STIMULI-RESPONSIVE POLYMER SYSTEMS THAT RESPOND TO REDOX POTENTIAL AND pH FOR CONTROLLED DRUG RELEASE

APPROVED BY SUPERVISORY COMMITTEE

John B. MacMillan, PhD

Daniel J. Siegwart, PhD

Jacques Lux, PhD

Mihaela C. Stefan, PhD

DEDICATION

Dedicated to my mentors who helped shaped me to who I am today academically and professionally. My parents, Ahmed and Sahar, and sisters, Tammara and Diana, for their continuous support and encouragement throughout my graduate career. I further wish to thank my husband, Saadi, for his unconditional love and patience as I promised him I would be graduating "soon, in the next two months" for almost a year now.

ACKNOWLEDGEMENT

I would like to greatly thank my mentor, Dr. Daniel Siegwart, for his considerable guidance, support, and training to become an independent thinker. Also, for allowing me to participate in internships and fellowships that would apply towards my future career endeavors. I would like to thank my graduate thesis committee, Dr. John MacMillan, Dr. Mihaela Stefan, and Dr. Jacques Lux, for always making time in their busy schedules to nurture my progress throughout this journey. Specifically, thank you Dr. MacMillan for assisting me during my graduate course work, Dr. Lux for aiding in experimental suggestions and techniques, and Dr. Stefan for being my first ever mentor and introducing me to research as an undergraduate student. Also, thank you to Ms. Carla Childers for her guidance on the formalities and financial accounts of the graduate program and the fellowships I received.

I would like to thank my lab members for making the Siegwart Lab a collaborative teaching environment and my home-away-from-home. In particular, thank you, Dr. Jing Hao, Dr. Petra Kos, Dr. Hu Xiong, Dr. Yunfeng Yan, Dr. Jason Miller, and Dr. Kejin Zhou for your patience in training me, your experimental discussions, and your personal support throughout this journey. Thank you to my colleagues, classmates and friends who also played similar roles.

Thank you to Dr. Nancy Street who was always there during my time as a UTSW Green Fellow, National Science Foundation (NSF) Graduate Research Fellow, University of Texas Archer Fellow, National Institute of Health National Cancer Institute Technology Transfer Center (NIH/NCI TTC) Fellow, UTSW graduate student, and UTD undergraduate student. Dr. Street you truly were my rock throughout all these experiences and I can never thank you enough for everything that you have done.

Thank you to the NSF Graduate Research Fellowship Program for their financial support towards both my academic and professional career. Thank you to the UTSW Office for Technology and Development (OTD) staff, the UT Archer Program staff, and the NIH/NCI TTC staff in helping me pursue my future career goals. I would individually like to thank Dr. Natalie Lundsteen, Mr. Ray Wheatley, Ms. Anna Benfield, Dr. Frank Grassler, Mr. Richard Rodriquez, Dr. Surekha Vathyam, Dr. Joel Swerdlow, Dr. Michelle Chin, Vice Chancellor William Shute, and Mr. Steve Alvarez.

My parents, Ahmed and Sahar, and sisters, Tammara and Diana, for their continual support, example, and motivation. My unborn child, who I hope to one day inspire. Lastly, my husband, Saadi, for waiting three years for me to complete my doctoral work and finally live with him full-time, for encouraging me to never give up, for always saying how proud of me he is, and for reassuring me that all will be well. Saadi, you are the love of my life, the future father of my child, and my forever best friend.

STIMULI-RESPONSIVE POLYMER SYSTEMS THAT RESPOND TO REDOX POTENTIAL AND pH FOR CONTROLLED DRUG RELEASE

by

SUSSANA A. ELKASSIH

DISSERTATION / THESIS

Presented to the Faculty of the Graduate School of Biomedical Sciences

The University of Texas Southwestern Medical Center at Dallas

In Partial Fulfillment of the Requirements

For the Degree of

DOCTOR OF PHILOSOPHY

The University of Texas Southwestern Medical Center at Dallas

Dallas, Texas

May, 2018

STIMULI-RESPONSIVE POLYMER SYSTEMS THAT RESPOND TO REDOX POTENTIAL AND pH FOR CONTROLLED DRUG RELEASE

Publication No._____

SUSSANA A. ELKASSIH, PhD

The University of Texas Southwestern Medical Center at Dallas, 2018

Supervising Professor: DANIEL J. SIEGWART, PhD

Nanocarriers are widely investigated drug delivery systems that can overcome physiological barriers by tuning nanocarrier size, shape, surface chemistry, targeting ligand conjugation, and material composition. Furthermore, they have stimuli-responsive moieties that translate physiological signals, such as pH and redox potential, at the tumor microenvironment into nanocarrier behaviors, like swelling, degradation, morphological change, and charge reversal. Stimuli-responsive nanocarriers exhibit better pharmacokinetic profiles with reduced premature cargo leakage during circulation time and improved tumor targeting efficacies. pH is the most commonly explored stimuli for designing nanocarriers, however there has been a recent interest in redox stimuli-responsive nanocarriers. Redox stimuli-responsive nanocarriers are often incorporated with a glutathione (GSH) sensitive bond, typically disulfide bonds, for intracellular activation or degradation.

In these documented series of experiments, I first focus on poly(disulfide)s and report on the synthesis of fully degradable poly(disulfide) cross-linked nanogel drug carriers formed by oxidative radical polymerization of 2,2'-(ethylenedioxy)diethanethiol (EDDET) as a monomer with different cross-linkers, including pentaerythritol tetramercaptoacetate (PETMA), via a single-electron transfer mechanism. Because the poly(EDDET) backbone repeat structure and cross-linking junctions are composed entirely of disulfide bonds, these nanogels specifically degrade to small molecule dithiols intracellularly in response to the reducing agent glutathione present inside of cells. Due to the ease of synthesis, rapid gelation times, and tunable functionality, these non-toxic and fully degradable nanogels offer excellent potential for use in a variety of drug delivery applications.

In addition to disulfide bonds, esters are another attractive functional group for the synthesis of degradable polymers for drug delivery, therefore I later discuss experiments and research that I worked on with Dr. Jing Hao, a postdoc in the Siegwart Lab, that describes how polyesters can be synthesized in a controlled fashion and how they can be used to deliver siRNA molecules *in vitro* and *in vivo*. Specifically, the synthesis of a lipocationic polyester library via ring-opening polymerization (ROP) of functional valerlactones for efficacious siRNA delivery is described. The 139 polymers in the lipocationic polyester library were synthesized in high yield, fast time (minutes), and gram scale. Precise monomer incorporation ratios were achieved to enable tunable hydrophobicity and pKa. Nanoparticles formulated with these polymers were able to enable gene silencing *in vitro* and *in vivo* at low doses.

TABLE OF CONTENTS

PRIOR PUBLICATIONS

Elkassih, Sussana A.; Kos, Petra; Xiong, Hu; Siegwart, Daniel J. Degradable Redox-Responsive Disulfide-Based Nanogel Drug Carriers via Dithiol Oxidation Polymerization. *Submitted*. (2018).

Yan, Yunfeng; Liu, Li; Xiong, Hu; Miller, Jason B.; Zhou, Kejin; Kos, Petra; Huffman, K. E.; Elkassih, Sussana A.; Norman, John W.; Carstens, Ryan; Kim, James; Minna, John D. and Siegwart, Daniel J. Functional Polyesters Enable Selective siRNA Delivery to Lung Cancer Over Matched Normal Cells. *Proceedings of the National Academy of Sciences, U.S.A*. (2016), *113*, E5702-E5710.

Xiong, Hu; Kos, Petra; Yan, Yunfeng; Zhou, Kejin, Miller Jason B.; Elkassih, Sussana A.; Siegwart, Daniel J. Activatable Water Soluble Probes Enhance Tumor Imaging By Responding to Dysregulated pH and Exhibiting High Tumor-To-Liver Fluorescence Emission Contrast. *Bioconjugate Chemistry* (2016), *27*, 1737-1744.

Hao, Jing; Elkassih, Sussana A.; Siegwart, Daniel J. Progress Towards the Synthesis of Amino Polyesters Via Ring-Opening Polymerization (ROP). *Synlett* (2016), *27*, 2285-2292.

Nagai, Atsushi; Miller, Jason B.; Kos, Petra; Elkassih, Sussana A.; Xiong, Hu; Siegwart, Daniel J. Tumor Imaging Based on Photon Upconversion of Pt(II) Porphyrin Rhodamine Co-Modified NIR Excitable Cellulose Enhanced by Aggregation. *ACS Biomaterials Science & Engineering* (2015), *1*, 1206-1210.

Hao, Jing; Kos, Petra; Zhou, Kejin; Miller, Jason B.; Xue, Lian; Yan, Yunfeng; Xiong, Hu; Elkassih, Sussana A.; Siegwart, Daniel J. Rapid Synthesis of a Lipocationic Polyester Library via Ring-Opening Polymerization of Functional Valerolactones for Efficacious siRNA Delivery. *Journal of the American Chemical Society* (2015), *137*, 9206-9209.

Yan, Yunfeng; Xue, Lian; Miller, Jason B.; Zhou, Kejin; Kos, Petra; Elkassih, Sussana A.; Liu, Li; Nagai, Atsushi; Xiong, Hu; Siegwart, Daniel J. One-Pot Synthesis of Functional Poly(amino ester sulfide)s and Utility in Delivering pDNA and siRNA. *Polymer* (2015), *72*, 271-280.

Elkassih, Sussana A.; Sista, Prakash; Magurudeniya, Harsha D.; Papadimitratos, Alexios; Zakhidov, Anvar A.; Biewer, Michael C.; Stefan, Mihaela C. Synthesis and Characterization of Benzodithiophene with Phenylethynyl Substituents. *Macromolecular Chemistry and Physics* (2013), *214*, 572-577.

Sista, Prakash; Hao, Jing; Elkassih, Sussana A.; Sheina, Elena E.; Biewer, Michael C.; Janesko, Benjamin G.; Stefan, Mihaela C. Synthesis, Characterization, and Computational Modeling of Benzodithiophene Donor-Acceptor Semiconducting Polymers. *Journal of Polymer Science, Part A: Polymer Chemistry* (2011), *49*, 4172-4179.

LIST OF FIGURES

LIST OF SCHEMES

LIST OF TABLES

LIST OF ABBREVIATIONS

αIεCL - α-iodo-ε-caprolactone

AIBN - Azobisisobutyronitrile

AT1 - 2-(dimethylamino)ethane-1-thiol

AT2 - 2-(diethylamino)ethane-1-thiol

AT3 - 2-(dipropylamino)ethane-1-thiol

AT4 - 2-(dibutylamino)ethane-1-thiol

AT5 - 2-(pyrrolidin-1-yl)ethane-1-thiol

AT6 - 2-(piperidine-1-yl)ethane-1-thiol

AT7 - 2-(azepan-1-yl)ethane-1-thiol

ATR - Attenuated Total Reflection

ATRP - Atom Transfer Radical Polymerization

BDE - Bond Dissociation Energy

BLI - Bioluminescense Imaging

BnOH - Benzyl Alcohol

Br - Broad Signal Quint

Boc - tert-ButyloxycarbonylBOP - (Benzotriazol-1-yloxy)tris(dimethylamino) phosphonium hexafluorophosphate

^{13}C-NMR - Carbon-13 NMR

CABCL - γ-(carbamic acid benzyl ester)-3-caprolactone

Chol - Cholesterol

CL - Crosslinker

CPD - Cell-Penetrating Poly(disulfide)

CRP - Controlled/Living Radical Polymerization

DAPI - 4',6-diamidino-2-phenylindole

DBU - 1,8-Diazabicyclo[5.4.0]undec-7-ene

DCC - Dicyclohexylcarbodiimide

DCM - Dichloromethane

D_H - Hydrodynamic Diameter

DIPEA - *N,N*-Diisopropylethylamine

DLS - Dynamic Light Scattering

DMAP - 4-(dimethylamino)pyridine

DMEM - Dulbecco Modified Eagle Medium

DMF - Dimethylformamide

DMPP - Dimethylphenhylpiperazinium

DOX - Doxorubicin

DP - *N*,*N*-dimethyldipropylenetriamine

DPO - 5,6-dihydro-2H-pyran-2-one

DSDOP - 2,2-dibutyl-2-stanna-1,3-dioxepane

DSPC - 1,2-distearoyl-sn-glycero-3-phosphocholine

DTNB - 5,5'-dithio-bis-(2-nitrobenzoic acid)

DTT - Dithiothreitol

EDDET - 2,2'-(ethylenedioxy)diethanethiol

EGFR - Epidermal Growth Factor Receptor

ELSD - Evaporative Light Scattering Detector

EPR - Enhanced Permeability and Retention

$(Et)_3N$ - Triethylamine

EtOH - Ethanol

FBS - Fetal Bovine Serum

FDA - Food and Drug Administration

FITC - Fluorescein Isothiocyanate

FRET - Förster Resonance Energy Transfer

FTIR - Fourier Transform Infrared

GI - Gastrointestinal

GPC - Gel Permeation Chromatography

GP_x - Gluthathione Peroxidase

GR - Glutathione Reductase

GSH - Glutathione

GSSG - Glutathione Disulfide

^{1}H-NMR - Hydrogen-1 (Proton) NMR

HeLa-Luc - Hela Luciferase

IT - Intratumoral

IV - Intravenous

LC-MS - Liquid Chromatography-Mass Spectroscopy

LDA - Lithium Diisopropylamide

LHRH - Luteinizing Hormone Releasing Hormone

LiHa - Liquid Handling Arm

LNP - Lipid Nanoparticle

Luc - Luciferase

m/z - Mass/Charge Number of Ions

MCA - Multi-Channel Arm

mCPBA - meta-Chloroperbenzoic Acid

miRNA - Micro RNA

M_n - Number Average Molecular Weight

M_w - Weight Average Molecular Weight

MWCO - Molecular Weight Cut-Off

N1C4 - poly{4-((2-(dimethylamino)ethyl) thio)tetrahydro- 2H-pyran-2-one}-r-poly{4-(butylthio)tetrahydro-2H-pyran-2-one}

N1C8 - poly{4-((2-(dimethylamino)ethyl) thio)tetra hydro-2H-pyran-2-one}-r-poly{4-(octylthio)tetrahydro-2H-pyran-2-one}

N1C6 - poly{4-((2-(dimethylamino)ethyl) thio)tetra hydro-2H-pyran-2-one}-r-poly{4-(hexylthio)tetrahydro-2H-pyran-2-one}

NHS - N-Hydroxysuccinimide

NIH - National Institute of Health

NMR - Nuclear Magnetic Resonance

NP - Nanoparticle

PAMAM - polyamidoamine

PBS - Phosphate Buffered Saline

PCL - poly(ε-caprolactone)

Pd/C - Palladium on Carbon

PDI - Polydispersity Index

pDNA - Plasmid Deoxyribonucleic Acid

PEG. - poly(ethylene glycol)

PETMA - pentaerythritol tetramercaptoacetate

PETMP - pentaerythritol tetra(3-mercaptopropionate)

PFA - Paraformaldehyde

PGA - poly(glycolic acid)

pKa - $-\log_{10}(Ka)$

PLA - poly(lactic acid)

PLGA - poly(lactic-co-glycolic acid)

PLU127 - Pluronic-127

PTA - Phosphotungstic

RAFT - Reversible-Addition Fragmentation Chain-Transfer Polymerization

RI - Refractive Index

RNA - Ribonucleic Acid

RNAi - RNA Interference

RoMa - Robotic Manipulator Arm

ROMP - Ring-Opening Metathesis Polymerization

ROP - Ring Opening Polymerization

rt - Room Temperature

SAR - Structure-Activity Relationship

siControl - siRNA Control

siCPD - Self-Inactivating Cell-Penetrating Poly(disulfide)

siLuc - Small Interfering Luciferase

siRNA - Small Interfering Ribonucleic Acid

SP - Spermine

STDEV - Standard Deviation

TEA - Triethylamine

TEM - Transmission Electron Microscopy

TFA - Trifluoroacetic Acid

THF - Tetrahydrofuran

TNB - 2-nitro-5-thiobenzoic acid

TP - Tetramethylenepentamine

UV-Vis - Ultraviolet-Visible Spectroscopy

5-NHZ-VL - 5-Z-amino-δ-valerolactone

CHAPTER ONE

REDOX STIMULI-RESPONSIVE POLY(DISULFIDE) NANOCARRIERS

REVIEW OF THE LITERATURE

1.1 INTRODUCTION

Drug delivery systems have evolved during the last six decades and can be briefly classified by three generations.[1,2] In the 1950s, early systems were designed as oral formulations[3] or transdermal patches for delayed drug release.[4] In the 1980s, the focus was on controlled release, which refers to the efforts to maintain a constant drug concentration in the blood.[5] Around this time, there was the development of bioresponsive polymers, which led the way for more controllable drug delivery systems.[6] Since 2010, the third generation of drug delivery systems has been based on nanomaterials with modular and tunable physiochemical properties.[7-10] To meet the physiological requirements of various drug targets, numerous types of drug delivery systems were developed ranging from macro-, to micro-, and to nanoscale. Nanocarriers are a widely investigated drug delivery system, where they can overcome physiological barriers by tuning the nanocarrier size, shape, surface chemistry, targeting ligand conjugation and material composition. Furthermore, stimuli-responsive nanocarriers have stimuli-responsive moieties that translate physiological signals (such as, pH and redox potential) at the tumor microenvironment into behaviors of the nanocarriers, such as swelling, degradation, morphological change, and charge reversal.[11] Stimuli-responsive nanocarriers exhibit better pharmacokinetic profiles with reduced concern of premature cargo leakage during circulation and improved tumor targeting efficacies.[12] pH is the most commonly explored stimuli for designing nanocarriers, however there has been a recent interest in redox stimuli-responsive nanocarriers. Redox stimuli-responsive nanocarriers are often incorporated with a glutathione (GSH) sensitive bond, typically disulfide bonds, for intracellular activation or degradation. This chapter will give an overview of controlled drug delivery as it discusses advantages of controlled drug delivery, the numerous types of drug delivery systems, the physiological barriers drug delivery systems must overcome, design criteria, and the

emergence of stimuli-responsive drug delivery systems. Because there is an increasing interest in redox stimuli-responsive drug delivery systems in the field, the last half of the chapter will primarily focus on poly(disulfide) redox responsive nanocarriers.

1.2 ADVANTAGES OF CONTROLLED DRUG DELIVERY

Controlled drug delivery carriers can improve the pharmacokinetic properties of a wide variety of drugs. In addition to controlled release of small molecules, such as in FDA-approved microparticle drug depots and chemotherapeutic drug-loaded liposomes,[13] nanoparticle carriers are essential for the delivery of biomacromolecular drugs including nucleic acids that cannot cross cell membranes on their own.[13-15] Embedding drugs into nanoparticles not only effectively suppresses interaction with blood components, but also enhances drug targeting specificity, lowers systemic drug toxicity, improves treatment absorption rates, and provides protection for pharmaceuticals against degradation.[16-18]

1.3 MACRO-, MICRO-, and NANO-CONTROLLED DRUG DELIVERY SYSTEMS

To meet the physiological requirements of various drug targets, numerous types of drug delivery systems were developed ranging from macro-, to micro-, to nanoscale.

1.3.1 Macroscale

Macroscale drug delivery systems generally refer to drug delivery devices with at least one dimension greater than 1 mm in size.[19,20] Macroscale devices were developed in varying forms,

such as wearable devices,[21,22] mucoadhesives,[23] and long-term drug-releasing implants.[24,25] From the perspective of material, polymers are preferred for preparing physiologically compatible drug delivery systems.[26-29] Representative polymers for these devices include natural polymers like dextran, alginate, chitosan, gelatin, or synthetic polymers such as poly(lactic-co-glycolic acid) (PLGA) or poly(aminoester).[30] Drugs could be loaded into either a reservoir, where the drugs are enclosed by a polymeric membrane, or a matrix, where the drugs are embedded in polymeric networks.[31] Release of the drugs could be through diffusion, where the steric hindrance from the polymer scaffold dominates; competitive dissociation, where the drug exhibits specific affinity towards the polymeric carrier; or degradation, where the polymer scaffold could be eroded via dissolution, hydrolysis, or enzymatic digestion.[32] Sensitivity to environmental signals could also be incorporated into polymeric systems for smart drug delivery.[33]

1.3.2 Microscale

Microscale drug delivery systems are generally referred as microparticles that are injected locally in the tissue. Microparticles with a large diameter (1 μm) would get stuck in the capillary bed or get caught by Kupffer cells in the liver, making them unsuitable for systemic injection.[34] When administered locally, steric hindrance from the extracellular matrix will limit the movement of microparticles and hold the microparticles in the site of injection. This feature leads to widespread applications of microparticles as drug depots.[35]

1.3.3 Nanoscale

Nanocarriers are generally 30-300 nm and this size enables them to filter through the fenestrations of liver blood vessels as well as penetrate into tumor tissue by the enhanced

permeability and retention (EPR) effect.[36-38] Note that nanocarriers (>500 nm) are susceptible to macrophage uptake while smaller nanocarriers (<10 nm) are easily cleared out via renal excretion pathway.[12] Nanocarriers have become a widely investigated drug delivery systems with cancer as the most researched target.[39]

1.4 PHYSIOLOGICAL BARRIERS

The main goal of drug delivery systems is to reach the desired site and release the cargo to achieve efficacious outcomes in threating a variety of diseases. Cancer is the best representative of these diseases, where sufficient accumulation of potent anticancer drugs is the goal for applying nanocarriers. Therefore, in this chapter, cancer as a model disease will be used to describe physiological barriers and designing criteria for drug delivery systems.

When the nanocarriers are injected into blood circulation, rapid adsorption of serum proteins onto the nanocarrier occurs. Various proteins, such as fibrinogen, globulin, and albumin, will form a corona around the nanocarriers, a process termed as opsonization. This nanoparticle-protein complex is susceptible for uptake by circulating or residential phagocytes.[40,41] The opsonization-internalization mediated nanocarrier clearance is the first and major barrier in the blood potentially, causing up to 50% loss of the administered dose hours after injection and leading to nonspecific accumulation of nanocarriers in organs like the liver and spleen.[42] In addition, the opsonization prevents the targeting ligands conjugated/attached on nanocarriers from interacting with the targeted receptors.[43] In the blood flow, fluid dynamics of the nanocarrier influence their margination towards vascular walls.[44] The low permeability of vascular endothelium is the next significant hurdle for nanocarriers.[45,46] After extravasation into tumor microenvironment, the

nanocarrier needs to diffuse through the dense extracellular matrix against high interstitial pressure to reach the tumor cells.[47]

Small molecular therapeutics, especially those with high hydrophobicity, are capable of passively diffusing through the lipid bilayer plasma membrane.[48] However, for protein or nucleic acid-based therapeutics, nanocarriers are generally needed for transportation into the cells.[49,50] Numerous internalization pathways exist, and the entry is affected by various properties of the nanocarrier, such as particle size, surface charge, physiochemical composition, and the modification with targeting ligands.[51] For nanocarriers that are not modified with any specific targeting ligand, the uptake is mainly through endocytosis,[52] where vesicles emerge from plasma membrane to encapsulate and internalize the nanocarriers together with extracellular fluids. Those nanocarriers that are modified with targeting ligands, take advantage of specific receptors overexpressed on cancer cell membranes for facilitated and selective internalization. For example, epidermal growth factor receptor (EGFR),[53] folate receptor,[54] transferrin receptor,[55] lectins,[56] and low-density lipoprotein receptor[57] are well-characterized receptors to induce efficient cellular uptake. Different types of targeting ligands, including small molecules,[58] antibodies,[59] peptides,[60] and aptamers[61] can be easily functionalized onto the surface of the nanocarriers.[62,63]

For drugs that work in intracellular compartments, the nanocarrier needs to be internalized through endocytosis and escape the endosome to reach other organelles. After internalization of the nanoparticles through plasma membrane invagination, the nanocarriers are generally trapped inside endosomes.[64-66] As the endosome matures, it fuses with the lysosome, where the acidic and enzyme-rich environment would lead to the degradation of both the nanocarrier and cargo.[67] The endo-lysosome entrapment poses the most critical barrier for the intracellular drug delivery, especially for macromolecular therapeutics. The methods for endosome escape can be classified

into different mechanisms, such as proton-sponge effect,[68] nanoparticle-endosome membrane fusion,[69,70] and photochemical disruption.[71] Acidification of the endosome plays an important role for cellular uptake of nanoparticles.[65,66]

After overcoming the multiple barriers, the delivery may still fail, especially for chemotherapeutics, due to the potential drug resistance of the cells. Drug resistance develops either intrinsically before administering the therapeutics or externally after extended exposure to chemotherapeutics.[72] The chemotherapeutic resistance stems from complex mechanisms that involve defects in the apoptosis machineries, induction of alternative DNA repair pathways, structural changes of the drug targets, and elevated expression of drug efflux pumps.[73] Among the different mechanisms, the drug efflux pump is the most significant barrier that could pump out not only the administered nanocarrier, but also a wide range of therapeutics, leading to multidrug resistance.[74-76]

1.5 DESIGN CRITERIA

To overcome physiological barriers nanocarrier size, shape, surface chemistry, targeting ligand conjugation and material composition can be tailored modularly.

1.5.1 Size

Nanocarriers that are too small (<10 nm) are easily cleared from the circulation through glomerular filtration,[77] while nanocarriers that are too large (>2 μm) will clog the blood vessel due to the limited diameter of the capillaries (~5 μm).[78] For tumor-targeted nanocarriers, the size should be tailored to take advantage of the enhanced permeability and retention (EPR) effect, which limits the particle size within 500 nm[79] and preferentially <200 nm.[80] Nanocarriers >200

nm also risk clearance by other organs, such as liver, spleen, or lung, reducing their circulation half-time. In addition to tumor accumulation, the ability to penetrate dense solid tumors makes nanocarriers within sub-100 nm range more efficient carriers. Overall, nanocarriers within the size range of 10–200 nm, preferentially <100 nm,[81] are ideal for tumor targeted drug delivery.

1.5.2 Shape

Nanocarrier shape can significantly affect the delivery efficacy from multiple aspects of the delivery process, including circulation, extravasation, and internalization by targeted cells.[82-84] Currently, nanospheres, nanodiscs, nanorods, and nanocylinders are among the most investigated geometries. From the perspective of circulation, nanocarriers with a cylindrical[85] or disc-like[86] structure showed distinct hemodynamic patterns versus spherical ones; circulation half-time could be enhanced either by orienting the nanocarrier to follow blood flow or by tumbling in the blood vessels. In addition, the shape of the nanocarriers affects macrophage recognition,[87] further affecting the biodistribution patterns. For targeted internalization by cancer cells, nanocarriers with a bacteria-like rod shape, generally demonstrate higher intracellular up- take efficiencies than their spherical shape.[12]

1.5.3 Surface Chemistry

The interaction of nanocarrier surface components with cells affect the efficacy. Due to the negative charge of cell membranes,[88] positively charged nanocarriers typically exhibit superior *in vitro* internalization efficacy versus negatively charged or neutral ones.[89,90] Generally, positively charged nanocarriers are endocytosed through the clathrin-dependent pathway while negatively charged nanoparticles tend to be internalized through the caveolae-mediated pathway.[91,92]

However, for *in vivo* administration, positive charges on nanocarriers could easily attract serum proteins, which are mostly negatively charged.[93,94] pH stimuli-responsive nanocarriers are specifically tailored to maintain a neutral or slightly negative charge while in circulation but shift to a positive charge when reaching the tumor microenvironment.[12] The acidic tumor microenvironment will trigger the pH stimuli-responsive nanocarriers to shed their negatively charged shells from the positively charged cores[95] or switching the charge of a synthetic peptide.[96] Cellular internalization is significantly affected by the hydrophobicity or hydrophilicity of the nanocarrier surface, where hydrophobic nanocarriers are easily internalized.[97] Commonly, attachment of poly(ethylene glycol) (PEG) (PEGylation) is used to increase the hydrophilicity of the surfaces and elongates nanocarrier circulation time.[12]

1.5.4 Targeting Ligand Conjugation

Besides avoiding macrophage recognition, the presence or absence of targeting ligands on nanocarrier surfaces can influence their adhesion and entry into targeted cancer cells.[12] The overexpressed receptors on tumors, as well as, vascular proximal endothelial cells make targeting ligands a useful component for targeted delivery with improved precision.[98] Note that healthy cells also share the receptors of the tumor cells, although at a lower expression level.[99,100]

1.5.5 Material Composition

Various types of materials have been used to construct nanocarriers,[101] such as polymer-based nanogels, micelles, polymersomes, and dendrimers;[102,103] lipid-based solid lipid nanocarriers, liposomes,[104] and lipid-like lipidoids;[105] inorganic nanocarriers, including gold nanoparticles,[106,107] carbon nanotubes, graphene[108], nanodiamonds,[109] magnetic particles[110], and

liquid metal nanoparticles;[111] macromolecular assembly-based DNA[112-114] and protein nanocarriers[115]. This chapter will focus on polymer-based nanocarriers, because of the ability to readily control polymer chemical and physical properties via chemical synthesis and their ease of processing.

1.6 STIMULI RESPONSIVE DRUG DELIVERY

Stimuli-responsive drug delivery systems have stimuli-responsive moieties that translate physiological signals (such as, pH and redox potential) at tumor microenvironment into behaviors of the nanocarriers, such as swelling, degradation, morphological change, and charge reversal.[11] Stimuli-responsive nanocarriers exhibit better pharmacokinetic profiles with reduced concern of premature drug leakage during circulation and improved tumor targeting efficacies.[12]

1.6.1 Acidic Environment

A local decrease of pH in different tissues, such as the GI tract and vagina, subcellular compartments, such as the endosome and lysosome, or disease-associated conditions, such as infection, inflammation, and tumor microenvironment, provides a reliable signal to trigger cargo release from drug delivery systems.[12] For tumors, the abnormal metabolic activities, like the elevated rate of glycolysis, together with poor lymphatic drainage lead to the accumulation of lactic acid, hence establishing an acidic tumor-microenvironment. Tumor-targeted nanocarriers will experience subtle pH changes when moving from blood circulation (pH 7.4) to tumors extracellular space (pH 6–7.2).[116] Nanocarriers internalized into intracellular space will undergo a further decrease of pH in endosomes (pH 5.0 – 6.0) and lysosomes (pH 4.0 –5.0).[117] Numerous

pH-responsive drug delivery systems have been developed to take advantage of this pH gradient. Formulation is generally based on two mechanisms: (1) incorporating protonatable polymers, such as polyacids, polybases, or poly-amino acids, that could allow solubility or conformational changes upon acid stimulation; (2) utilizing acid-labile moieties, like bicarbonate salts, or acid-cleavable bonds, such as hydrazines, acetals and esters, to enable disassembly of the nanocarriers in acidic environments.[96] Nanocarriers comprising of aliphatic polyesters, such as poly(lactic acid) (PLA), poly(glycolic acid) (PGA), poly(ε-caprolactone) (PCL), polycarbonates, and their copolymers are commonly used polyesters, where they degrade under physiological conditions. However, aliphatic polyesters are generally hydrophobic and lack the functional groups required for delivery of drugs that require electrostatic interactions (e.g. nucleic acids), bioconjugation reactions, and attachment of targeting ligands.[118,119] Also, ester bond degradation generates acidic products, which can cause an undesirable local decrease in pH.

1.6.2 Redox Environment

The reducing gradient between the intracellular compartment and the extracellular environment is a physiological stimulus that has attracted great interest for controlled drug delivery. Intracellular concentrations of the glutathione (GSH) is 2–10 mM, which is maintained in reducing the state by other reducing factors.[120] Furthermore, the GSH level is at least four folds higher in tumor when compared with normal tissues,[121,122] making the reduction gradient-based nanocarriers more tumor selective. Also, it was reported that GSH level is related to many human diseases, such as neurodegenerative diseases, liver diseases, stroke, seizures, and diabetes.[121,123-126] For example, an abnormally high concentration of GSH in cancerous cells protects the cells against the anti-cancer drugs and free radicals generated during radiation therapy, which results in

multi-drug and radiation resistance.[121,124,127] This could provide a potential physiological trigger for poly(disulfide) degradation and drug delivery to diseased tissues.[12] Nanocarriers are often incorporated with GSH-sensitive bond, typically the disulfide bond, for intracellular activation or degradation. The disulfide bond is stable in the mildly oxidative extracellular space, but after crossing the plasma membrane it will be converted into thiols or undergo thiol-disulfide exchange by interaction with reducing agents.

1.7 DISULFIDE BONDS

The disulfide bond is a dynamic covalent bond, which can be easily cleaved and reformed on demand, but is stronger than the non-covalent interactions present in supramolecular polymers.[128] The dynamic nature of disulfide accounts for unique properties in poly(disulfide)s such as adaptability, stress resistance, self-repair, or degradability in response to physical or chemical stimulation. Poly(disulfide)s are dynamic polymers with disulfide repeats in their main chain.[129]

1.7.1 Dynamic Covalent Bond

The disulfide bond is a dynamic covalent bond. Dynamic covalent bonds combine the characteristics of covalent and non-covalent bonds.[130-132] Under certain conditions, they can reversibly form and break, like non-covalent bonds. Under different conditions, they can be as strong and permanent as covalent bonds. The disulfide bond, for example, is stable under neutral and acidic conditions, but under reductive or basic conditions in the presence of thiolates, disulfides exchange rapidly.

1.7.2 S—H Bond Dissociation Energies in Thiols

Alkanethiols have similar S—H bond dissociation energies, generally to be around 87 kcal mol^{-1} regardless of the structure of the alkyl residue, therefore alkanethiols act similarly toward hydrogen atom abstraction (**Scheme 1.1**).[133,134] The S—H bond in cysteine is slightly weaker (86 kcal mol^{-1}),[133] while hydrogen sulfide is significantly less reactive (91 kcal mol^{-1}).[135] The S-H bond in thioacids is found to be in the same range (from 87 kcal mol^{-1} for thiobenzoic acid to 99 kcal mol^{-1} for thioacetic acid),[135] and they generally display hemolytic reactivity analogous to that of alkanethiols. Thiophenols are excellent hydrogen atom donors due to the stabilization by resonance of the corresponding arenethiyl radical (**Scheme 1.1**). Thiophenol has a S—H bond dissociation energy around 79 kcal mol^{-1}, but electron-donating *para*-substituents decrease the S—H bond dissociation energy (BDE), whereas electron-withdrawing ones increase it (**Scheme 1.1**).[136,137] Hydropersulfides (RSSH) have very weak S—H bonds (around 65 kcal mol^{-1}) (**Scheme 1.1**).[135]

Alkanethiols: similar S-H BDEs around 87 kcal mol^{-1} regardless of the structure of the alkyl residue

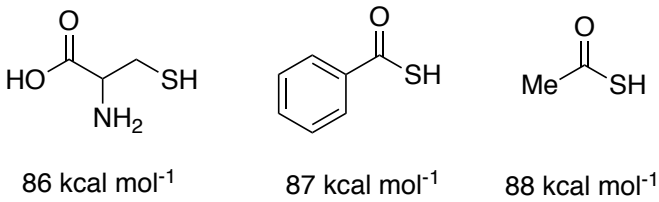

Thiophenols: weaker S-H BDEs due to teh stabilization by resonance of the corresponding arenethiyl radial

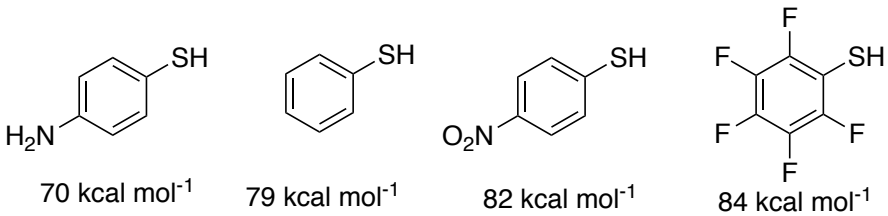

Dialkyldisulfides: around 65 kcal mol^{-1}

Diaryldisulfides: around 50 kcal mol^{-1}

Scheme 1.1. S-H and S-S bond dissociation energies (BDEs).

1.7.3 S—S Bond Dissociation Energies in Disulfides

Sulfur-sulfur bonds in disulfides are stronger than O—O, Se—Se, or Te—Te bonds.[138] Regardless, S—S are easily cleaved, where the stability of the resulting radical governs the S—S BDE.[135]

1.7.4 Generation of Thiyl Radicals

Thiyl radicals can rapidly couple with each other to form disulfide bonds and polymers.[139] Generation of a thiyl radical can be accomplished via hydrogen atom abstraction by other radicals having a corresponding higher X-H BDE, one-electron oxidation, one-electron reduction of disulfides, and hemolytic cleavage by radiolysis or light irradiation (**Scheme 1.2**). Thiols can rapidly transfer a hydrogen atom to most types of radical $X^{\bullet}$ having a corresponding higher X—H BDE. Therefore, all of the commonly used initiators such as azo-compounds or peroxides that generate alkyl or alkoxyl radicals are efficient to initiate thiol-mediated radical transformations (**Scheme 1.2A**). Thiyl radicals may be generated from a thiol and a one-electron oxidant such as Mn(III) compounds (**Scheme 1.2B**).[140] Similarly, electron transfer from thiolate anions results in the formation of thiyl radicals, which has been proposed to occur with oxygen in the autoxidation of thiolate solutions.[141] Homolytic cleavage of S—H or S—S bonds can be induced by radiolysis or under light irradiation (**Scheme 1.2D**). Thiols have a maximum of absorbance around 300 nm, thus irradiation above 300 nm is rather inefficient in generating substantial amounts of thiyl radicals.[142] However, in preparative chain reactions, where only initiation is required, continuous irradiation using a sun lamp can be used and in such cases, the slow but constant initiations is an advantage because the steady-state concentration of radicals remains low, diminishing the

importance of termination reactions.[143] Ketones are commonly used as sensitizers under light irradiation because the triplet state of carbonyl compounds rapidly abstracts a hydrogen atom from thiols.[144] Because the S—S bonds in disulfides are much weaker than any S—H bonds, they are easier to cleave photochemically.[145]

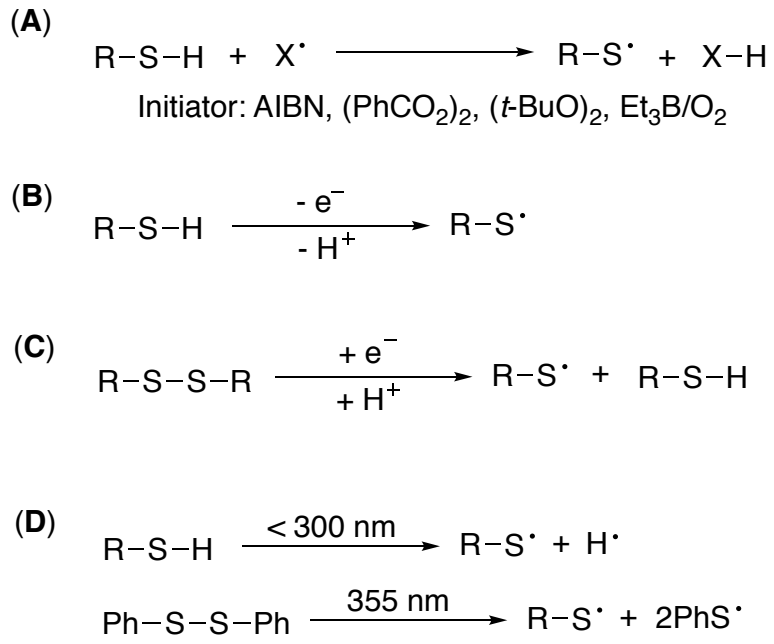

Scheme 1.2. Generation of thiyl radicals. (**A**) Hydrogen atom abstraction by other radicals having a corresponding higher X-H BDEs. (**B**) One-electron oxidation by $Mn(OAc)_3$, O_2. (**C**) One-electron reduction of disulfides. (**D**) Homolytic cleavage by radiolysis or light irradiation.

1.7.5 Termination Reactions

Alkylthiyl radicals recombine rapidly ($2k_t$ = (1-3) X 10^9 M^{-1} s^{-1}).[146,147] Similarly, unhindered arenethiyl radicals have been considered to dimerize at diffusion-controlled rates.[148]

1.8 POLY(DISULFIDE)S

1.8.1 Field Overview

As mentioned earlier, the reducing gradient between the intracellular compartment and the extracellular environment is a physiological stimulus that has attracted great interest in the field for controlled drug delivery and has been explored for developing stimuli-responsive drug delivery systems. Disulfide bonds have been incorporated into polymeric materials in a variety of ways,[17] including the use of disulfide containing cross-linkers,[149-157] redox-responsive self-assembly of amphiphilic polymers in the form of micelles or polymersomes,[158,159] biodegradable polymers, both linear and dendritic from disulfide-containing monomers,[160-164] and redox-responsive drug/polymer conjugates or polymer prodrugs.[165] To date, the majority of these approaches have been limited to polymerization of vinyl monomers, cross-linked by disulfide containing cross-linkers, such as star polymers, micelles, branched polymers, and gels.[157] These structures degrade to the original carbon-carbon bond-based polymer upon disulfide reduction, thus limiting the extent of degradation to long polymer chains. For example, McAlpine *et al*. used reversible addition-fragmentation chain-transfer (RAFT) polymerization to prepare star polymer comprising of PEG attached to a predesigned functional core.[166] The stars were cross-linked using disulfide linkers (**Scheme 1.3**). Tang *et. al.* used the disulfide bond to link low-generation polyamidoamine (PAMAM) dendrimers with branched PEG shells for enhanced gene and chemotherapeutic delivery.[167] Intracellular degradation of the disulfide bond exposed the siRNA and DOX co-loaded PAMAM dendrimer for passive drug release. DeSimone *et. al.* devised a siRNA pro-drug by covalently conjugating siRNA onto a hydrogel nanocarrier via a disulfide linker.[168] The nanocarrier was prepared by the particle replication in nonwetting templates method to enable either entrapment or conjugation of the siRNA. The covalent conjugation reduced the risk of burst

release compared with the gel entrapment-based loading method. The disulfide linker allowed selective release of siRNA inside targeted cells, while the control conjugate with a noncleavable linker failed to release the drug. Using a disulfide containing crosslinker, Zhao *et al.* prepared a GSH-degradable nanogel for intra-cellular delivery of various types of anticancer proteins, such as caspase-3,[169] apoptin, or p53[170]. Cellular entry could be mediated either by a positively charged monomeric component[169,171] or by a cancer-specific targeting ligand to target the overexpressed luteinizing hormone releasing hormone (LHRH) receptors.[170] After internalization, the polymeric shell sheds off intracellularly to release the encapsulated payload for inducing apoptosis.

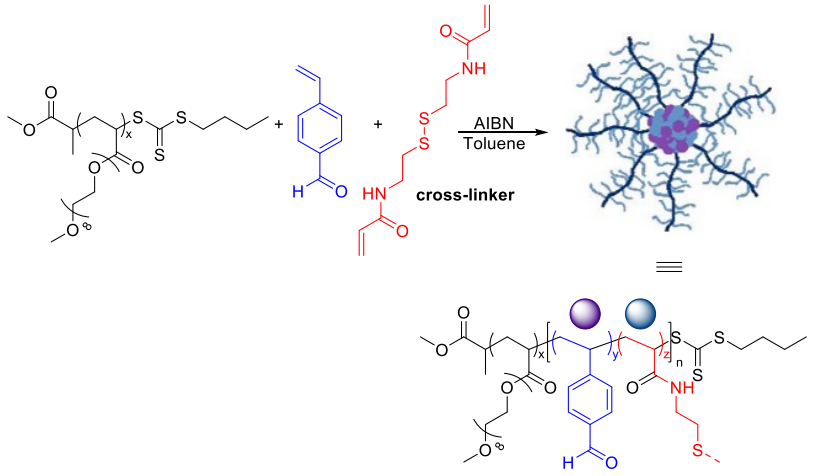

Scheme 1.3. Synthesis of cross-linked star polymer.[168] Arm homopolymer, vinyl benzaldehyde, and disulfide containing crosslinker were applied in a radical reaction to form star polymer.

Direct incorporation of disulfides into the polymer backbone would allow for tunable levels of degradation and has been accomplished to some extent by controlled/living radical polymerization methods (**Scheme 1.4**).[157] However, the preparation of linear polymers composed entirely of poly(disulfide) bonds (no vinyl comonomers) remains challenging. Matyjaszewski *et al*. employed atom transfer radical polymerization (ATRP) to synthesize α,ω-bromine-

functionalized polystryrene (**Scheme 1.4A**). The terminal bromine atoms were then replaced by thiol groups using thiodimethylformamide.[172] The dithiol-functionalized polystyrene were oxidized using Fe(III)Cl_3 to produce polymers. Hakwer.*et al.* synthesized well-defined linear copolymers via reversible-addition fragmentation chain-transfer (RAFT) polymerization using novel cyclic monomers with various methacrylate derivatives. Cyclic monomers contained ester, thioester, and disulfide functionalities (**Scheme 1.4B**).[173] Emerik *et al s*ynthesized disulfide-containing polyolefins by ring-opening metathesis polymerization (ROMP) of disulfide containing cyclic olefin (**Scheme 1.4C**).[174]

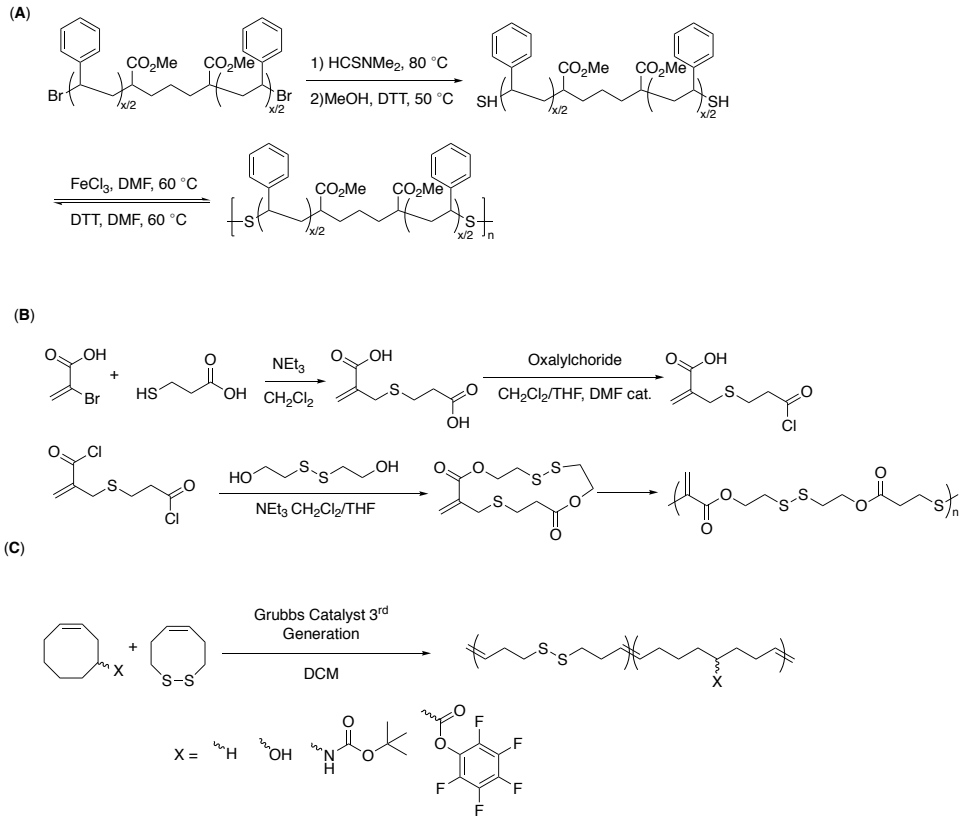

Scheme 1.4. Examples of direct incorporation of disulfides into polymer backbone using controlled/living radical polymerization to allow for tunable levels of degradation: (**A**) ATRP;[172] (**B**) RAFT;[173] and (**C**) ROMP.[174]

1.8.2 Synthesis & Mechanism

The synthesis of poly(disulfide)s has been investigated since the second half of the 1940s.[175] Four general routes exist: (1) ring-opening thiol-disulfide exchange polymerization of disulfide monomers or larger oligio(disulfide)s; (2) oxidative polymerization of dithiols; (3) conjugate addition to polymerize monomeric disulfides, which proceeds by nucleophilic substitution with sulfur acting as both electrophile and nucleophile; and (4) ring-opening disulfide metathesis, which can occur with thiolate initiators or with heat and proceeds via sulfenyl radicals (**Scheme 1.5**).[176] Oxidative and thiol-disulfide exchange polymerization are two most commonly used routes, where they offer different advantages. Both oxidative and thiol-disulfide exchange polymerization are mild and tolerate the presence of many functional groups, whereas disulfide exchange polymerization, initiated by heat, requires harsher conditions. All four approaches are reversible and thus compatible with reactivation, self-repair, recycling and responsiveness to templates. Disadvantages included in all four cases is the occurrence of macrocyclic side products originating from "backbiting", that is intramolecular disulfide exchange, and is difficult to avoid.[177] Ring-opening thiol-disulfide exchange polymerization is directional and requires neither oxidative conditions nor heat. Initiators and terminators can be used for controlling and suppressing macrocyclic side products, polymerizing from surfaces, introducing labels or creating sequences in multicomponent copolymers.[178]

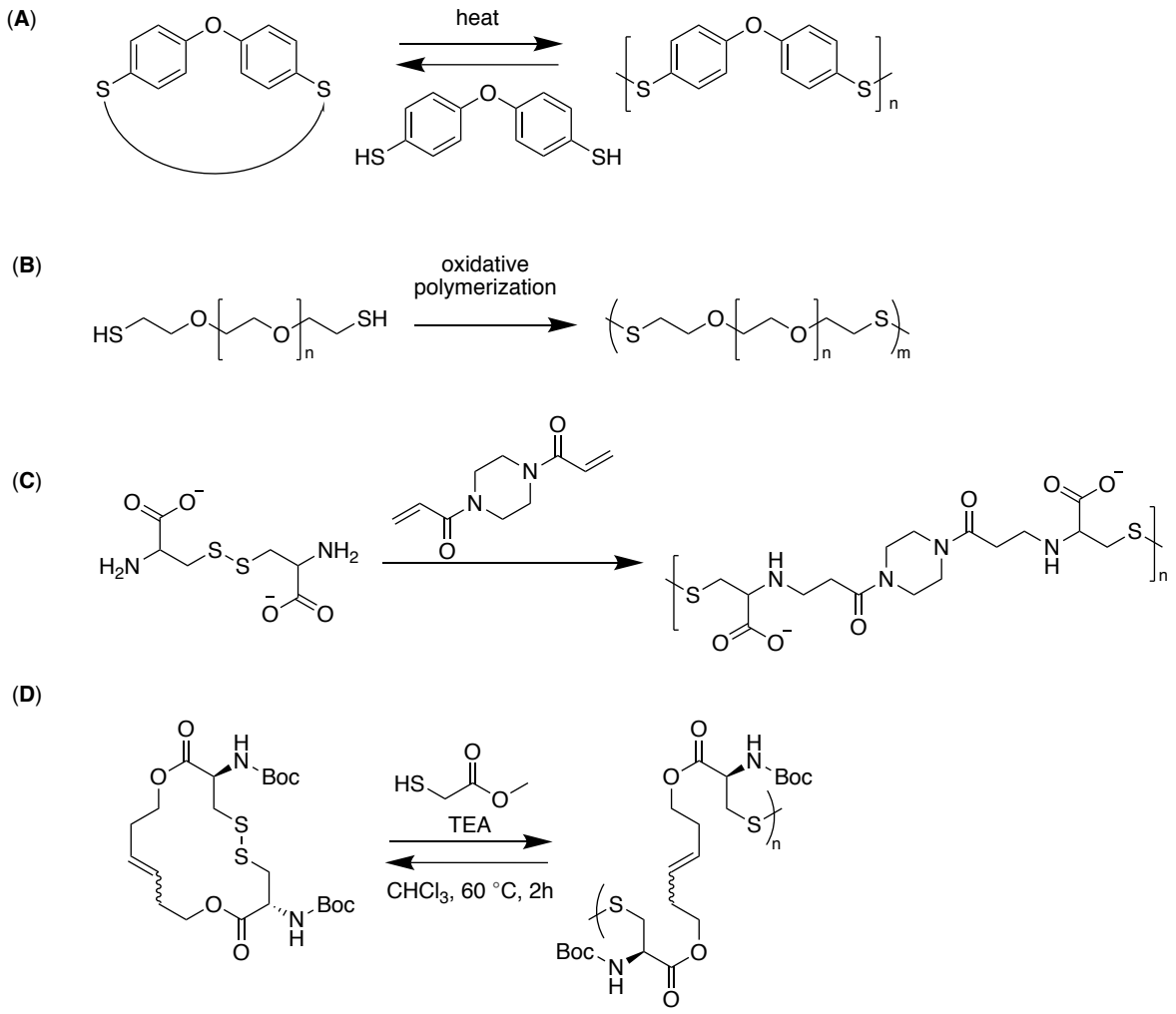

Scheme 1.5. General routes for poly(disulfide) synthesis. (**A**) ring-opening thiol-disulfide exchange polymerization of disulfide monomers or larger oligio(disulfide)s; (**B**) oxidative polymerization of dithiols; (**C**) conjugate addition to polymerize monomeric disulfides; and (**D**) ring-opening disulfide metathesis.

In general, thiols are more acidic than their alcohol analogues, allowing deprotonation to occur under milder conditions.[179] Once deprotonated, the thiolate anion is open to a spectrum of processes that lead to disulfide formation.[180] At one end of the spectrum is a single electron transfer process to a reducible species.[139,181] The oxidation, which results in the formation of the thiyl

radical, is the rate-determining step.[182] Thiyl radicals then couple rapidly with each other to form the disulfide bond. At the other end of the spectrum, the nucleophilic thiolate anion may attack another disulfide bond resulting in the formation of a new disulfide and a new thiolate anion.[179] Rosenthal-Kim and Puskas *et al.* reported on a highly efficient oxidative system for the polymerization of dithiols to high molecular weight poly(disulfide) polymers via a base-catalyzed thiol oxidation mechanism (**Scheme 1.6**).[179] Once sulfhydryl groups are deprotonated,[183] the thiolate anion can undergo two separate processes that lead to disulfide formation. In one process, the nucleophilic thiolate anion may attack another disulfide bond resulting in the formation of a new disulfide and a new thiolate anion. This mechanism has been utilized in the context of cell-penetrating poly(disulfide)s, which have been shown to efficiently internalize into cells and rapidly degrade in the cytosol by GSH-assisted depolymerization with minimal cytotoxicity.[184-189] In an alternative process, a single electron transfer step leads to generation of thiyl radicals, which rapidly couple with each other to form disulfide bonds and polymers.[139,190]

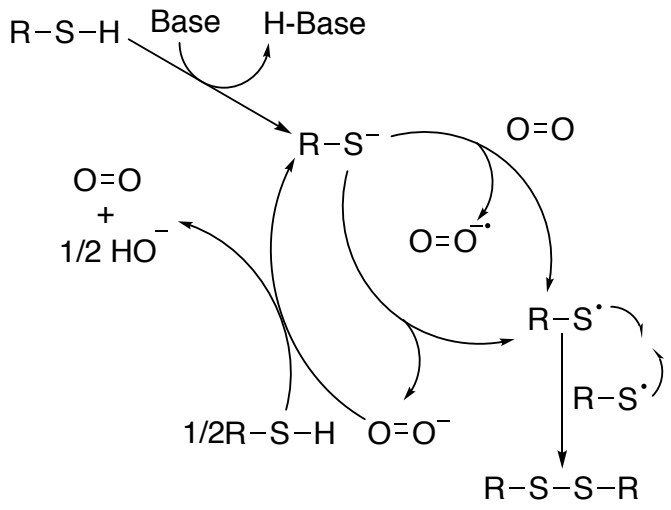

Scheme 1.6. Base-catalyzed thiol oxidation.[179]

The reverse reaction of thiol oxidation is disulfide reduction (**Scheme 1.7**). One of the most widely used disulfide-reducing agents is dithiothreitol (DTT) (**Scheme 1.7A**).[191] Upon oxidation, the dithiol compound forms an intramolecular disulfide bond that results in a stable six-membered ring. DTT has significant synthetic utility for maintaining thiol functionality by preventing oxidation.[192-194]. Another commonly used reducing agent is tris(2-carboxyethyl) phosphine (**Scheme 1.7B**).[175,195] As mentioned previously, GSH, a cysteine-containing tripeptide, is the most abundant reducing agent found in biological systems, where GSH is able to hydrogen bond in a β-sheet-like manner with the disulfide bridge above the plane of the molecule (**Scheme 1.7C**).[196] GSH is also a cofactor in many redox enzyme systems. For example, the GSH enzyme system includes the enzymes glutathione reductase (GR), selenoprotein glutathione peroxidase (GPx), glutathione disulfide (GSSG), and hydrogen peroxide.[197,198] It is particularly important in the regulation of the concentration of thiols, disulfides, and hydrogen peroxide within cells.

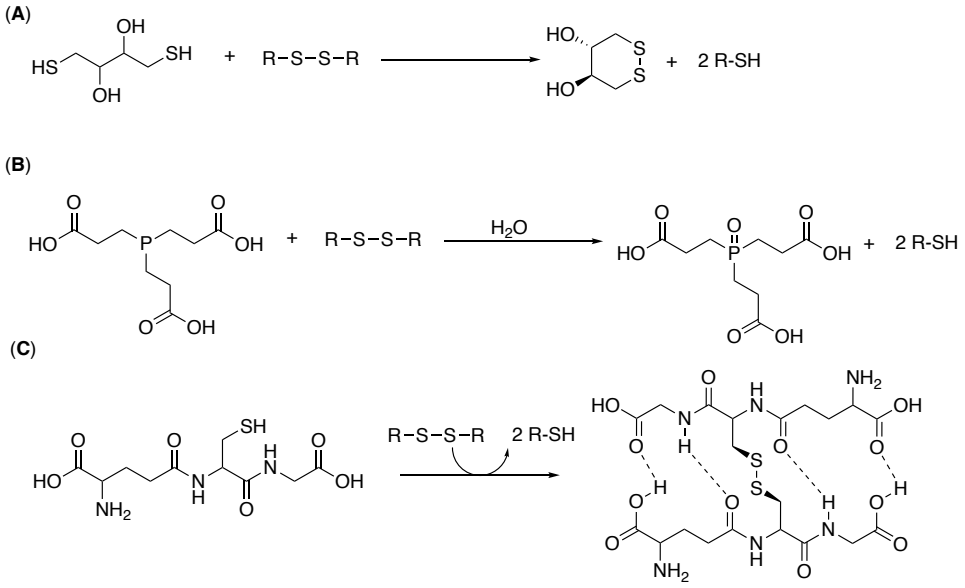

Scheme 1.7. Disulfide reduction using (**A**) dithiothreitol (DTT), (**B**) tris(2-carboxyethyl) phosphine (TCEP), and (**C**) glutathione (GSH).

1.8.3 Intracellular Internalization

Previous studies by Matile *et al.* [185] and Yao *et al.*[189] indicate that poly(disulfide) nanocarriers may utilize unconventional internalization pathways—a thiol-mediated cargo delivery mechanisms. Matile *et al.* first reported on a thiol-mediated cargo delivery mechanism with substrate-initiated, self-inactivating, cell-penetrating poly(disulfide)s (siCPDs). Namely, siCPDs bind covalently to the membrane surface by disulfide exchange with exofacial thiols, cross the membrane along transient micellar defects, and detach into the cytosol by disulfide exchange with intracellular glutathione. Matile *et al.* demonstrated this by the inhibition of thiol-mediated translocation with Ellman's reagent (i.e., 5,5′- dithiobis-2-nitrobenzoic acid, or DTNB) directly in HeLa cells. The cells were incubated with the cell-impermeable DTNB for 30 min to convert all free thiols at the surface into disulfides. According to their flow cytometry measurements, cellular uptake of siCPDs was significantly reduced in the absence of exofacial thiols. Also, the efficiency of thiol-mediated translocation is determined by the velocity of disulfide exchange, hence the faster the siCPD depolarizes the more pronounced the Ellman's reagent had on impeding thiol-mediated translocation. Similarly, Yao *et al.* carried out detailed uptake studies of their cell-penetrating poly(disulfide)s (CPDs) by HeLa cells at different temperatures and in the presence of endocytosis inhibitors, where in general, cell uptake profiles observed with these CPD-conjugated proteins were similar to what was previously reported with Matile's et al. siCPDs. Reduced temperature decreased protein delivery efficiency but did not block the process completely. The insensitivity of protein delivery to endocytosis-related inhibitors used (chlorpromazine, wortmannin, and methyl-β-cyclodextrin) ruled out the endocytosis pathway but blocking exofacial thiols on the cell surface with 5,5′-dithiobis-2- nitrobenzoic acid significantly suppressed protein uptake, further supporting unconventional thiol-mediated cargo delivery mechanisms.

1.9 CONCLUSION & OUTLOOK

In conclusion, controlled drug delivery carriers can improve the pharmacokinetic properties of a wide variety of drugs. Embedding drugs into drug delivery systems not only effectively suppresses interaction with blood components, but also enhances drug targeting specificity, lowers systemic drug toxicity, improves treatment absorption rates, and provides protection for pharmaceuticals against degradation. To meet the physiological requirements of various drug targets, numerous types of drug delivery systems were developed ranging from macro-, to micro-, and to nanoscale, but nanocarriers have become a widely investigated drug delivery system. Nanocarriers can overcome physiological barriers by tuning the nanocarrier size, shape, surface chemistry, targeting ligand conjugation and material composition. Furthermore, stimuli-responsive nanocarriers have stimuli-responsive moieties that translate physiological signals (such as, pH and redox potential) at tumor microenvironment into behaviors of the nanocarriers. There has been an increasing interest in redox-responsive nanocarriers, however, there remains a need to develop redox stimuli-responsive nanocarriers that have high stability, high loading efficiency, fast degradation kinetics, and the ability to completely degrade down to non-toxic small molecule components.

In the next chapter, a facile and convenient way to prepare redox responsive nanogel drug carriers via dithiol oxidation is described. A dithiol monomer, 2,2'-(ethylenedioxy)diethanethiol (EDDET) was polymerized along with the cross-linkers ethoxylated-trimethylolpropan tri(3-mercaptopropionate) (ETTMP), pentaerythritol tetra(3-mercaptopropionate) (PETMP), and pentaerythritol tetramercaptoacetate (PETMA) into nanogels via a base-catalyzed thiol oxidation mechanism. Mechanistic studies indicated that a single electron transfer step occurred and FT-IR confirmed disulfide formation. The generation of bulk gels was possible and nanogels were

engineered using microfluidic mixing and incorporation of a non-ionic surfactant to impart colloidal stability. Control over mesh size was achieved for nanogels. An assay using Ellman's Reagent was employed to quantify the cross-linking density and number of free –SH groups. Nanogels were characterized by dynamic light scattering (DLS) and transmission electron microscopy (TEM) and the weight percent loading and entrapment efficiency was measured. *In vitro* cell viability assays and cellular uptake studies were performed in HeLa cells. Lastly, quenching studies and degradation kinetics were completed. These nanogel drug carriers provide a versatile platform that can be customized to fit a specific application. Furthermore, the free –SH groups could potentially be used to attach targeting moieties, drugs, or stabilizing chemical functionalities. Due to the rapid and facile synthesis with a variety of thiol building blocks, tunable physical properties, high biocompatibility, and fully degradable nature, the resulting nanogels are potentially useful in a wide variety of drug delivery applications.

1.10 BIBLIOGRAPHY

1 Park, K. Facing the Truth About Nanotechnology in Drug Delivery. *ACS Nano* **7**, 7442-7447, (2013).

2 Peppas, N. A. Historical perspective on advanced drug delivery: How engineering design and mathematical modeling helped the field mature. *Adv. Drug Delivery Rev.* **65**, 5-9, (2013).

3 Moroz, E., Matoori, S. & Leroux, J.-C. Oral delivery of macromolecular drugs: Where we are after almost 100years of attempts. *Adv. Drug Delivery Rev.* **101**, 108-121, (2016).

4 Rodriguez-Gascon, A., del Pozo-Rodriguez, A., Isla, A. & Solinís, M. A. Vaginal gene therapy. *Adv. Drug Delivery Rev.* **92**, 71-83, (2015).

5 Park, K. Controlled drug delivery systems: past forward and future back. *J. Control. Release* **190**, 3-8, (2014).

6 Peppas, N. A., Hilt, J. Z., Khademhosseini, A. & Langer, R. Hydrogels in biology and medicine: from molecular principles to bionanotechnology. *Adv. Mater.* **18**, 1345-1360, (2006).

7 Farokhzad, O. C. & Langer, R. Impact of nanotechnology on drug delivery. *ACS Nano* **3**, 16-20, (2009).

8 Coombes, R. C. Drug testing in the patient: toward personalized cancer treatment. *Sci. Transl. Med.* **7**, 284-294, (2015).

9 Langer, R. & Weissleder, R. Scientific discovery and the future of medicine. *Nanotechnology. JAMA* **313**, 135-136, (2015).

10 Traverso, G. & Langer, R. Engineering Precision. *Sci. Transl. Med.* **7**, 1, (2015).

11 Lu, Y., Sun, W. & Gu, Z. Stimuli-responsive nanomaterials for therapeutic protein delivery. *J. Control. Release* **194**, 1-19, (2014).

12 Sun, W., Ji, W., Hu, Q. & Gu, Z. Leveraging physiology for precision drug delivery. *Physiol. Rev.* **97**, 189-225, (2017).

13 Anselmo, A. C. & Mitragotri, S. An Overview of Clinical and Commercial Impact of Drug Delivery Systems. *J. Control. Release* **190**, 15-28, (2014).

14 Davis, M. E., Chen, Z. G. & Shin, D. M. Nanoparticle therapeutics: an emerging treatment modality for cancer. *Nat. Rev. Drug Discov.* **7**, 771-782, (2008).

15 Jain, R. K. & Stylianopoulos, T. Delivering nanomedicine to solid tumors. *Nat. Rev. Clin. Oncol.* **7**, 653-664, (2010).

16 Peer, D., Karp, J. M., Hong, S., Farokhzad, O. C., Margalit, R. & Langer, R. Nanocarriers as an emerging platform for cancer therapy. *Nat. Nanotechnol.* **2**, 751-760, (2007).

17 Cheng, W., Gu, L., Ren, W. & Liu, Y. Stimuli-responsive polymers for anti-cancer drug delivery. *Mater. Sci. Eng. C* **45**, 600-608, (2014).

18 Kanasty, R., Dorkin, J. R., Vegas, A. & Anderson, D. Delivery materials for siRNA therapeutics. *Nat. Mater.* **12**, 967-977, (2013).

19 Kearney, C. J. & Mooney, D. J. Macroscale delivery systems for molecular and cellular payloads. *Nat. Mater.* **12**, 1004, (2013).

20 Porter, C. J., Trevaskis, N. L. & Charman, W. N. Lipids and lipid-based formulations: optimizing the oral delivery of lipophilic drugs. *Nat. Rev. Drug Discov.* **6**, 231, (2007).

21 Ayoob, A. M. & Borenstein, J. T. The role of intracochlear drug delivery devices in the management of inner ear disease. *Expert Opin. Drug Deliv.* **12**, 465-479, (2015).

22 Kovatchev, B. P., Renard, E., Cobelli, C., Zisser, H. C., Keith-Hynes, P., Anderson, S. M., Brown, S. A., Chernavvsky, D. R., Breton, M. D. & Mize, L. B. Safety of outpatient closed-loop control: first randomized crossover trials of a wearable artificial pancreas. *Diabetes Care* **37**, 1789-1796, (2014).

23 Ugwoke, M. I., Agu, R. U., Verbeke, N. & Kinget, R. Nasal mucoadhesive drug delivery: background, applications, trends and future perspectives. *Adv. Drug Delivery Rev.* **57**, 1640-1665, (2005).

24 Trajkovski, B., Petersen, A., Strube, P., Mehta, M. & Duda, G. N. Intra-operatively customized implant coating strategies for local and controlled drug delivery to bone. *Adv. Drug Delivery Rev.* **64**, 1142-1151, (2012).

25 Kleiner, L. W., Wright, J. C. & Wang, Y. Evolution of implantable and insertable drug delivery systems. *J. Control. Release* **181**, 1-10, (2014).

26 Delplace, V. & Nicolas, J. Degradable vinyl polymers for biomedical applications. *Nat. Chem.* **7**, 771, (2015).

27 Folkman, J. & Long, D. M. The use of silicone rubber as a carrier for prolonged drug therapy. *J. Surgical Res.* **4**, 139-142, (1964).

28 Langer, R. & Folkman, J. Polymers for the sustained release of proteins and other macromolecules. *Nature* **263**, 797, (1976).

29 Webber, M. J., Appel, E. A., Meijer, E. & Langer, R. Supramolecular biomaterials. *Nat. Mater.* **15**, 13, (2016).

30 Mo, R., Jiang, T., Di, J., Tai, W. & Gu, Z. Emerging micro-and nanotechnology based synthetic approaches for insulin delivery. *Chem. Soc. Rev.* **43**, 3595-3629, (2014).

31 Stevenson, C. L., Santini Jr, J. T. & Langer, R. Reservoir-based drug delivery systems utilizing microtechnology. *Adv. Drug Delivery Rev.* **64**, 1590-1602, (2012).

32 Liechty, W. B., Kryscio, D. R., Slaughter, B. V. & Peppas, N. A. Polymers for drug delivery systems. *Annu. Rev. Chem. Biomol. Eng.* **1**, 149-173, (2010).

33 Qiu, Y. & Park, K. Environment-sensitive hydrogels for drug delivery. *Adv. Drug Delivery Rev.* **53**, 321-339, (2001).

34 Moon, J. J., Huang, B. & Irvine, D. J. Engineering nano-and microparticles to tune immunity. *Adv. Mater.* **24**, 3724-3746, (2012).

35 Gu, Z., Dang, T. T., Ma, M., Tang, B. C., Cheng, H., Jiang, S., Dong, Y., Zhang, Y. & Anderson, D. G. Glucose-responsive microgels integrated with enzyme nanocapsules for closed-loop insulin delivery. *ACS Nano* **7**, 6758-6766, (2013).

36 Maeda, H. Toward a full understanding of the EPR effect in primary and metastatic tumors as well as issues related to its heterogeneity. *Adv. Drug Delivery Rev.* **91**, 3-6, (2015).

37 Marguet, M., Bonduelle, C. & Lecommandoux, S. Multicompartmentalized polymeric systems: towards biomimetic cellular structure and function. *Chem. Soc. Rev.* **42**, 512-529, (2013).

38 Prabhakar, U., Maeda, H., Jain, R. K., Sevick-Muraca, E. M., Zamboni, W., Farokhzad, O. C., Barry, S. T., Gabizon, A., Grodzinski, P. & Blakey, D. C. (AACR, 2013).

39 Chow, E. K.-H. & Ho, D. Cancer Nanomedicine: From Drug Delivery to Imaging. *Sci. Transl. Med.* **5**, 216, (2013).

40 Wan, S., Kelly, P. M., Mahon, E., Stöckmann, H., Rudd, P. M., Caruso, F., Dawson, K. A., Yan, Y. & Monopoli, M. P. The “sweet” side of the protein corona: effects of glycosylation on nanoparticle–cell interactions. *ACS Nano* **9**, 2157-2166, (2015).

41 Tenzer, S., Docter, D., Kuharev, J., Musyanovych, A., Fetz, V., Hecht, R., Schlenk, F., Fischer, D., Kiouptsi, K. & Reinhardt, C. Rapid formation of plasma protein corona critically affects nanoparticle pathophysiology. *Nat. Nanotechnol.* **8**, 772, (2013).

42 Moghimi, S. M. Chemical camouflage of nanospheres with a poorly reactive surface: towards development of stealth and target-specific nanocarriers. *Biochim. Biophys. Acta* **1590**, 131-139, (2002).

43 Salvati, A., Pitek, A. S., Monopoli, M. P., Prapainop, K., Bombelli, F. B., Hristov, D. R., Kelly, P. M., Åberg, C., Mahon, E. & Dawson, K. A. Transferrin-functionalized nanoparticles lose their targeting capabilities when a biomolecule corona adsorbs on the surface. *Nat. Nanotechnol.* **8**, 137, (2013).

44 Mitchell, M. J., Wayne, E., Rana, K., Schaffer, C. B. & King, M. R. TRAIL-coated leukocytes that kill cancer cells in the circulation. *Proc. Natl. Acad. Sci. USA* **111**, 930-935, (2014).

45 D'apolito, R., Tomaiuolo, G., Taraballi, F., Minardi, S., Kirui, D., Liu, X., Cevenini, A., Palomba, R., Ferrari, M. & Salvatore, F. Red blood cells affect the margination of microparticles in synthetic microcapillaries and intravital microcirculation as a function of their size and shape. *J. Control. Release* **217**, 263-272, (2015).

46 Dahlman, J. E., Barnes, C., Khan, O. F., Thiriot, A., Jhunjunwala, S., Shaw, T. E., Xing, Y., Sager, H. B., Sahay, G. & Speciner, L. In vivo endothelial siRNA delivery using polymeric nanoparticles with low molecular weight. *Nat. Nanotechnol.* **9**, 648, (2014).

47 Lu, P., Weaver, V. M. & Werb, Z. The extracellular matrix: a dynamic niche in cancer progression. *J. Cell. Biol.* **196**, 395-406, (2012).

48 Veber, D. F., Johnson, S. R., Cheng, H.-Y., Smith, B. R., Ward, K. W. & Kopple, K. D. Molecular properties that influence the oral bioavailability of drug candidates. *J. Med. Chem.* **45**, 2615-2623, (2002).

49 Gu, Z., Biswas, A., Zhao, M. & Tang, Y. Tailoring nanocarriers for intracellular protein delivery. *Chem. Soc. Rev.* **40**, 3638-3655, (2011).

50 Panyam, J. & Labhasetwar, V. Biodegradable nanoparticles for drug and gene delivery to cells and tissue. *Adv. Drug Delivery Rev.* **55**, 329-347, (2003).

51 Zhang, S., Gao, H. & Bao, G. Physical principles of nanoparticle cellular endocytosis. *ACS Nano* **9**, 8655-8671, (2015).

52 Sigismund, S., Confalonieri, S., Ciliberto, A., Polo, S., Scita, G. & Di Fiore, P. P. Endocytosis and signaling: cell logistics shape the eukaryotic cell plan. *Physiol. Rev.* **92**, 273-366, (2012).

53 Ruiz de Almodovar, C., Lambrechts, D., Mazzone, M. & Carmeliet, P. Role and therapeutic potential of VEGF in the nervous system. *Physiol. Rev.* **89**, 607-648, (2009).

54 Van Dam, G. M., Themelis, G., Crane, L. M., Harlaar, N. J., Pleijhuis, R. G., Kelder, W., Sarantopoulos, A., De Jong, J. S., Arts, H. J. & Van Der Zee, A. G. Intraoperative tumor-specific fluorescence imaging in ovarian cancer by folate receptor-α targeting: first in-human results. *Nat. Med.* **17**, 1315, (2011).

55 Yu, Y. J., Atwal, J. K., Zhang, Y., Tong, R. K., Wildsmith, K. R., Tan, C., Bien-Ly, N., Hersom, M., Maloney, J. A. & Meilandt, W. J. Therapeutic bispecific antibodies cross the blood-brain barrier in nonhuman primates. *Sci. Transl. Med.* **6**, 261ra154-261ra154, (2014).

56 Pinho, S. S. & Reis, C. A. Glycosylation in cancer: mechanisms and clinical implications. *Nat. Rev. Cancer* **15**, 540, (2015).

57 Lin, C.-Y. & Gustafsson, J.-Å. Targeting liver X receptors in cancer therapeutics. *Nat. Rev. Cancer* **15**, 216, (2015).

58 Yang, Z., Lee, J. H., Jeon, H. M., Han, J. H., Park, N., He, Y., Lee, H., Hong, K. S., Kang, C. & Kim, J. S. Folate-based near-infrared fluorescent theranostic gemcitabine delivery. *J. Am. Chem. Soc.* **135**, 11657-11662, (2013).

59 Pridgen, E. M., Alexis, F., Kuo, T. T., Levy-Nissenbaum, E., Karnik, R., Blumberg, R. S., Langer, R. & Farokhzad, O. C. Transepithelial transport of Fc-targeted nanoparticles by the neonatal fc receptor for oral delivery. *Sci. Transl. Med.* **5**, 213ra167-213ra167, (2013).

60 Sugahara, K. N., Teesalu, T., Karmali, P. P., Kotamraju, V. R., Agemy, L., Greenwald, D. R. & Ruoslahti, E. Coadministration of a tumor-penetrating peptide enhances the efficacy of cancer drugs. *Science* **328**, 1031-1035, (2010).

61 Xing, H., Wong, N. Y., Xiang, Y. & Lu, Y. DNA aptamer functionalized nanomaterials for intracellular analysis, cancer cell imaging and drug delivery. *Curr. Opin. Chem. Biol.* **16**, 429, (2012).

62 Bertrand, N., Wu, J., Xu, X., Kamaly, N. & Farokhzad, O. C. Cancer nanotechnology: the impact of passive and active targeting in the era of modern cancer biology. *Adv. Drug Delivery Rev.* **66**, 2-25, (2014).

63 Srinivasarao, M., Galliford, C. V. & Low, P. S. Principles in the design of ligand-targeted cancer therapeutics and imaging agents. *Nat. Rev. Drug Discov.* **14**, 203, (2015).

64 Gilleron, J., Querbes, W., Zeigerer, A., Borodovsky, A., Marsico, G., Schubert, U., Manygoats, K., Seifert, S., Andree, C. & Stöter, M. Image-based analysis of lipid

nanoparticle–mediated siRNA delivery, intracellular trafficking and endosomal escape. *Nat. Biotechnol.* **31**, 638, (2013).

65 Sahay, G., Querbes, W., Alabi, C., Eltoukhy, A., Sarkar, S., Zurenko, C., Karagiannis, E., Love, K., Chen, D. & Zoncu, R. Efficiency of siRNA delivery by lipid nanoparticles is limited by endocytic recycling. *Nat. Biotechnol.* **31**, 653, (2013).

66 Wittrup, A., Ai, A., Liu, X., Hamar, P., Trifonova, R., Charisse, K., Manoharan, M., Kirchhausen, T. & Lieberman, J. Visualizing lipid-formulated siRNA release from endosomes and target gene knockdown. *Nat. Biotechnol.* **33**, 870-976, (2015).

67 Settembre, C. & Ballabio, A. Lysosome: regulator of lipid degradation pathways. *Trends Cell. Biol.* **24**, 743-750, (2014).

68 Benjaminsen, R. V., Mattebjerg, M. A., Henriksen, J. R., Moghimi, S. M. & Andresen, T. L. The possible "proton sponge" effect of polyethylenimine (PEI) does not include change in lysosomal pH. *Mol. Therapy* **21**, 149-157, (2013).

69 Ohya, T., Miaczynska, M., Coskun, Ü., Lommer, B., Runge, A., Drechsel, D., Kalaidzidis, Y. & Zerial, M. Reconstitution of Rab-and SNARE-dependent membrane fusion by synthetic endosomes. *Nature* **459**, 1091, (2009).

70 Xu, W., Nathwani, B., Lin, C., Wang, J., Karatekin, E., Pincet, F., Shih, W. & Rothman, J. E. A programmable DNA origami platform to organize SNAREs for membrane fusion. *J. Am. Chem. Soc.* **138**, 4439-4447, (2016).

71 Kim, H., Lee, D., Kim, J., Kim, T.-i. & Kim, W. J. Photothermally triggered cytosolic drug delivery via endosome disruption using a functionalized reduced graphene oxide. *ACS Nano* **7**, 6735-6746, (2013).

72 Chaudhary, P. M. & Roninson, I. B. Induction of multidrug resistance in human cells by transient exposure to different chemotherapeutic drugs. *J. Natl. Cancer Inst.* **85**, 632-639, (1993).

73 Bredesen, D. E., Mehlen, P. & Rabizadeh, S. Apoptosis and dependence receptors: a molecular basis for cellular addiction. *Physiol. Rev.* **84**, 411-430, (2004).

74 Deeley, R. G., Westlake, C. & Cole, S. P. Transmembrane transport of endo-and xenobiotics by mammalian ATP-binding cassette multidrug resistance proteins. *Physiol. Rev.* **86**, 849-899, (2006).

75 Sarkadi, B., Homolya, L., Szakács, G. & Váradi, A. Human multidrug resistance ABCB and ABCG transporters: participation in a chemoimmunity defense system. *Physiol. Rev.* **86**, 1179-1236, (2006).

76 Stein, W. D. Kinetics of the multidrug transporter (P-glycoprotein) and its reversal. *Physiol. Rev.* **77**, 545-590, (1997).

77 Tenzer, S., Docter, D., Rosfa, S., Wlodarski, A., Kuharev, J. r., Rekik, A., Knauer, S. K., Bantz, C., Nawroth, T. & Bier, C. Nanoparticle size is a critical physicochemical determinant of the human blood plasma corona: a comprehensive quantitative proteomic analysis. *ACS Nano* **5**, 7155-7167, (2011).

78 Peppiatt, C. M., Howarth, C., Mobbs, P. & Attwell, D. Bidirectional control of CNS capillary diameter by pericytes. *Nature* **443**, 700, (2006).

79 Yuan, F., Dellian, M., Fukumura, D., Leunig, M., Berk, D. A., Torchilin, V. P. & Jain, R. K. Vascular permeability in a human tumor xenograft: molecular size dependence and cutoff size. *Cancer Res.* **55**, 3752-3756, (1995).

80 Hobbs, S. K., Monsky, W. L., Yuan, F., Roberts, W. G., Griffith, L., Torchilin, V. P. & Jain, R. K. Regulation of transport pathways in tumor vessels: role of tumor type and microenvironment. *Proc. Natl. Acad. Sci. USA* **95**, 4607-4612, (1998).

81 Chauhan, V. P. & Jain, R. K. Strategies for advancing cancer nanomedicine. *Nat. Mater.* **12**, 958, (2013).

82 Hu, X., Hu, J., Tian, J., Ge, Z., Zhang, G., Luo, K. & Liu, S. Polyprodrug amphiphiles: hierarchical assemblies for shape-regulated cellular internalization, trafficking, and drug delivery. *J. Am. Chem. Soc.* **135**, 17617-17629, (2013).

83 Tao, L., Hu, W., Liu, Y., Huang, G., Sumer, B. D. & Gao, J. Shape-specific polymeric nanomedicine: emerging opportunities and challenges. *Exp. Biol. Med.* **236**, 20-29, (2011).

84 Truong, N. P., Whittaker, M. R., Mak, C. W. & Davis, T. P. The importance of nanoparticle shape in cancer drug delivery. *Expert Opin. Drug Deliv.* **12**, 129-142, (2015).

85 Geng, Y., Dalhaimer, P., Cai, S., Tsai, R., Tewari, M., Minko, T. & Discher, D. E. Shape effects of filaments versus spherical particles in flow and drug delivery. *Nat. Nanotechnol.* **2**, 249, (2007).

86 Muro, S., Garnacho, C., Champion, J. A., Leferovich, J., Gajewski, C., Schuchman, E. H., Mitragotri, S. & Muzykantov, V. R. Control of endothelial targeting and intracellular delivery of therapeutic enzymes by modulating the size and shape of ICAM-1-targeted carriers. *Mol. Therapy* **16**, 1450-1458, (2008).

87 Champion, J. A. & Mitragotri, S. Role of target geometry in phagocytosis. *Proc. Natl. Acad. Sci. USA* **103**, 4930-4934, (2006).

88 Yeung, T., Gilbert, G. E., Shi, J., Silvius, J., Kapus, A. & Grinstein, S. Membrane phosphatidylserine regulates surface charge and protein localization. *Science* **319**, 210-213, (2008).

89 He, C., Hu, Y., Yin, L., Tang, C. & Yin, C. Effects of particle size and surface charge on cellular uptake and biodistribution of polymeric nanoparticles. *Biomaterials* **31**, 3657-3666, (2010).

90 Kim, B., Han, G., Toley, B. J., Kim, C.-k., Rotello, V. M. & Forbes, N. S. Tuning payload delivery in tumour cylindroids using gold nanoparticles. *Nat. Nanotechnol.* **5**, 465, (2010).

91 Harush-Frenkel, O., Rozentur, E., Benita, S. & Altschuler, Y. Surface charge of nanoparticles determines their endocytic and transcytotic pathway in polarized MDCK cells. *Biomacromolecules* **9**, 435-443, (2008).

92 Sahay, G., Alakhova, D. Y. & Kabanov, A. V. Endocytosis of nanomedicines. *J. Control. Release* **145**, 182-195, (2010).

93 Arvizo, R. R., Miranda, O. R., Thompson, M. A., Pabelick, C. M., Bhattacharya, R., Robertson, J. D., Rotello, V. M., Prakash, Y. & Mukherjee, P. Effect of nanoparticle surface charge at the plasma membrane and beyond. *Nano Lett.* **10**, 2543-2548, (2010).

94 Yu, T., Malugin, A. & Ghandehari, H. Impact of silica nanoparticle design on cellular toxicity and hemolytic activity. *ACS Nano* **5**, 5717-5728, (2011).

95 Han, S. S., Li, Z. Y., Zhu, J. Y., Han, K., Zeng, Z. Y., Hong, W., Li, W. X., Jia, H. Z., Liu, Y. & Zhuo, R. X. Dual-pH Sensitive Charge-Reversal Polypeptide Micelles for Tumor-Triggered Targeting Uptake and Nuclear Drug Delivery. *Small* **11**, 2543-2554, (2015).

96 Huang, Y., Tang, Z., Zhang, X., Yu, H., Sun, H., Pang, X. & Chen, X. pH-triggered charge-reversal polypeptide nanoparticles for cisplatin delivery: preparation and in vitro evaluation. *Biomacromolecules* **14**, 2023-2032, (2013).

97 Nel, A. E., Mädler, L., Velegol, D., Xia, T., Hoek, E. M., Somasundaran, P., Klaessig, F., Castranova, V. & Thompson, M. Understanding biophysicochemical interactions at the nano–bio interface. *Nat. Mater.* **8**, 543, (2009).

98 Takahashi, Y., Kitadai, Y., Bucana, C. D., Cleary, K. R. & Ellis, L. M. Expression of vascular endothelial growth factor and its receptor, KDR, correlates with vascularity, metastasis, and proliferation of human colon cancer. *Cancer Res.* **55**, 3964-3968, (1995).

99 Demoulin, J.-B. & Essaghir, A. PDGF receptor signaling networks in normal and cancer cells. *Cytokine & Growth Factor Rev.* **25**, 273-283, (2014).

100 Lu, Y. & Low, P. S. Folate-mediated delivery of macromolecular anticancer therapeutic agents. *Adv. Drug Delivery Rev.* **64**, 342-352, (2012).

101 Godwin, H., Nameth, C., Avery, D., Bergeson, L. L., Bernard, D., Beryt, E., Boyes, W., Brown, S., Clippinger, A. J. & Cohen, Y. (ACS Publications, 2015).

102 Appel, E. A., del Barrio, J., Loh, X. J. & Scherman, O. A. Supramolecular polymeric hydrogels. *Chem. Soc. Rev.* **41**, 6195-6214, (2012).

103 Chacko, R. T., Ventura, J., Zhuang, J. & Thayumanavan, S. Polymer nanogels: a versatile nanoscopic drug delivery platform. *Adv. Drug Delivery Rev.* **64**, 836-851, (2012).

104 Pattni, B. S., Chupin, V. V. & Torchilin, V. P. New developments in liposomal drug delivery. *Chem. Rev.* **115**, 10938-10966, (2015).

105 Akinc, A., Zumbuehl, A., Goldberg, M., Leshchiner, E. S., Busini, V., Hossain, N., Bacallado, S. A., Nguyen, D. N., Fuller, J. & Alvarez, R. A combinatorial library of lipid-like materials for delivery of RNAi therapeutics. *Nat. Biotechnol.* **26**, 561, (2008).

106 Jans, H. & Huo, Q. Gold nanoparticle-enabled biological and chemical detection and analysis. *Chem. Soc. Rev.* **41**, 2849-2866, (2012).

107 Langille, M. R., Personick, M. L., Zhang, J. & Mirkin, C. A. Defining rules for the shape evolution of gold nanoparticles. *J. Am. Chem. Soc.* **134**, 14542-14554, (2012).

108 Mao, H. Y., Laurent, S., Chen, W., Akhavan, O., Imani, M., Ashkarran, A. A. & Mahmoudi, M. Graphene: promises, facts, opportunities, and challenges in nanomedicine. *Chem. Rev.* **113**, 3407-3424, (2013).

109 Mochalin, V. N., Shenderova, O., Ho, D. & Gogotsi, Y. The properties and applications of nanodiamonds. *Nat. Nanotechnol.* **7**, 11, (2012).

110 Gao, J., Gu, H. & Xu, B. Multifunctional magnetic nanoparticles: design, synthesis, and biomedical applications. *Accounts Chem. Res.* **42**, 1097-1107, (2009).

111 Lu, Y., Hu, Q., Lin, Y., Pacardo, D. B., Wang, C., Sun, W., Ligler, F. S., Dickey, M. D. & Gu, Z. Transformable liquid-metal nanomedicine. *Nat. Commun.* **6**, 10066, (2015).

112 Chen, Y.-J., Groves, B., Muscat, R. A. & Seelig, G. DNA nanotechnology from the test tube to the cell. *Nat. Nanotechnol.* **10**, 748, (2015).

113 Ohta, S., Glancy, D. & Chan, W. C. DNA-controlled dynamic colloidal nanoparticle systems for mediating cellular interaction. *Science* **351**, 841-845, (2016).

114 Tjong, V., Tang, L., Zauscher, S. & Chilkoti, A. “Smart” DNA interfaces. *Chem. Soc. Rev.* **43**, 1612-1626, (2014).

115 Jones, L. H. Recent advances in the molecular design of synthetic vaccines. *Nat. Chem.* **7**, 952, (2015).

116 Estrella, V., Chen, T., Lloyd, M., Wojtkowiak, J., Cornnell, H. H., Ibrahim-Hashim, A., Bailey, K., Balagurunathan, Y., Rothberg, J. M. & Sloane, B. F. Acidity generated by the tumor microenvironment drives local invasion. *Cancer Res.* **73**, 1524-1535, (2013).

117 Fleige, E., Quadir, M. A. & Haag, R. Stimuli-responsive polymeric nanocarriers for the controlled transport of active compounds: concepts and applications. *Adv. Drug Delivery Rev.* **64**, 866-884, (2012).

118 Albertsson, A. C. & Varma, I. K. Aliphatic polyesters: Synthesis, properties and applications. *Adv. Polym. Sci.* **157**, 1-40, (2002).

119 Tian, H., Tang, Z., Zhuang, X., Chen, X. & Jing, X. Biodegradable synthetic polymers: Preparation, functionalization and biomedical application. *Prog. Polym. Sci.* **37**, 237-280, (2012).

120 Lei, X. G., Zhu, J.-H., Cheng, W.-H., Bao, Y., Ho, Y.-S., Reddi, A. R., Holmgren, A. & Arnér, E. S. Paradoxical roles of antioxidant enzymes: basic mechanisms and health implications. *Physiol. Rev.* **96**, 307-364, (2015).

121 Estrela, J. M., Ortega, A. & Obrador, E. Glutathione in cancer biology and therapy. *Crit. Rev. Clin. Lab Sci.* **43**, 143-181, (2006).

122 Kuppusamy, P., Li, H., Ilangovan, G., Cardounel, A. J., Zweier, J. L., Yamada, K., Krishna, M. C. & Mitchell, J. B. Noninvasive imaging of tumor redox status and its modification by tissue glutathione levels. *Cancer Res.* **62**, 307-312, (2002).

123 Djuric, Z., Malviya, V. K., Deppe, G., Malone, J. M., McGunagle, D. L., Heilbrun, L. K., Reading, B. A. & Lawrence, W. D. Detoxifying enzymes in human ovarian tissues:

comparison of normal and tumor tissues and effects of chemotherapy. *J. Cancer Res. Clin. Oncol.* **116**, 379-383, (1990).

124 Balendiran, G. K., Dabur, R. & Fraser, D. The role of glutathione in cancer. *Cell Biochem. Funct.* **22**, 343-352, (2004).

125 Franco, R., Schoneveld, O. J., Pappa, A. & Panayiotidis, M. I. The central role of glutathione in the pathophysiology of human diseases. *Arch. Physiol. Biochem.* **113**, 234-258, (2007).

126 Valko, M., Leibfritz, D., Moncol, J., Cronin, M. T., Mazur, M. & Telser, J. Free radicals and antioxidants in normal physiological functions and human disease. *Int. J. Biochem. Cell Biol.* **39**, 44-84, (2007).

127 Stavrovskaya, A. A. Cellular mechanisms of multidrug resistance of tumor cells. *Biochemistry. Biokhimiia.* **65**, 95-106, (2000).

128 Lehn, J.-M. Dynamers: dynamic molecular and supramolecular polymers. *Prog. Polym. Sci.* **30**, 814-831, (2005).

129 Kishore, K. & Ganesh, K. (Springer: Berlin Heidelberg, 1995).

130 Li, J., Nowak, P. & Otto, S. Dynamic combinatorial libraries: from exploring molecular recognition to systems chemistry. *J. Am. Chem. Soc.* **135**, 9222-9239, (2013).

131 Cougnon, F. B. & Sanders, J. K. Evolution of dynamic combinatorial chemistry. *Accounts Chem. Res.* **45**, 2211-2221, (2011).

132 Lehn, J.-M. in *Constitutional Dynamic Chemistry* 1-32 (Springer, 2011).

133 Denisov, E., Chatgilialoglu, C., Shestakov, A. & Denisova, T. Rate constants and transition-state geometry of reactions of alkyl, alkoxyl, and peroxyl radicals with thiols. *Int. J. Chem. Kinet.* **41**, 284-293, (2009).

134 Ito, O. & Alfassi, Z. S-Centered Radicals. *by Alfassi ZB, Wiley, Chichester*, 193-224, (1999).

135 Luo, Y.-R. *Handbook of bond dissociation energies in organic compounds*. (CRC press, 2002).

136 Bordwell, F., Zhang, X.-M., Satish, A. & Cheng, J.-P. Assessment of the importance of changes in ground-state energies on the bond dissociation enthalpies of the OH bonds in phenols and the SH bonds in thiophenols. *J. Am. Chem. Soc.* **116**, 6605-6610, (1994).

137 Nau, W. M. Computational assessment of polar ground-state effects on the bond dissociation energies of benzylic and related bonds. *The Journal of organic chemistry* **61**, 8312-8314, (1996).

138 Voronkov, M. G. & Deryagina, E. N. Thermal reactions of thiyl radicals. *Russ. Chem. Rev.* **59**, 778, (1990).

139 Holmgren, A. & Bjornstedt, M. Thioredoxin and thioredoxin reductase. *Methods Enzymol.* **252**, 199-208, (1995).

140 Nguyen, V.-H., Nishino, H., Kajikawa, S. & Kurosawa, K. Mn (III)-based reactions of alkenes and alkynes with thiols. An approach toward substituted 2, 3-dihydro-1, 4-oxathiins and simple route to (E)-vinyl sulfides. *Tetrahedron* **54**, 11445-11460, (1998).

141 Misra, H. P. Generation of superoxide free radical during the autoxidation of thiols. *J. Biol. Chem.* **249**, 2151-2155, (1974).

142 Dénès, F., Pichowicz, M., Povie, G. & Renaud, P. Thiyl radicals in organic synthesis. *Chem. Rev.* **114**, 2587-2693, (2014).

143 Pryor, W. A. & Stanley, J. P. Reactions of the hydrogen atom in solution. IV. Photolysis of deuterated thiols. *J. Am. Chem. Soc.* **93**, 1412-1418, (1971).

144 Zepp, R. G. & Wagner, P. J. Slow quenching of triplet ketones by alkyl thiols. *J. Chem. Soc., Chem. Commun.*, 167b-168, (1972).

145 Ito, O. Flash photolysis study on reversible addition reactions of thiyl radicals. *Res. Chem. Intermed.* **21**, 69-93, (1995).

146 Hoffman, M. Z. & Hayon, E. Pulse radiolysis study of sulfhydryl compounds in aqueous solution. *J. Phys. Chem.* **77**, 990-996, (1973).

147 Madej, E., Folkes, L. K., Wardman, P., Czapski, G. & Goldstein, S. Thiyl radicals react with nitric oxide to form S-nitrosothiols with rate constants near the diffusion-controlled limit. *Free Radic. Biol. Med.* **44**, 2013-2018, (2008).

148 Ito, O. & Matsuda, M. Evaluation of addition rates of the thiyl radicals to vinyl monomers by flash photolysis. 2. Substituent effect on addition of substituted benzenethiyl radicals to methyl methacrylate or styrene. *J. Am. Chem. Soc.* **101**, 5732-5735, (1979).

149 Wang, Y.-C., Li, Y., Sun, T.-M., Xiong, M.-H., Wu, J., Yang, Y.-Y. & Wang, J. Core–Shell–Corona Micelle Stabilized by Reversible Cross-Linkage for Intracellular Drug Delivery. *Macromol. Rapid Commun.* **31**, 1201-1206, (2010).

150 Lv, L.-P., Xu, J.-P., Liu, X.-S., Liu, G.-Y., Yang, X. & Ji, J. Disulfide-Crosslinked Biomimetic Micelles: Formation, Thiol Reactivity and Cytotoxicity Behavior. *Macromol. Chem. Phys.* **211**, 2292-2300, (2010).

151 Koo, A. N., Lee, H. J., Kim, S. E., Chang, J. H., Park, C., Kim, C., Park, J. H. & Lee, S. C. Disulfide-cross-linked PEG-poly(amino acid)s copolymer micelles for glutathione-mediated intracellular drug delivery. *Chem. Commun. (Camb)*, 6570-6572, (2008).

152 Zhang, A., Zhang, Z., Shi, F., Ding, J., Xiao, C., Zhuang, X., He, C., Chen, L. & Chen, X. Disulfide crosslinked PEGylated starch micelles as efficient intracellular drug delivery platforms. *Soft. Matter.* **9**, 2224-2233, (2013).

153 Oh, J. K., Siegwart, D. J., Lee, H. I., Sherwood, G., Peteanu, L., Hollinger, J. O., Kataoka, K. & Matyjaszewski, K. Biodegradable nanogels prepared by atom transfer radical polymerization as potential drug delivery carriers: Synthesis, biodegradation, in vitro release, and bioconjugation. *J. Am. Chem. Soc.* **129**, 5939-5945, (2007).

154 Oh, J. K., Siegwart, D. J. & Matyjaszewski, K. Synthesis and biodegradation of nanogels as delivery carriers for carbohydrate drugs. *Biomacromolecules* **8**, 3326-3331, (2007).

155 Oh, J., Drumright, R., Siegwart, D. & Matyjaszewski, K. The development of microgels/nanogels for drug delivery applications. *Prog. Polym. Sci.* **33**, 448-477, (2008).

156 Siegwart, D. J., Srinivasan, A., Bencherif, S., Karunanidhi, A., Oh, J., Vaidya, S., Jin, R., Hollinger, J. & Matyjaszewki, K. Cellular uptake of functional nanogels prepared by inverse miniemulsion ATRP with encapsulated proteins, carbohydrates, and gold nanoparticles. *Biomacromolecules* **10**, 2300-2309, (2009).

157 Siegwart, D. J., Oh, J. K. & Matyjaszewski, K. ATRP in the design of functional materials for biomedical applications. *Prog. Polym. Sci.* **37**, 18-37, (2012).

158 Hu, X., Zhang, Y., Xie, Z., Jing, X., Bellotti, A. & Gu, Z. Stimuli-Responsive Polymersomes for Biomedical Applications. *Biomacromolecules* **18**, 649-673, (2017).

159 Kataoka, K., Harada, A. & Nagasaki, Y. Block copolymer micelles for drug delivery: design, characterization and biological significance. *Adv. Drug. Deliv. Rev.* **47**, 113-131, (2001).

160 Cheng, W., Kumar, J. N., Zhang, Y. & Liu, Y. pH- and redox-responsive poly(ethylene glycol) and cholesterol-conjugated poly(amido amine)s based micelles for controlled drug delivery. *Macromol. Biosci.* **14**, 347-358, (2014).

161 Sun, Y., Yan, X., Yuan, T., Liang, J., Fan, Y., Gu, Z. & Zhang, X. Disassemblable micelles based on reduction-degradable amphiphilic graft copolymers for intracellular delivery of doxorubicin. *Biomaterials* **31**, 7124-7131, (2010).

162 Luo, P., Luo, Y., Huang, J., Lu, W., Luo, D., Yu, J. & Liu, S. Incorporation of camptothecin into reduction-degradable supramolecular micelles for enhancing its stability. *Colloids Surf. B Biointerfaces* **109**, 167-175, (2013).

163 Liu, J., Pang, Y., Huang, W., Zhu, Z., Zhu, X., Zhou, Y. & Yan, D. Redox-Responsive Polyphosphate Nanosized Assemblies: A Smart Drug Delivery Platform for Cancer Therapy. *Biomacromolecules* **12**, 2407-2415, (2011).

164 Navath, R. S., Wang, B., Kannan, S., Romero, R. & Kannan, R. M. Stimuli-responsive star poly(ethylene glycol) drug conjugates for improved intracellular delivery of the drug in neuroinflammation. *J. Control. Release* **142**, 447-456, (2010).

165 Khandare, J. & Minko, T. Polymer-drug conjugates: Progress in polymeric prodrugs. *Prog. Polym. Sci.* **31**, 359-397, (2006).

166 Kim, S. J., Ramsey, D. M., Boyer, C., Davis, T. P. & McAlpine, S. R. Effectively delivering a unique Hsp90 inhibitor using star polymers. *ACS Med. Chem. Lett.* **4**, 915-920, (2013).

167 Wang, K., Hu, Q., Zhu, W., Zhao, M., Ping, Y. & Tang, G. Structure-Invertible Nanoparticles for Triggered Co-Delivery of Nucleic Acids and Hydrophobic Drugs for Combination Cancer Therapy. *Adv. Funct. Mater.* **25**, 3380-3392, (2015).

168 Dunn, S. S., Tian, S., Blake, S., Wang, J., Galloway, A. L., Murphy, A., Pohlhaus, P. D., Rolland, J. P., Napier, M. E. & DeSimone, J. M. Reductively responsive siRNA-conjugated hydrogel nanoparticles for gene silencing. *J. Am. Chem. Soc.* **134**, 7423-7430, (2012).

169 Zhao, M., Biswas, A., Hu, B., Joo, K.-I., Wang, P., Gu, Z. & Tang, Y. Redox-responsive nanocapsules for intracellular protein delivery. *Biomaterials* **32**, 5223-5230, (2011).

170 Zhao, M., Liu, Y., Hsieh, R. S., Wang, N., Tai, W., Joo, K.-I., Wang, P., Gu, Z. & Tang, Y. Clickable protein nanocapsules for targeted delivery of recombinant p53 protein. *J. Am. Chem. Soc.* **136**, 15319-15325, (2014).

171 Zhao, M., Hu, B., Gu, Z., Joo, K.-I., Wang, P. & Tang, Y. Degradable polymeric nanocapsule for efficient intracellular delivery of a high molecular weight tumor-selective protein complex. *Nano Today* **8**, 11-20, (2013).

172 Tsarevsky, N. V. & Matyjaszewski, K. Reversible Redox Cleavage/Coupling of Polystyrene with Disulfide or Thiol Groups Prepared by Atom Transfer Radical Polymerization. *Macromolecules* **35**, 9009-9014, (2002).

173 Paulusse, J. M., Amir, R. J., Evans, R. A. & Hawker, C. J. Free radical polymers with tunable and selective bio- and chemical degradability. *J. Am. Chem. Soc.* **131**, 9805-9812, (2009).

174 Chang, C.-C. & Emrick, T. Functional Polyolefins Containing Disulfide and Phosphoester Groups: Synthesis and Orthogonal Degradation. *Macromolecules* **47**, 1344-1350, (2014).

175 Meng, F., Hennink, W. E. & Zhong, Z. Reduction-sensitive polymers and bioconjugates for biomedical applications. *Biomaterials* **30**, 2180-2198, (2009).

176 Bang, E.-K., Lista, M., Sforazzini, G., Sakai, N. & Matile, S. Poly(disulfide)s. *Chem. Sci.* **3**, 1752-1763, (2012).

177 Oae, S., Kim, Y. H., Fukushima, D. & Takata, T. in *Pure Appl. Chem.* Vol. 49 153 (1977).

178 Wilson, A., Gasparini, G. & Matile, S. Functional systems with orthogonal dynamic covalent bonds. *Chem. Soc. Rev.* **43**, 1948-1962, (2014).

179 Rosenthal-Kim Emily, Q. & Puskas Judit, E. in *Pure Appl. Chem.* Vol. 84 2121 (2012).

180 Harman, L. S., Mottley, C. & Mason, R. P. Free radical metabolites of L-cysteine oxidation. *J. Biol. Chem.* **259**, 5606-5611, (1984).

181 Holmgren, A. in *Methods Enzymol.* Vol. 107 295-300 (Elsevier, 1984).

182 Shigeru, O. (London: CRC Press, 1991).

183 Ballinger, P. & Long, F. A. Acid Ionization Constants of Alcohols. II. Acidities of Some Substituted Methanols and Related Compounds1,2. *J. Am. Chem. Soc.* **82**, 795-798, (1960).

184 Bang, E. K., Gasparini, G., Molinard, G., Roux, A., Sakai, N. & Matile, S. Substrate-initiated synthesis of cell-penetrating poly(disulfide)s. *J. Am. Chem. Soc.* **135**, 2088-2091, (2013).

185 Gasparini, G., Bang, E.-K., Molinard, G., Tulumello, D. V., Ward, S., Kelley, S. O., Roux, A., Sakai, N. & Matile, S. Cellular Uptake of Substrate-Initiated Cell-Penetrating Poly(disulfide)s. *J. Am. Chem. Soc.* **136**, 6069-6074, (2014).

186 Chuard, N., Gasparini, G., Roux, A., Sakai, N. & Matile, S. Cell-penetrating poly(disulfide)s: the dependence of activity, depolymerization kinetics and intracellular localization on their length. *Org. Biomol. Chem.* **13**, 64-67, (2015).

187 Gasparini, G., Sargsyan, G., Bang, E. K., Sakai, N. & Matile, S. Ring Tension Applied to Thiol-Mediated Cellular Uptake. *Angew. Chem. Int. Edit.* **54**, 7328-7331, (2015).

188 Son, S., Namgung, R., Kim, J., Singha, K. & Kim, W. J. Bioreducible polymers for gene silencing and delivery. *Acc. Chem. Res.* **45**, 1100-1112, (2012).

189 Fu, J., Yu, C., Li, L. & Yao, S. Q. Intracellular Delivery of Functional Proteins and Native Drugs by Cell-Penetrating Poly(disulfide)s. *J. Am. Chem. Soc.* **137**, 12153-12160, (2015).

190 Dittmer, D. C. Organic sulfur chemistry: Structure and mechanisms, by Shigeru Oae, Associate Editor, Joyce T. Doi, CRC Press: Boca Raton, Florida, 1991. 433 pp. U.S. $175. ISBN 0-8493-4739-4. *Heteroat. Chem.* **4**, 531-531, (1993).

191 Whitesides, G. M., Lilburn, J. E. & Szajewski, R. P. Rates of thiol-disulfide interchange reactions between mono-and dithiols and Ellman's reagent. *J. Org. Chem.* **42**, 332-338, (1977).

192 Wang, X.-L., Jensen, R. & Lu, Z.-R. A novel environment-sensitive biodegradable polydisulfide with protonatable pendants for nucleic acid delivery. *J. Control. Release* **120**, 250-258, (2007).

193 Chen, Y.-M., Huang, B.-H. & Lin, J.-J. Synthesis and properties of cross-linkable macromers from the selective substitution of poly (oxyalkylene)-amines and cyanuric chloride. *Polymer* **46**, 4619-4626, (2005).

194 Matsumoto, S., Christie, R. J., Nishiyama, N., Miyata, K., Ishii, A., Oba, M., Koyama, H., Yamasaki, Y. & Kataoka, K. Environment-responsive block copolymer micelles with a disulfide cross-linked core for enhanced siRNA delivery. *Biomacromolecules* **10**, 119-127, (2009).

195 Brocchini, S., Godwin, A., Balan, S., Choi, J.-w., Zloh, M. & Shaunak, S. Disulfide bridge based PEGylation of proteins. *Adv. Drug Delivery Rev.* **60**, 3-12, (2008).

196 Lyon, R. P. & Atkins, W. M. Self-assembly and gelation of oxidized glutathione in organic solvents. *J. Am. Chem. Soc.* **123**, 4408-4413, (2001).

197 Arteel, G. E. & Sies, H. The biochemistry of selenium and the glutathione system. *Environ. Toxicol. Chem.* **10**, 153-158, (2001).

198 Bindoli, A., Rigobello, M. P., Scutari, G., Gabbiani, C., Casini, A. & Messori, L. Thioredoxin reductase: a target for gold compounds acting as potential anticancer drugs. *Coord. Chem. Rev.* **253**, 1692-1707, (2009).

CHAPTER TWO

DEGRADABLE REDOX-RESPONSIVE DISULFIDE-BASED NANOGEL DRUG CARRIERS VIA DITHIOL OXIDATION POLYMERIZATION

2.1 INTRODUCTION

Controlled drug delivery carriers can improve the pharmacokinetic properties of a wide variety of drugs. In addition to controlled release of small molecules, such as in FDA-approved microparticle drug depots and chemotherapeutic drug-loaded liposomes,[1] nanoparticle carriers are essential for the delivery of biomacromolecular drugs including nucleic acids that cannot cross cell membranes on their own.[1-3] Embedding drugs into nanoparticles not only effectively suppresses interaction with blood components, but also enhances drug targeting specificity, lowers systemic drug toxicity, improves treatment absorption rates, and provides protection for pharmaceuticals against degradation.[4-6]

Polymer-based drug carriers are an important class of materials because of the ability to readily control their chemical and physical properties via chemical synthesis and their ease of processing. Furthermore, stimuli-responsive polymers enable targeted delivery and controlled release in response to biological stimuli changes, such as pH, temperature, or redox potential to trigger cargo release.[7] Drug delivery systems (e.g. micelles, liposomes, dendrimers, nanogels, and hydrogels) composed of responsive polymers can release the cargo in response to specific triggers resulting in degradation or collapse and expansion of the network in an aqueous environment.[8] Aliphatic polyesters, such as poly(lactic acid) (PLA), poly(glycolic acid) (PGA), poly(ε-caprolactone) (PCL), polycarbonates, and their copolymers degrade under physiological conditions, but are generally hydrophobic and lack the functional groups required for delivery of drugs that require electrostatic interactions (e.g. nucleic acids), bioconjugation reactions, and attachment of targeting ligands.[9,10] Also, ester bond degradation generates acidic products, which can cause an undesirable local decrease in pH.

Poly(disulfides), on the other hand, can be degraded specifically in response to redox potential through thiol-disulfide exchange reactions.[11] Intracellular compartments of cells are much more reductive than the extracellular matrix, and the glutathione/glutathione disulfide (GSH/GSSG) couple is regarded as the representative cellular redox mechanism that plays a critical role in redox homeostasis.[12] The concentration of GSH is found in millimolar concentrations inside of cells, and is 100-1000 times lower outside of cells.[13] Therefore, poly(disulfide)s can degrade in physiological settings (i.e., in cells), potentially with reduced cytotoxicity. It was also reported that the GSH level is related to many human diseases like neurodegenerative diseases, liver diseases, stroke, seizures, and diabetes.[14-18] For example, an abnormally high concentration of GSH in cancerous cells protects the cells against the anti-cancer drugs and free radical generated during radiation therapy, which results in multi-drug and radiation resistance.[14,16] This could provide a potential physiological trigger for poly(disulfide) degradation and drug delivery to diseased tissues.[8]

The significant difference in the redox environment has been explored for developing stimuli-responsive drug delivery systems. Disulfide bonds have been incorporated into polymeric materials in a variety of ways,[5] including the use of disulfide containing cross-linkers,[19-27] redox-responsive self-assembly of amphiphilic polymers in the form of micelles or polymersomes,[28,29] biodegradable polymers, both linear and dendritic from disulfide-containing monomers,[30-34] and redox-responsive drug/polymer conjugates or polymer prodrugs.

Disulfide-containing polymers and nanogels have synthesized by controlled/living radical polymerization (CRP) methods as well.[27] To date, the majority of these approaches have been limited to polymerization of vinyl monomers, cross-linked by disulfide containing cross-linkers (e.g., star polymers, micelles, branched polymers, and gels).[27] These structures degrade to the original carbon-carbon bond-based polymer upon disulfide reduction, thus limiting the extent of

degradation to long polymer chains. Direct incorporation of disulfides into the polymer backbone would allow for tunable levels of degradation and has been accomplished to some extent in a small number of examples.[35-37] However, the preparation of linear polymers composed entirely by poly(disulfide) bonds (no vinyl comonomers) remains challenging.

We were attracted to recent reports on a highly efficient oxidative system for the polymerization of dithiols to high molecular weight poly(disulfide) polymers via a base-catalyzed thiol oxidation mechanism.[38] Once sulfhydryl groups are deprotonated,[39] the thiolate anion can undergo two separate processes that lead to disulfide formation. In one process, the nucleophilic thiolate anion may attack another disulfide bond resulting in the formation of a new disulfide and a new thiolate anion. This mechanism has been utilized in the context of cell-penetrating poly(disulfide)s, which have been shown to efficiently internalize into cells and rapidly degrade in the cytosol by GSH-assisted depolymerization with minimal cytotoxicity.[40-45] In an alternative process, a single electron transfer step leads to generation of thiyl radicals, which rapidly couple with each other to form disulfide bonds and polymers.[46]

Inspired by this thiyl radical process, we aimed to synthesize fully degradable disulfide cross-linked nanogel drug carriers formed by oxidative radical polymerization of 2,2'-(ethylenedioxy)diethanethiol (EDDET) as a monomer with different cross-linkers. Numerous studies show that nanogels are excellent drug carriers due to their high drug loading capacity, stability, and responsiveness to a wide variety of environmental stimuli.[47,48] Regarding disulfide redox-responsive nanogels, literature reports are limited to fabrication of the nanogels using polymer precursors and crosslinking the polymer strands.[49-52] For example, nanogels were prepared using dextran-lipoic acid derivatives cross-linked by dithiothreitol (DTT).[53] The nanogels showed a high drug loading efficiency and delivery of doxorubicin into the cells. There remains a

need to develop nanogels that have high stability, high loading efficiency, fast degradation kinetics, and the ability to completely degrade down to non-toxic small molecule components.

In this chapter, a facile method to prepare redox responsive nanogel drug carriers via dithiol oxidation is described. A dithiol monomer, 2,2'-(ethylenedioxy)diethanethiol (EDDET) was co-polymerized with the cross-linkers ethoxylated-trimethylolpropan tri(3-mercaptopropionate) (ETTMP), pentaerythritol tetra(3-mercaptopropionate) (PETMP), and pentaerythritol tetramercaptoacetate (PETMA) into nanogels via a base-catalyzed thiol oxidation mechanism. Mechanistic studies indicated that a single electron transfer step occurred, and disulfide formation was confirmed by Fourier Transform Infrared (FTIR) spectroscopy. Polymerization occurred in bulk or solution. Nanogels were engineered using microfluidic mixing and a non-ionic surfactant was incorporated to impart colloidal stability. Control over mesh size was achieved for both bulk and formulated nanogels. An assay using Ellman's Reagent was employed to quantify the cross-linking density and number of free –SH groups. Nanogels were characterized by dynamic light scattering (DLS) and transmission electron microscopy (TEM). The weight percent loading and entrapment efficiency was also measured. *In vitro* cell viability assays and cellular uptake studies were performed in HeLa cells. Lastly, quenching studies and degradation kinetics were completed. These nanogel drug carriers provide a versatile platform that can be customized to fit a specific application (e.g. via incorporation of functional thiols). Furthermore, the free –SH groups could potentially be used to attach targeting moieties, drugs, or stabilizing chemical functionalities. Due to the rapid and facile synthesis with a variety of thiol building blocks, tunable physical properties, high biocompatibility, and fully degradable nature, the resulting nanogels are potentially useful in a wide variety of drug delivery applications.

2.2 METHODOLOGY

2.2.1 MATERIALS

Unless otherwise noted, all chemicals were purchased from Sigma-Aldrich and used as received. Organic solvents were purchased from Fisher Scientific and purified with a solvent purification system (Innovative Technology). The multifunctional THIOCURE cross-linkers were provided by Bruno Bock.

2.2.2 METHODS

2.2.2.1 Homopolymerization of EDDET

2,2'-(ethylenedioxy) diethanethiol (EDDET) and trimethylamine (TEA) were dissolved in tetrahydrofuran (THF) at room temperature. While stirring, 3 wt. % hydrogen peroxide (*aq.*) was added dropwise. The same polymerization procedure could be performed in water instead of THF. After 10 minutes, the molecular weight and polydisperisity index (PDI) for the homopolymer was measured by GPC. An example synthesis is as follows: In a glass vial equipped with a stir bar, 600 μL EDDET (3.84 mmol, 700 mg) was dissolved in 1.2 mL TEA (8.45 mmol, 855 mg), then 2.3 mL 3 wt. % H_2O_2 (2.20 mmol, 68.2 mg) was added dropwise over 5 minutes.

2.2.2.2 Hydrogel Polymerization

EDDET, cross-linker (PETMA, PETMP, or ETTMP), and TEA were dissolved in water:acetone 1:1 (vol/vol). The solution was then added into excess 3 wt. % hydrogen peroxide solution (*aq.*) and gelation occurred within seconds to give a white or opaque hydrogel. A molar equivalence of the following was used CL:M:Base = 1:5:0.1, 1:10:0.1, 1:25:0.1, 1:50:0.1, 1:75:0.1, 1:100:0.1 and 3 wt. % H_2O_2 was used in excess. Depending on the type of cross-linker used, the hydrogel texture varied from soft (ETTMP) to spongy (PETMA) to rubbery (PETMP).

2.2.2.3 Gelation Time Mechanistic Study

Hydrogel synthesis was carried out in four different reaction vials for each PETMA, PETMP, and ETTMP gel. The first reaction flask observed normal conditions; the second, omitted the addition of TEA; the third, included the addition of 1:1 molar equivalence of hydroquinone as a free radical inhibitor; and the fourth, included the addition of 1:500 molar equivalence of hydroquinone. The gelation time was recorded.

2.2.2.4 Degree of Swelling Study

Samples of PETMA, PETMP, and ETTMP hydrogels were completely dried for 48 hours under vacuum. The gel sample was allowed to fully swell for 4 hours in H_2O and the wet mass was measured. The gel sample was again allowed to completely dry for 48 hours under vacuum and

the dry mass was measured. The swelling ratio was calculated by the following: swelling ratio = [mass of swollen gel]/[mass of dry gel].

2.2.2.5 Quantification of Free –SH groups

5,5'-dithio-bis-(2-nitrobenzoic acid) (DTNB, Ellman's Reagent) stock solutions in water were prepared and used to establish a standard curve of absorbance versus free moles of –SH, where absorbance was measured using Tecan HP8300 plate reader. Samples were prepared at a concentration located in the working range of standard curve. Samples were incubated with 1 μg/μL stock Ellman's reagent for 15 minutes. Absorbance was measured at $\lambda = 412$ nm in a black 96-well clear bottom plate in triplicate. Moles of free –SH for each sample was determined using the standard curve.

2.2.2.6 Nanogel Synthesis

Nanogels were fabricated using a microfluidic mixing instrument with herringbone rapid mixing features (Precision Nanosystems NanoAssembler). EDDET, PETMA, and TEA were dissolved in water:acetone 1:1 (volume) and mixed with an aqueous phase containing different weight percentages of hydrogen peroxide (wt. %s tested included: 3%, 6%, 12%, 24%, and 30%) and surfactant (Pluronic F-127) (PLU-127) (wt. % of PLU-127: 0%, 25%, 50%, and 75%). The optimized conditions included a 1:10 ratio of organic:aqueous phase (volume), 12 mL/min flow rate, and 12 wt. % of hydrogen peroxide. Different cross-linking densities (CL:M:Base = 1:5:0.1,

1:10:0.1, 1:25:0.1, 1:50:0.1, 1:75:0.1, 1:100:0.1) were obtained using the same wt. % of surfactant and different cross-linker to monomer ratios.

2.2.2.7 Nanogel Purification

Nanogels were purified via dialysis using Spectrum Laboratories Regenerated Cellulose Dialysis Membrane with 1000 Dalton MWCO. The nanogel reaction mixture was placed into dialysis membrane tube and sealed at both ends. Dialysis was conducted against water:acetone 1:1 (volume) 3X for 4 hours, each run, and then against water 3X for 4 hours, each run. All water utilized was ultra-purified using a Milli-Q water purification system. After dialysis purification, an accurate small aliquot of nanogels solution was taken by pipette, placed in a pre-weighed glass vial, and allowed to dry for 24 hours under vacuum. The vial was re-weighed and the mass of the completely dried nanogels was calculated. The nanogels were re-dispersed in PBS (or another solvent for analysis) at determined concentrations.

2.2.2.8 Quantification of Dye Encapsulation

Nanogels with different mesh sizes were synthesized by varying the cross-linker:monomer ratio, all with the same initial 5 wt. % loading in the feed of Rhodamine B dye (5 wt. % loading of the total mass of monomer + crosslinker). Using the same concentration of all nanogel samples within the working range of the standard curve, the nanogels were degraded using 11 mM dithiothreitol (DTT) for 24 hours to allow all Rhodamine B to be freely soluble and detectable. Fluorescence was measured using a Tecan HP8300 plate reader, λ_{ex} = 540 nm and λ_{em} = 576 nm top-read in

solid black 96-well plates in triplicate. The mass of Rhodamine B loaded for each nanogel sample was determined using the standard curve. The weight percent loading was calculated by [(actual dye encapsulation)/(monomer + crosslinker)] x 100. The percent entrapment efficiency was calculated by [(actual dye encapsulation)/(theoretical dye encapsulation)] x 100.

2.2.2.9 Degradation of PETMA Rhodamine B Loaded Nanogels

5 wt. % Rhodamine B loaded nanogels were imaged on an EVOS optical fluorescence microscope. Thin films were drop cast onto a cleaned glass slide. Images were taken before and after the addition of 11 mM DTT.

2.2.2.10 Kinetic Study

Samples of 5 wt. % Rhodamine B dye loaded nanogels (CL:M = 1:25, 1:50, 1:70, and 1:100 (mol/mol)) were prepared using the experimentally determined % efficiencies (45.32%, 51.24%, 56.38%, and 75.88%, respectively) to provide samples each containing the same amount of Rhodamine B loaded dye. A stock solution of 11 mM GSH was prepared using Milli-Q water. Nanogel samples and 11 mM GSH were added into an Amicon Ultra-0.5 mL centrifugal filter tubes and allowed to incubate for the following time points: 0 min, 5 min, 10 min, 15 min, 30 min, 45 min, and 60 min. After each time interval, the nanogels + GSH mixture was centrifuged at 4,000 rcf for 10 min at 4 °C. A fluorescence measurement of the filtrate (filtrate A) was taken via triplicate (Tecan HP8300 plate reader, λ_{ex} = 540 nm and λ_{em} = 576). The % release of Rhodamine B dye was quantified using a standard curve. The remaining nanogels + GSH mixture (filtrate B)

was obtained by a reverse spinning step after collecting filtrate A. Reverse spinning step was centrifuged at 1,000 rfc for 2 min. DLS measurements were taken before addition GSH, filtrate A, and filtrate B.

2.2.2.11 Quenching Study

Nanogels were incubated with 11 mM GSH and a fluorescence time scan measurement was performed using a Hitachi F-7000 Fluorescence Spectrophotometer (λ_{em} = 590 nm λ_{ex} = 550 nm). Fluorescence intensity was normalized to baseline. DLS measurements were made before and after the addition of GSH.

2.2.2.12 Cell Culture

HeLa cells (ATCC) were maintained in RPMI-1640 (Life Technologies) supplemented with 5% fetal calf serum at 37 °C in a humidified atmosphere containing 5% CO_2 and 95% air.

2.2.2.13 Cell Viability Assay

Cytotoxicity of nanogels (1:25, 1:50, 1:70, and 1:100 cross-linker:monomer ratios) and nanogels degraded by 11 mM GSH for 24 hours was assessed in HeLa cells (10,000 cells/well in 96-well plates seeded 12 h prior to experiments). HeLa cells were incubated in DMEM with 5% FBS for 24 hours with a series of total nanogels or degraded nanogels products of 0 ng/μL, 2.5 ng/μL, 5 ng/μL, 10 ng/μL, 25 ng/μL, 50 ng/μL, 75 ng/μL, and 100 ng/μL. Cell viability was measured using

the CellTiter-Glo Luminescent Cell Viability Assay (Promega) following the recommended protocol.

2.2.2.14 Cellular Uptake Study

HeLa cells were seeded at a density of 30,000 cells/well in 8-chambered cover glass slides (Nunc) and allowed to attach for 24 hours (37 ^{o}C, 5% CO_2). 5 wt. % Rhodamine B dye loaded nanogels (1:25 cross-linker:monomer ratio) solutions were prepared via serial dilution from original stock using PBS (1.1 ng/μL, 2.3 ng/μL, 4.5 ng/μL, 11 ng/μL, 23 ng/μL, 34 ng/μL, and 45 ng/μL). After 24 h incubation, the cells were washed with PBS, fixed with 4% (volume) PFA, and stained with DAPI for confocal imaging. Confocal microscopy imaging was performed using a Zeiss LSM510 Confocal Microscope at 40X magnification and images were analyzed using ImageJ (NIH).

2.2.2.15 Time Course Study

HeLa cells were seeded at a density of 30,000 cells/well in 8-chambered cover glass slides (Nunc) and allowed to attach for 24 hours (37 ^{o}C, 5% CO_2). 5 wt. % Rhodamine B dye loaded nanogels (1:25, 1:50, 1:70, and 1:100 cross-linker:monomer ratio) with a final dye concentration of 23 ng/μL were prepared from original stock using PBS. Incubation time points included the following: 0 min, 15 min, 1 hr, 3 hr, 6 hr, 15 hr, and 24 hr. After each respective incubation period, the cells were washed with PBS, fixed with 4% (volume) PFA, and stained with DAPI for confocal imaging. Confocal microscopy imaging was performed using a Zeiss LSM510 Confocal Microscope at 40X magnification and images were analyzed using ImageJ (NIH).

2.2.3 INSTRUMENTATION

2.2.3.1 Molecular Weight Analysis

Molecular weights were measured by a Gel Permeation Chromatography (GPC) (Viscotek) system equipped with a refractive index (RI) detector and ViscoGEL I-series columns (Viscoteck I-MBLMW-3078) using DMF as the eluent at 0.75 mL/min and 45 °C. The instrument was calibrated with a series of 10 narrow polydispersity polystyrene standards (500 to 200,000 g/mol).

2.2.3.2 Fourier-Transform Infrared Resonance (FTIR) Spectroscopy

FTIR was performed on a Thermo Scientific Nicolet 380 FTIR instrument with an attenuated total reflection (ATR) accessory. After the universal diamond ATR top-plate was cleaned using a solvent soaked tissue and a background scan collected, a gel sample was placed onto the small crystal area. Enough sample to cover the crystal area and a height no more than a few millimeters was applied. Once the sold was placed on the crystal area, the pressure arm was positioned over the crystal/sample area. The pressure arm was locked into position above the diamond crystal and force was applied to the sample, pushing it onto the diamond surface. Spectra were collected using PerkinElmer's Spectrum FTIR software. The ATR top-plate was cleaned before and after each use.

2.2.3.3 Dynamic Light Scattering (DLS)

Hydrodynamic diameter analysis (particle sizes) were measured by Dynamic Light Scattering (DLS) using a Malvern Zetasizer Nano ZS (He-Ne laser, $\lambda = 632$ nm).

2.2.3.4 Transmission Electron Microscopy (TEM)

TEM was performed on a FEI Tecnai G2 Spirit Gatan Camera at 6,800X magnification and at an accelerated voltage of 120 kW. For sample preparation, a drop of nanogels stock was placed on a 200 mesh carbon film covered TEM grid using phosphotungstic (PTA) negative staining, excess liquid was then wicked by filter paper. The copper grid was then dried under vacuum for one hour.

2.3 RESULTS

2.3.1 POLYMERIZATION

Oxidative homopolymerization of EDDET produced high molecular weight poly(disulfide) chains.

Before preparing nanogels, we initially investigated whether EDDET could be homopolymerized by the proposed radical oxidative polymerization mechanism. EDDET was selected as the monomer due to the presence of ethylene oxide repeats, which would render the chemical structure of the resulting poly(disulfide)s as poly(ethylene glycol) (PEG) mimics. Due to the extensive use of PEG in drug delivery and bioconjugation applications, we envisioned that poly(EDDET) would be highly biocompatible. To deprotonate the thiols in EDDET, triethylamine (TEA) was employed. The resulting thiol anions then underwent a single electron transfer mechanism in the presence of 3 wt. % H_2O_2 to give thiyl radicals. It was found that the produced thiyl radicals quickly coupled together to produce high molecular weight poly(EDDET). Polymerization was successfully performed in either THF or H_2O as a solvent. Although EDDET is not water soluble, it dissolves readily in water after deprotonation by TEA. The number average molecular weights (M_n) were 106,900 g/mol and 156,700 g/mol, the weight average molecular weights (M_w) were 197,900 g/mol and 280,900 g/mol, and the polydisperisity indexes (PDI) were 1.85 and 1.79 for representative homopolymers in THF and H_2O solvent conditions, respectively (**Figure 2.1**). The large M_w and broad PDI indicates that a controlled polymerization did not occur. Homopolymerization of EDDET occurred rapidly (within seconds), thus making the polymerization facile and convenient

for bioengineering purposes, but difficult to control. We therefore reasoned that oxidative polymerization of EDDET would be best suited for construction of cross-linked materials, particularly nanogels as potential drug carriers responsive to GSH inside of cells. We therefore proceeded towards synthesis and characterization of poly(disulfide) hydrogels.

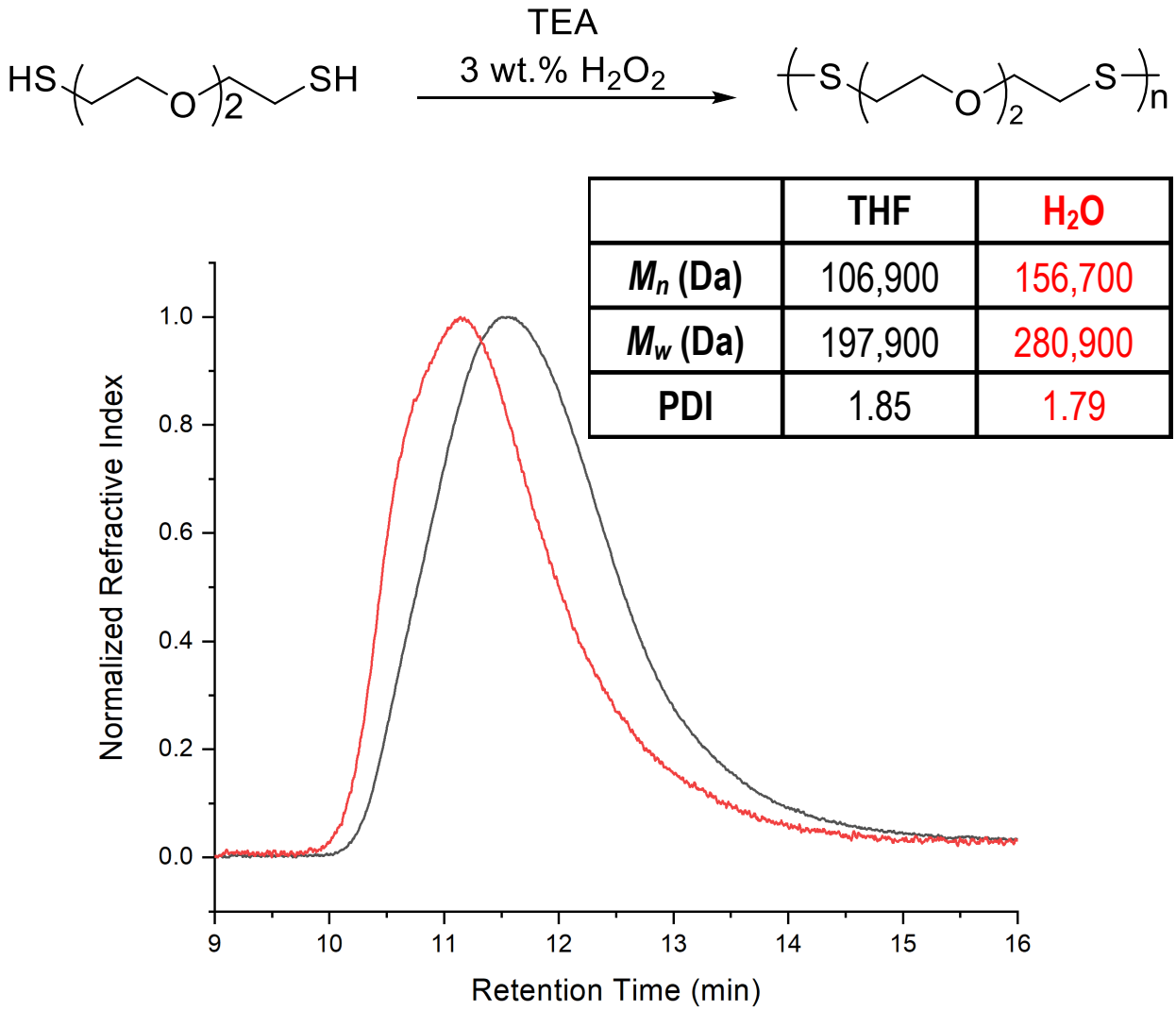

	THF	H_2O
M_n (Da)	106,900	156,700
M_w (Da)	197,900	280,900
PDI	1.85	1.79

Figure 2.1. GPC analysis of EDDET homopolymerization in THF (—) and H_2O (—).

2.3.2 HYDROGEL SYNTHESIS

Oxidative polymerization of EDDET in the presence of dithiol cross-linkers yielded hydrogels with tunable properties.

To investigate synthesis of hydrogels, we identified three thiol-based cross-linkers denoted as PETMA, PTMP, and ETTMP (**Scheme 2.1**). These tri- and tetra-functional cross-linkers repeat the chemical design themes of including ethers and esters in the hydrogel structure. Their low molecular weights ensure that the hydrogels will degrade to small molecules after disulfide bond cleavage in cells. Hydrogels with different degrees of cross-linking density were synthesized. EDDET and cross-linker thiols were deprotonated using TEA to give thiol anions, which generated thiyl radicals after addition of 3 wt. % H_2O_2 (*aq.*). The resulting thiyl radicals quickly coupled together to form disulfide cross-linked hydrogels. Materials with different cross-linking density was achieved by varying the crosslinker to monomer ratio (CL:M = 1:5, 1:10, 1:25, 1:50, 1:75, and 1:100). Depending on the chemical structure of the cross-linker used, the hydrogel texture varied from soft (ETTMP) to spongy (PETMA) to rubbery (PETMP) (**Scheme 2.1**). ETTMP was not used further because of prolonged degradation time exhibited by ETTMP due to the longer PEG chains that must completely swell before degradation begins, coupled to the inability to degrade to small molecules. PETMA and PETMP are very similar in structure (one carbon spacer difference), therefore PETMA was used in all further experiments due to its preferable, gel-like physical property.

To prove that the hydrogels formed via a radical mechanism, we performed mechanistic studies by measuring gelation time under different conditions that would examine either an ionic or a radical process. Under normal reaction conditions using TEA and 3 wt. % H_2O_2 (*aq.*), all gels

formed within approximately 5 seconds. If no base was added, no gelation occurred. This indicates that deprotonation (formation of thiol anions) is a required step for polymerization. Next, we examined if free radical inhibitors could slow or stop the polymerization. If a 1:1 molar equivalence of hydroquinone to monomer was added, then gelation did not occur for the ETTMP hydrogel and the gelation time was significantly delayed for the PETMA and PETMP gels. If a 1:500 molar equivalence of hydroquinone to monomer was added, then no hydrogels formed at all under any conditions with all three cross-linkers, even after an extended wait period (**Figure 2.2A**). The impeded gelation time by a radical inhibitor indicates that these gels form via a single electron transfer mechanism to provide a thiyl radical, which couple to form poly(disulfide)s.

To further confirm disulfide bond formation, we employed Fourier Transform Infrared Spectroscopy (FTIR). Both 2,2'-(ethylenedioxy)diethanethiol monomer and PETMA crosslinker FTIR traces revealed a clear –SH peak, which disappeared after gel formation (**Figure 2.2B**). Furthermore, different weight %s of H_2O_2 (0.1%, 1%, 3%) showed no change in FTIR traces, indicating minimal over oxidation (**Figure 2.2C**). The degree of swelling is used as a common measure of the degree of crosslinking, where the equilibrium degree of swelling will be smaller when the degree of cross-linking is higher. PETMA gels with different cross-linker to monomer ratios (CL:M = 1:5, 1:10, 1:25, 1:50, 1:75, and 1:100) were synthesized and showed a clear trend in crosslinking density. The measured swelling ratios were 1.65, 2.06, 2.24, 2.26, 2.32, and 3.03 for the 1:5, 1:10, 1:25, 1:50, 1:75, and 1:100 gels, respectively (**Figure 2.3**). Increasing the amount of monomer in the feed resulted in a larger equilibrium degree of swelling, hence a larger gel mesh size. Also, PETMA-based hydrogels degraded in response to DTT to release Rhodamine B. All dye molecules were released within two minutes (**Figure 2.4**).

After confirming that disulfide bond formation and no over oxidation occurs, as well as establishing an understanding of how cross-linker to monomer ratio can affect the cross-linking density via the swelling ratios, we wanted to see whether any free thiols remained in the gels. Quantification of free thiols is functionally important because free thiols could be used to click targeting moieties or therapeutic agents directly to the nanogels. 5,5'-dithio-bis-(2-nitrobenzoic acid) (DTNB or Ellman's Reagent) reacts with free thiols to produce 2-nitro-5-thiobenzoic acid (TNB). TNB is a colored species, where the absorbance can be measured and then the amount of free thiols can be quantified when compared to a standard curve. We found that the moles of free thiols decreased as the amount of monomer in the feed increased, hence indicating a larger mesh size that corresponded with the previous degree of swelling results (**Figure 2.2D**).

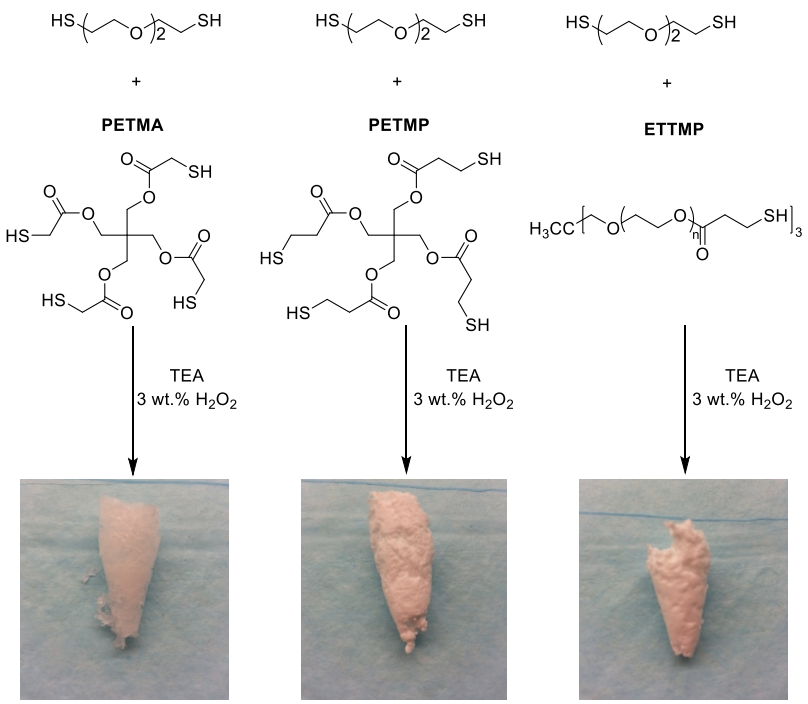

Scheme 2.1. Polymerization scheme to form hydrogels. Images of dried hydrogels synthesized using EDDET, PETMA, PETMP, and ETTMP.

A

Gelation Time			
	ETTMP	PETMA	PETMP
No Base (TEA)	----	----	----
Thiol:hydroquinone = 1:0 (mol/mol)	5	5	5
Thiol:hydroquinone = 1:1 (mol/mol)	*	30	180
Thiol:hydroquinone = 1:500 (mol/mol)	*	*	*
*No gelation occurred after a wait time of 30 minutes			

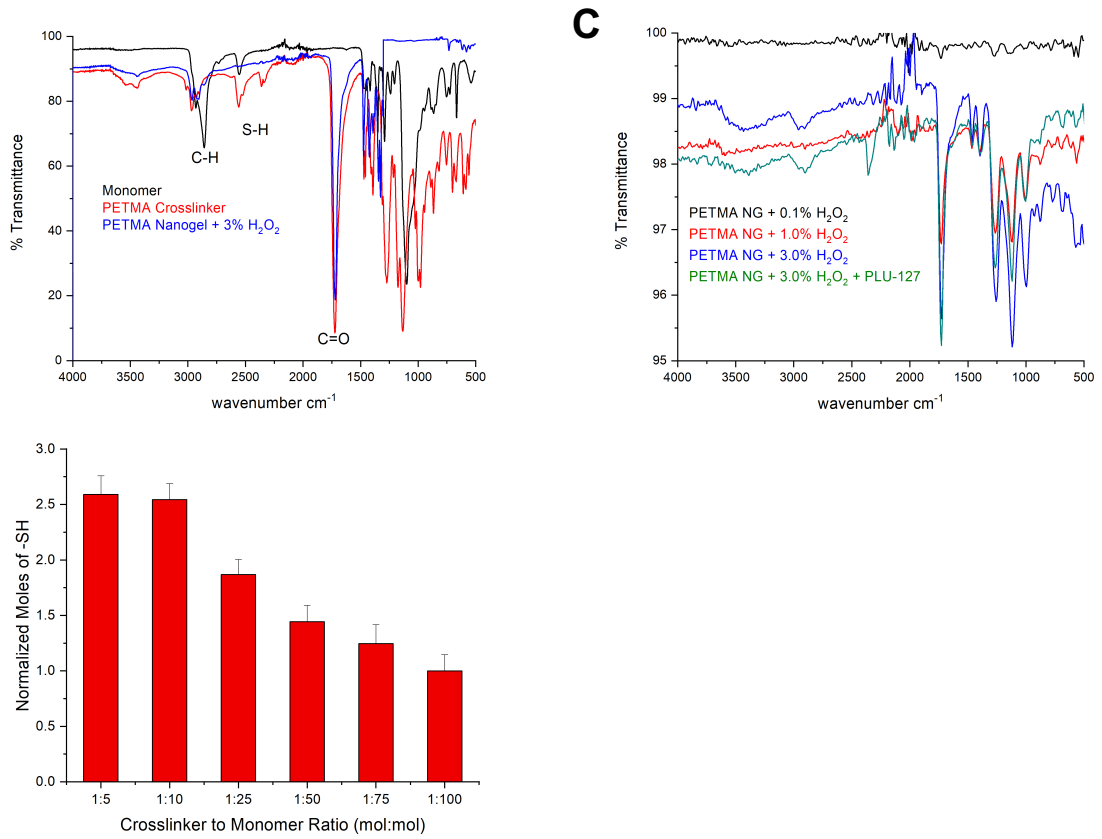

Figure 2.2. Hydrogels form via a single-electron transfer radical mechanism. (**A**) Table of gelation time of ETTMP, PETMA, and PETMP hydrogels in the absence of base (TEA), and 1:1 and 1:500 molar equivalence of free –SH to radical inhibitor. (**B**) FTIR traces of monomer (—), crosslinker (—), and hydrogel (—) for PETMA. (**C**) FTIR traces of PETMA synthesized in different weight %s of H_2O_2 0.1% (—), 1% (—), 3% (—), and (—) 3% with the addition of PLU127 surfactant. Moles of free –SH decreased as mesh size increased. (**D**) Calculated moles of free -SH of PETMA nanogels with different crosslinking densities.

Degree of Swelling			
CL:M	Dry Mass	Wet Mass	Swelling Ratio
1 to 5	0.2276	0.3752	1.65
1 to 10	0.2441	0.5029	2.06
1 to 25	0.5857	1.3128	2.24
1 to 50	1.3194	2.985	2.26
1 to 75	0.3822	0.8857	2.32
1 to 100	0.707	2.1412	3.03

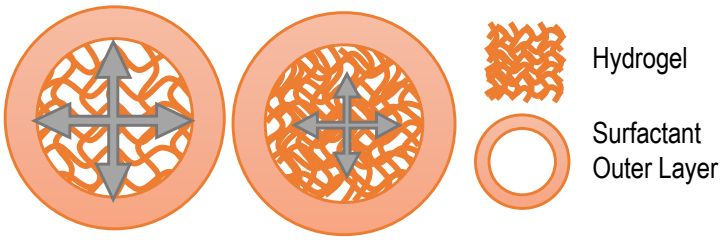

Figure 2.3. Decreasing the cross-linker to monomer ratio led to higher swelling of hydrogels. The equilibrium degree of swelling of different cross-linking densities of PETMA hydrogels.

Figure 2.4. PETMA-based hydrogels degraded in response to DTT to release Rhodamine B. All dye molecules were released within two minutes.

2.3.3 NANOGEL SYNTHESIS

Surfactant-stabilized, cross-linked nanogels were synthesized using controlled microfluidic mixing.

To formulate monodisperse nanogels, we employed microfluidic mixing, where optimized conditions resulted in >40% yield and well dispersed nanogels with opaque blue sheen in solution, which is characteristic of nanoparticles in solution (**Figure 2.5**). Because we found that purifying bare nanogels via dialysis resulted in aggregation, we therefore incorporated PLU-127 during nanogel formation. This polymer surfactant coating prevented aggregation of nanogels from occurring during further isolation and purification. Before and after dialysis purification, nanogels possessed a hydrodynamic diameter between 60-70 nm. Increasing the wt. % of PLU-127 (0%, 25%, 50%, and 100%) led to a smaller hydrodynamic diameter, as anticipated due to increased surface area of coated nanogels with more PLU-127 coating (**Figure 2.7A**). However, keeping the wt. % of PLU-127 constant and only adjusting the cross-linker to monomer ratio (CL:M = 1:0.5, 1:1, and 1:2) did not change nanogel hydrodynamic diameters (**Figure 2.7B**). Therefore, the wt. % of PLU-127 controlled the overall nanogel hydrodynamic diameter and the mesh size was tuned independently by altering the cross-linker to monomer ratio.

We then prepared uniformly sized nanogels with different mesh sizes (CL:M = 1:25, 1:50, 1:75, and 1:100) using a constant wt. % of surfactant and different cross-linker to monomer ratios. Nanogels exhibited similar hydrodynamic diameters (**Figure 2.6**) and TEM images of monodisperse nanogels showed uniform particles (**Figure 2.7C-2.7F**). We next examined dye encapsulation as a drug mimic and quantified the weight % loading and % entrapment efficiency. We used Rhodamine B to represent a model small molecule drug with 5 wt. % loading in the feed.

Dye encapsulation was quantified using dithiothreitol (DTT). DTT reduces disulfide bonds by two sequential thiol-disulfide exchange reactions. The amount of dye released was quantified by using a standard curve. Both the weight % loading and % entrapment efficiency showed a similar trend: As mesh size increased (CL:M = 1:25, 1:50, 1:75, and 1:100), the weight % loading and % entrapment efficiency increased (**Figure 2.7G**). The ability for π stacking in the larger mesh sized nanogels could potentially account for the increased Rhodamine B dye loading. These results indicated that the synthesis and purification conditions led to stable and reproducible nanogels and that these nanogels impart the ability to control the mesh size and loading capacity.

To demonstrate that these nanoparticles enable triggerable release of the encapsulated Rhodamine B in a reducing environment through disulfide-thiol chemistry, thin films of nanogel solution were drop cast onto a cleaned glass slide and images were taken before (**Figure 2.8A**) and after (**Figure 2.8B**) the addition of 11 mM DTT. After the addition of the reducing agent, the entire imaging field was flooded with a diffuse fluorescent signal which indicates the release of the Rhodamine B molecules from the nanogels. Hence, the degradation of nanogels could trigger the controlled release of encapsulated drug therapeutics in a reducing environment (**Figure 2.9**).

Total Flow Rate (mL/min)	H_2O_2 wt. %	DLS (nm)	Appearance	Ratio	Yield
12	3%	73	opaque blue sheen	1:10	22.41%
12	6%	69	opaque blue sheen	1:10	27.03%
12	12%	74	opaque blue sheen	1:10	40.39%
12	24%	70	opaque blue sheen	1:10	27.74%
12	30%	----	opaque blue sheen	1:10	N/A
nanoprecip.	3%	99	opaque blue sheen	1:10	28.63%

Before Dialysis
PETMA Nanogel = 63 nm

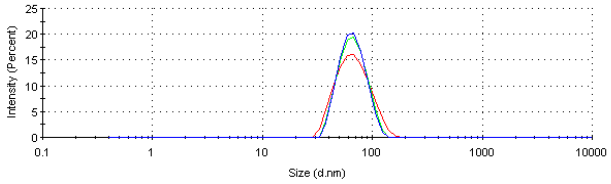

After Dialysis
PETMA Nanogel = 68 nm

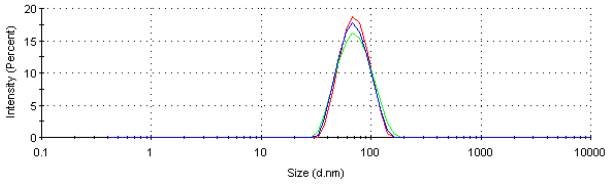

Figure 2.5. Table listing different formulation conditions. Formulated nanogels were prepared using a microfluidic mixing instrument. An organic phase containing monomer, cross-linker, and base dissolved in water:acetone 1:1 (volume) solution was combined with an aqueous phase containing different weight percentages of H_2O_2. The ratio of organic:aqueous phase was 1:10 (volume) and the flow rate was 12 mL/min.

A

Dynamic Light Scattering (DLS) of Different Mesh Size Nanogels (nm)						
CL:M	Intensity	STDEV	Volume	STDEV	Number	STDEV
1 to 5	55.56	18.44	42.18	14.08	34.19	9.124
1 to 25	111.5	33.92	93.59	32.32	74.30	20.64
1 to 50	111.2	31.84	95.28	30.82	77.73	20.48
1 to 75	92.30	23.70	89.70	22.48	77.83	16.53
1 to 100	99.37	24.58	87.37	23.97	75.15	17.75

B

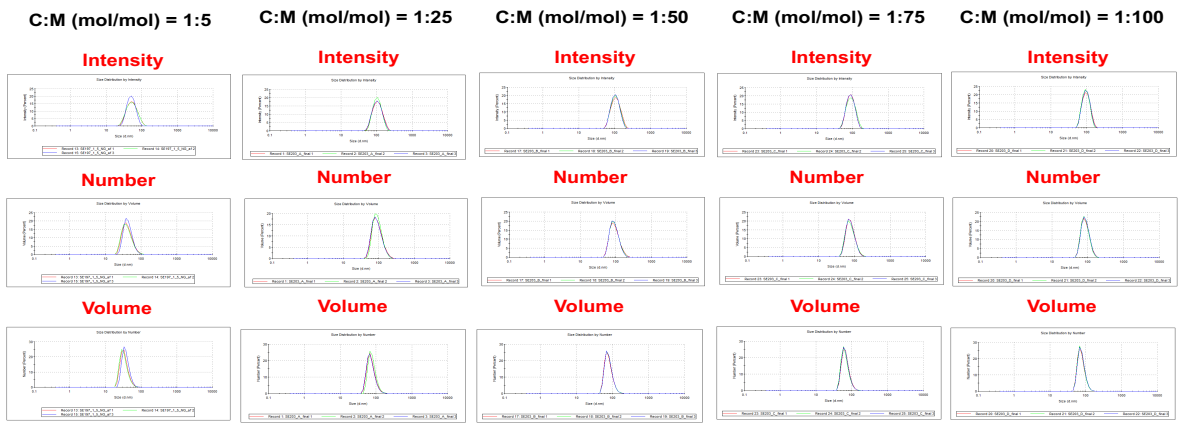

Figure 2.6. (**A**) Table of particle sizes of different PETMA nanogels of different cross-linking densities after dialysis purification. (**B**) Intensity-, number-, and volume-weighted DLS plots of corresponding nanogels. Formulated nanogels were prepared using a microfluidic mixing instrument. An organic phase containing monomer, cross-linker, and base dissolved in water:acetone 1:1 (volume) solution was combined with an aqueous phase containing 12 wt. % H_2O_2. The ratio of organic:aqueous phase was 1:10 (volume) and the flow rate was 12 mL/min. Particle sizes before after dialysis purification were measured by DLS.

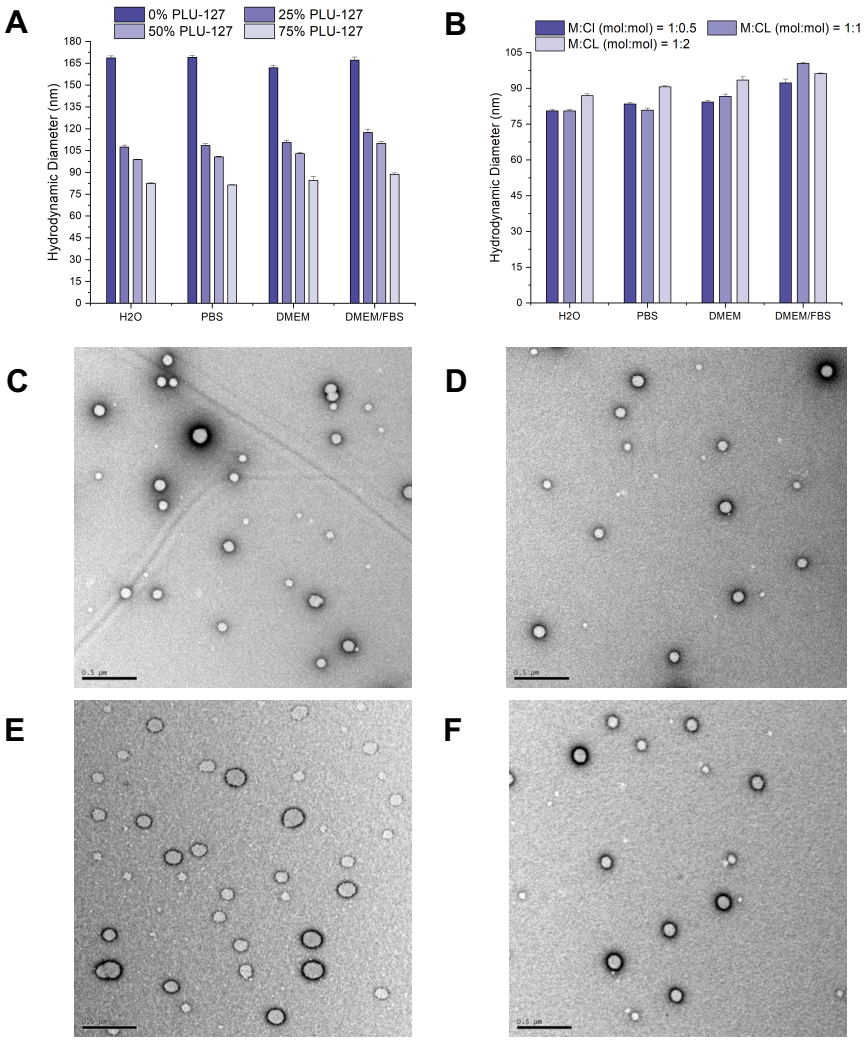

G

	Weight % Loading	% Entrapment Efficiency
1 to 5	1.44	28.74
1 to 25	2.27	45.32
1 to 50	2.56	51.24
1 to 75	2.82	56.38
1 to 100	3.79	75.88

Figure 2.7. Hydrodynamic diameter of nanogels after (**A**) varying the wt. % of surfactant PLU-127 and (**B**) varying the monomer:cross-linker ratio. TEM image of monodispersed disulfide cross-linked nanogels with (**C**) 1:25, (**D**) 1:50, (**E**) 1:75, and (**F**) 1:100 cross-linker:monomer (mol/mol) ratio. Scale bar = 0.5 µm. (**G**) Table of quantified dye encapsulation of different mesh size for 5 wt. % Rhodamine B loaded nanogels.

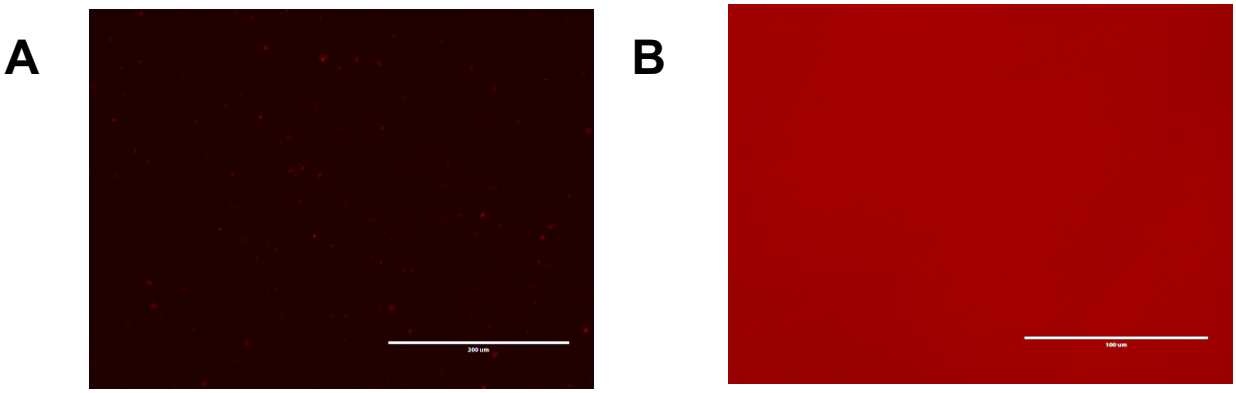

Figure 2.8. Optical fluorescence microscopy images of nanogel nanogels containing 5 wt. % Rhodamine B before (**A**) and after (**B**) the addition of 11 mM dithiothreitol (DTT). Scale bars = 100 µm.

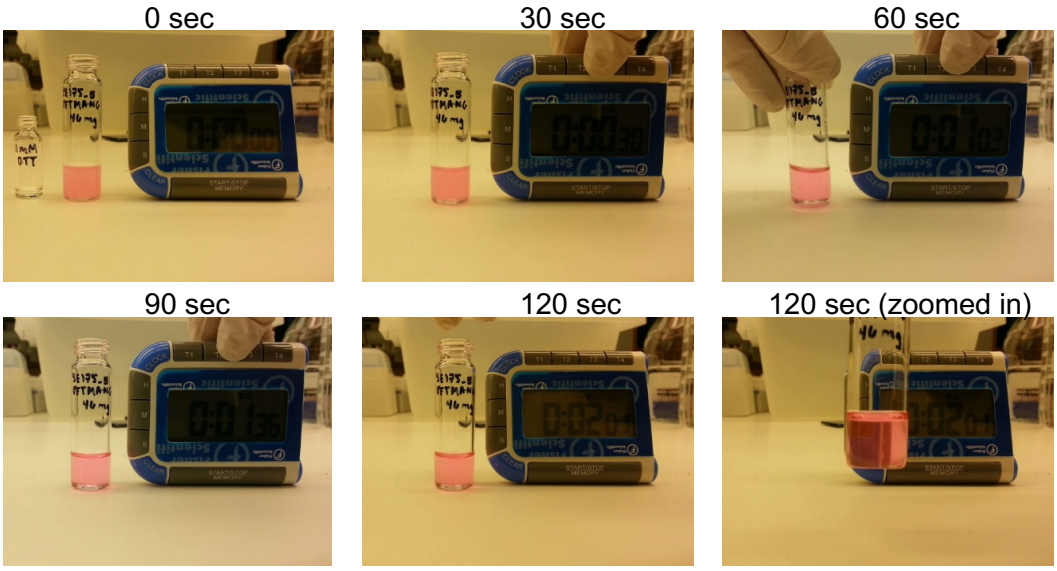

Figure 2.9. Degradation of PETMA, Rhodamine B loaded nanogels after the addition of dithiothreitol (DTT) disulfide bond reducing agent. Degradation occurred in less than two minutes for this sample size (10 mg).

2.3.4 IN VITRO, TOXICITY, AND KINETIC STUDIES

Nanogels demonstrated low toxicity, quick uptake, and fast degradation kinetics in vitro.

To examine applicability as drug carriers, we measured potential cytotoxicity from both the nanogels themselves, as well as the ultimate nanogel degradation products. HeLa cervical cancer cells were incubated with PBS suspensions of intact nanogels (**Figure 2.10A**) or degraded nanogel products (**Figure 2.10B**). High cell viability was quantified under all conditions, indicating limited to no pronounced cytotoxicity. Degradation products were isolated following a 24 hour incubation with 11 mM GSH.

Next, we examined the cellular uptake behavior of nanogels formed with different cross-linking densities (**Figure 2.12**). Loaded Rhodamine B dye was used to track the nanogels. It has been reported that disulfide materials may utilize reaction with surface thiols to aid internalization.[41,45] In our experiments, we observed that all nanogels with different cross-linking densities (CL:M = 1:25, 1:50, 1:75, and 1:100) began internalizing within 15 min and completed uptake by 6 hours (**Figure 2.12E**). Red fluorescence was observed in both puncta and diffuse signal suggesting some nanogels may be in endosomes while others had degraded and released free dye (**Figure 2.12A-2.12D**). Because high loading of Rhodamine B molecules within nanogels could potentially lead to quenched fluorescence emission by homo FRET, we decided to investigate this possibility by performing fluorescence time scan measurements before and after addition of GSH. Fluorescence intensity was normalized to baseline. Results indicated that no quenching occurred (**Figure 2.19A**). Furthermore, DLS measurements taken before and after the addition of 11 mM GSH revealed that nanogels degrade down to small molecules (**Figure 2.19B** and **2.19D**).

To further understand these results and characterize the nanogels, we measured degradation kinetics by looking at the change in fluorescence intensity over time as nanogels, loaded with Rhodamine dye, were degraded in 11 mM GSH. All nanogels began to degrade down within the first ten minutes and exhibited a burst release profile due to disulfide bond breakage (**Figure 2.19B**). Overall, *in vitro* studies show low toxicity, quick uptake, and fast degradation kinetics. Also, due to the ease of synthesis, rapid gelation times, and tunable functionality, these non-toxic and fully degradable nanogels offer excellent potential for use in a wide variety of drug delivery applications.

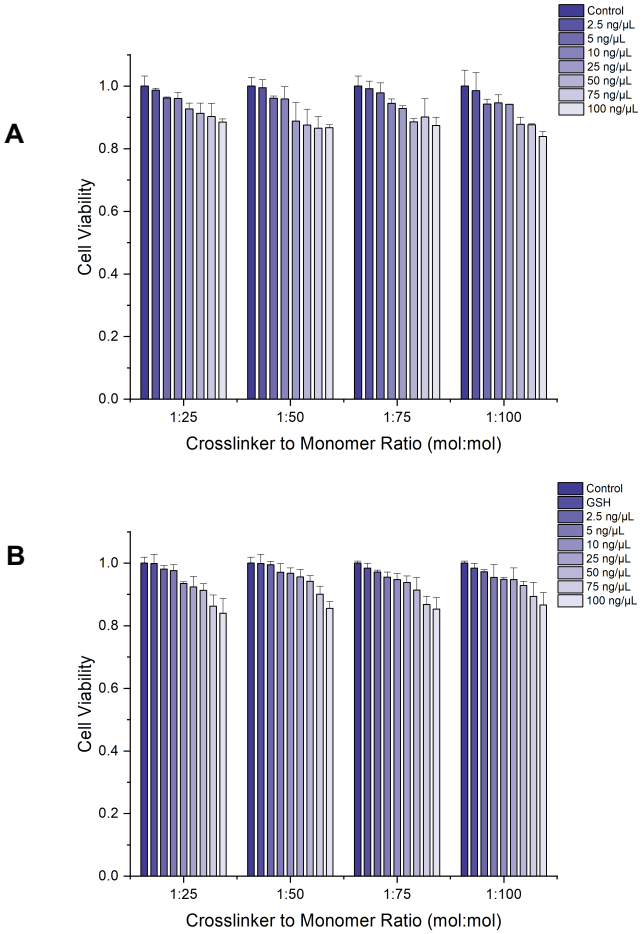

Figure 2.10. Cytotoxicity analysis of HeLa cells cultured with (**A**) PETMA nanogels and (**B**) degraded nanogel products. Results were normalized to untreated cells.

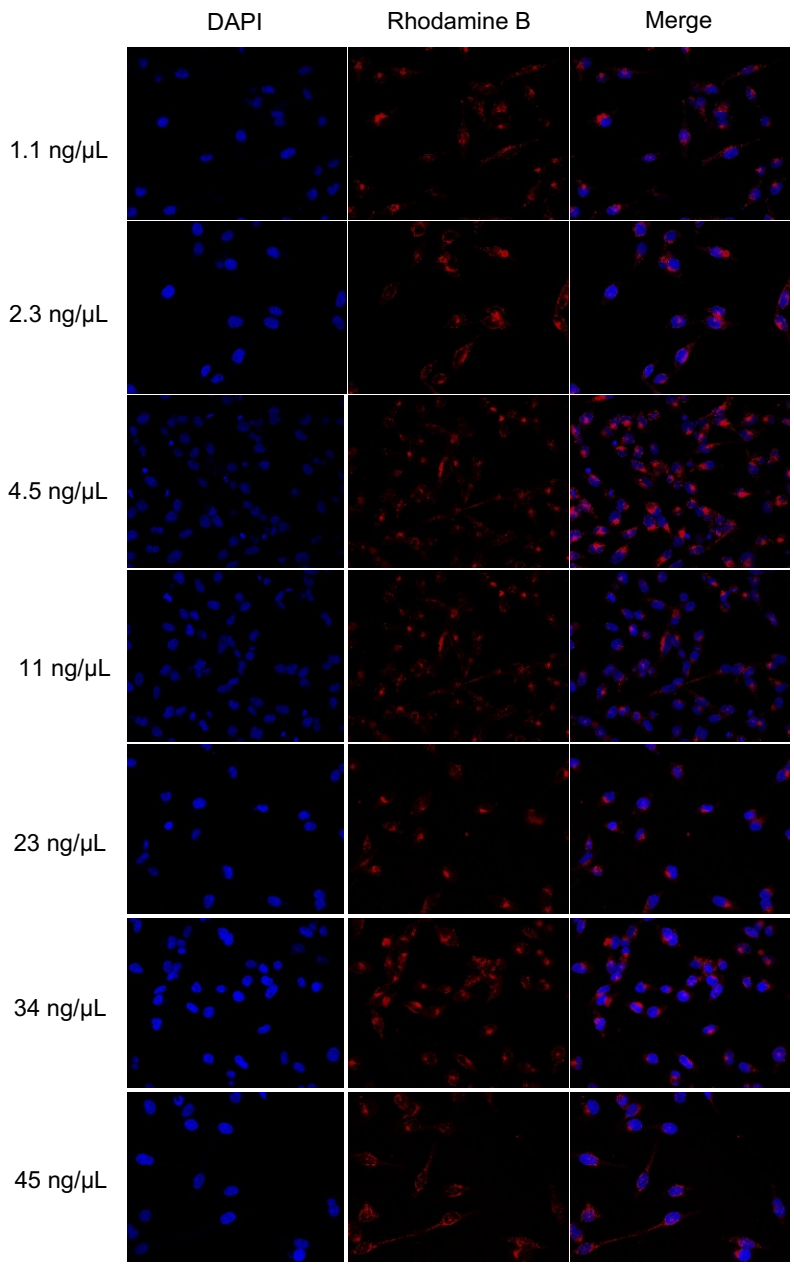

Figure 2.11. The optimum Rhodamine B dye concentration for analysis of cellular uptake was determined by incubating HeLa cells with increasing dye-loaded nanogel concentrations using the 1:25 nanogels for 24 hrs. HeLa cells were fixed using PFA and the nucleus stained with DAPI. Images taken on a confocal microscope at 40X magnification and images were analyzed using ImageJ.

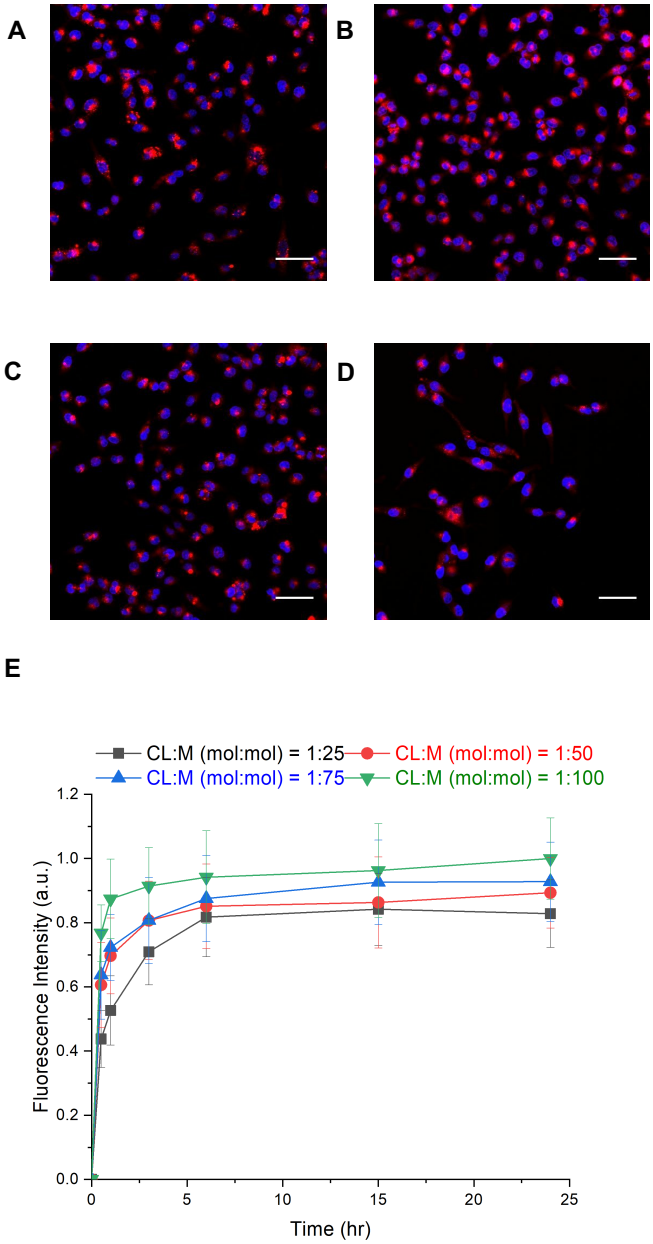

Figure 2.12. HeLa cells were incubated with 5 wt. % Rhodamine B loaded nanogels with a final dye concentration of 23 ng/μL and incubated at different time points (0 min, 15 min, 1 hr, 3 hr, 6 hr, 15 hr, and 24 hr). HeLa cells were fixed using PFA and the nucleus stained with DAPI. Images taken at 40X magnification and scale bars represent 50 μm scale. Confocal images of (**A**) 1:25, (**B**) 1:50, (**C**) 1:75, and (**D**) 1:100, monomer:cross-linker (mol/mol) at the 24 hr time point. (**E**) The rate of internalization was quantified by tracking fluorescence intensity over time.

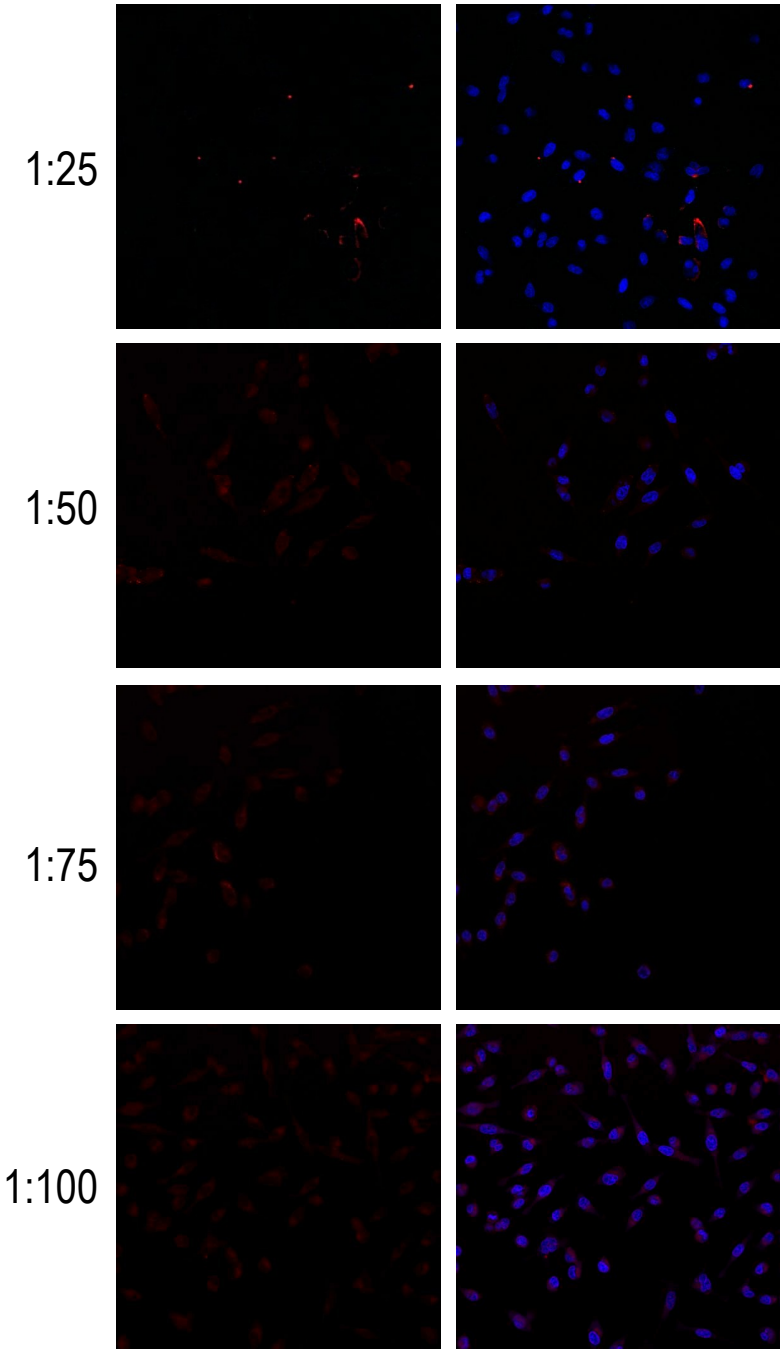

Figure 2.13. HeLa cells were incubated with 5 wt. % Rhodamine B loaded nanogels with a final dye concentration of 23 ng/μL and incubated 15 min. HeLa cells were fixed using PFA and the nucleus stained with DAPI. Images taken on a confocal microscope at 40X magnification and images were analyzed using ImageJ.

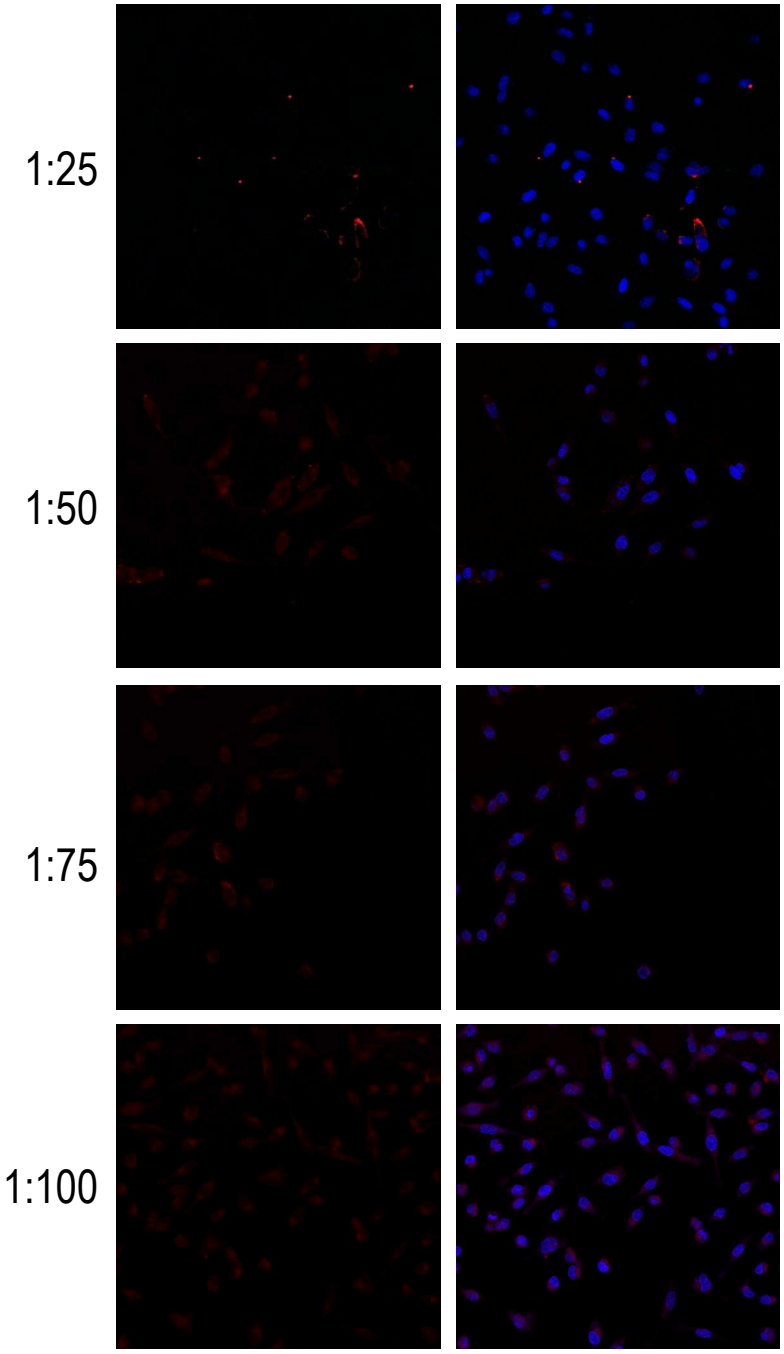

Figure 2.14. HeLa cells were incubated with 5 wt. % Rhodamine B loaded nanogels with a final dye concentration of 23 ng/μL and incubated 1 hr. HeLa cells were fixed using PFA and the nucleus stained with DAPI. Images taken on a confocal microscope at 40X magnification and images were analyzed using ImageJ.

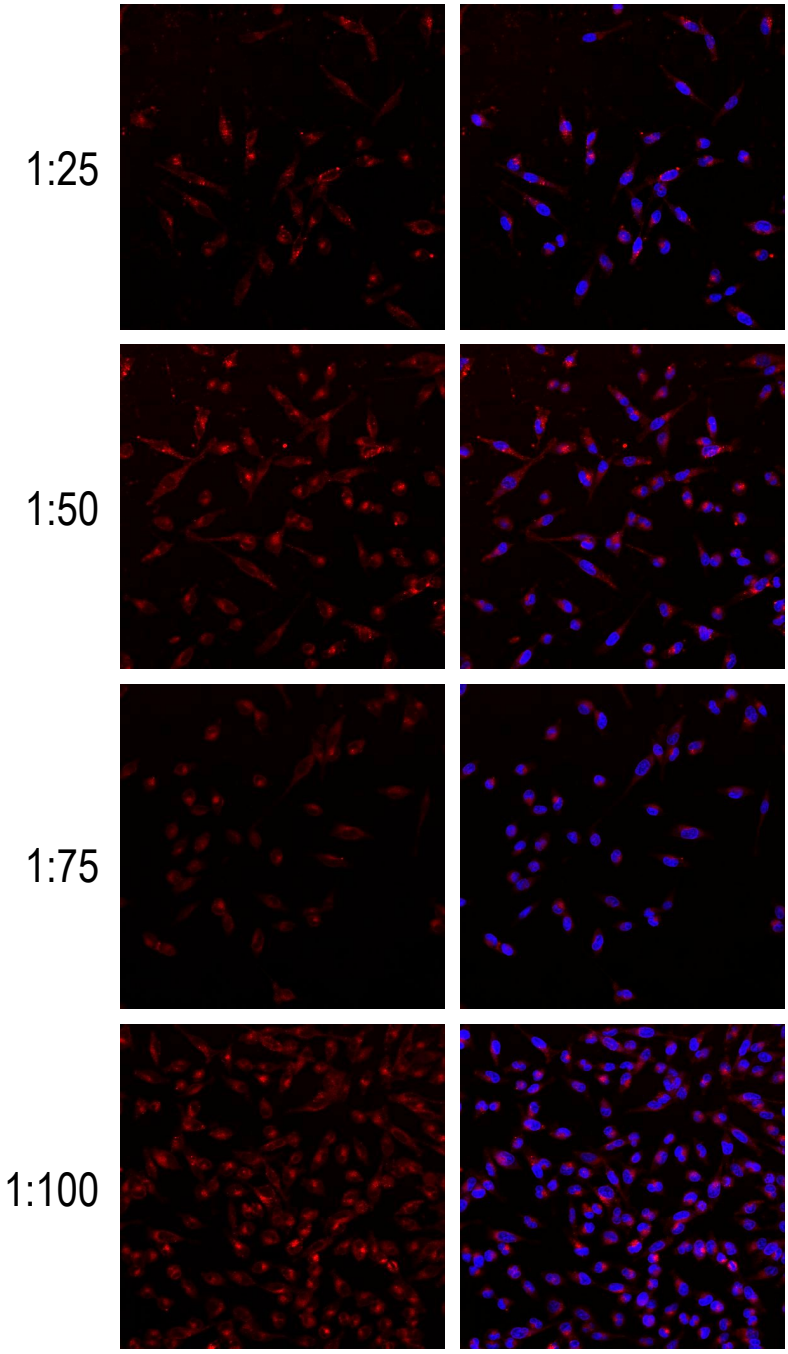

Figure 2.15. HeLa cells were incubated with 5 wt. % Rhodamine B loaded nanogels with a final dye concentration of 23 ng/μL and incubated 3 hr. HeLa cells were fixed using PFA and the nucleus stained with DAPI. Images taken on a confocal microscope at 40X magnification and images were analyzed using ImageJ.

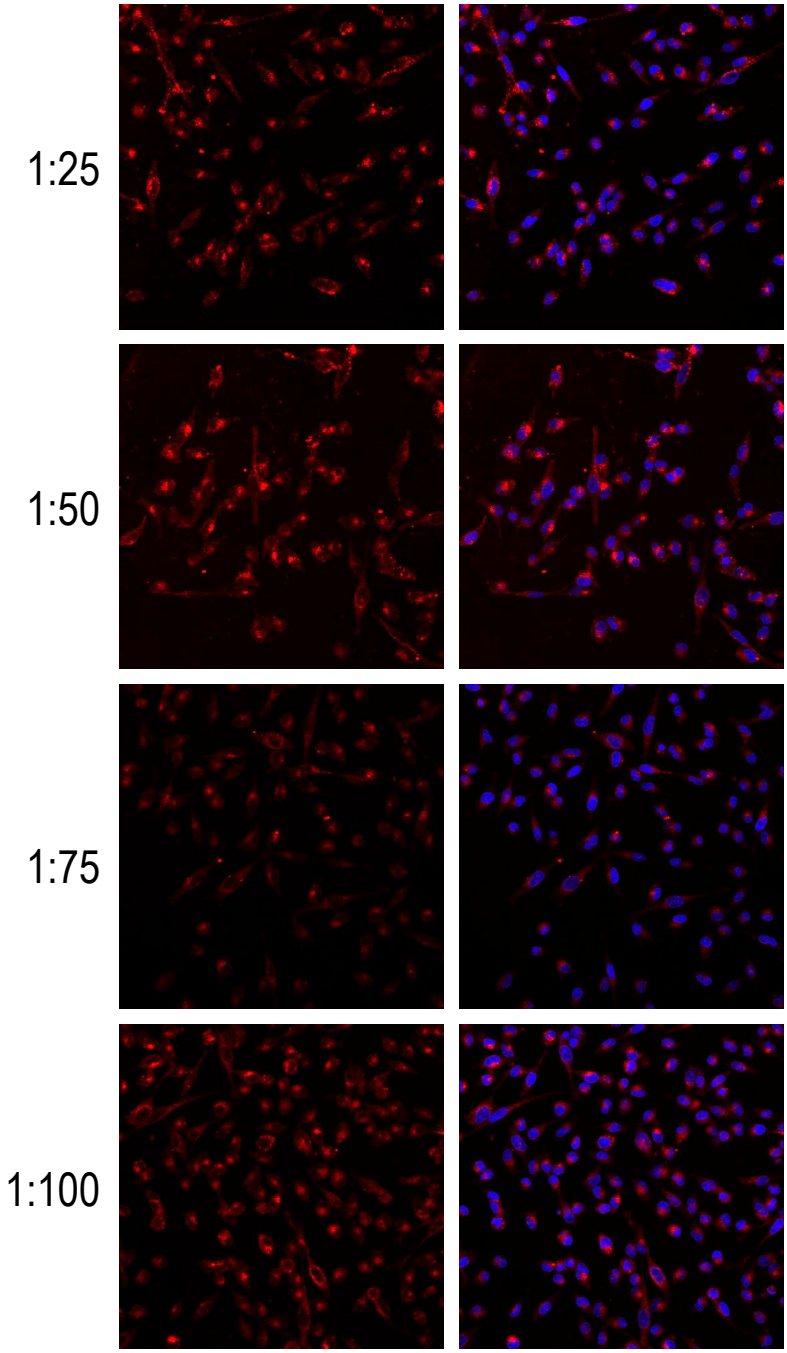

Figure 2.16. HeLa cells were incubated with 5 wt. % Rhodamine B loaded nanogels with a final dye concentration of 23 ng/μL and incubated 6 hr. HeLa cells were fixed using PFA and the nucleus stained with DAPI. Images taken on a confocal microscope at 40X magnification and images were analyzed using ImageJ.

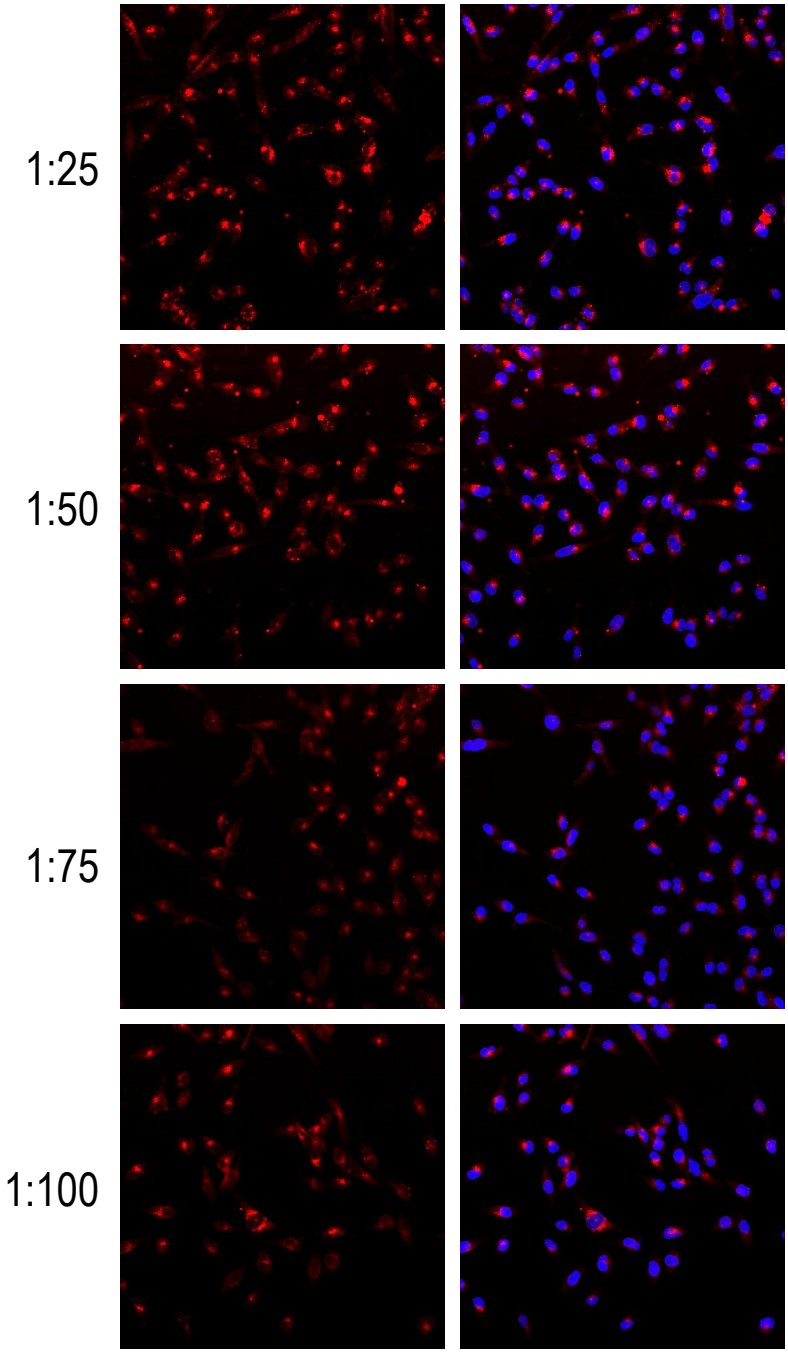

Figure 2.17. HeLa cells were incubated with 5 wt. % Rhodamine B loaded nanogels with a final dye concentration of 23 ng/μL and incubated 15 hr. HeLa cells were fixed using PFA and the nucleus stained with DAPI. Images taken on a confocal microscope at 40X magnification and images were analyzed using ImageJ.

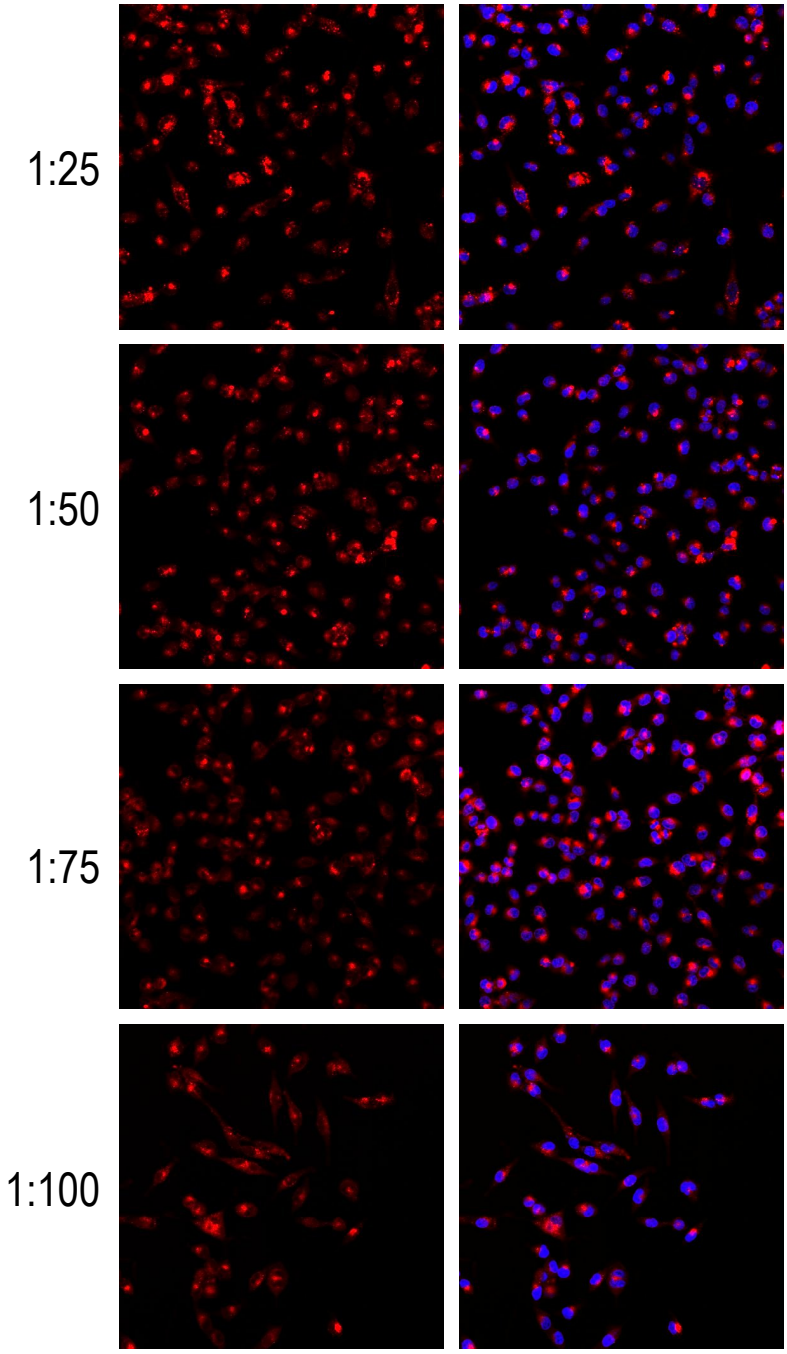

Figure 2.18. HeLa cells were incubated with 5 wt. % Rhodamine B loaded nanogels with a final dye concentration of 23 ng/μL and incubated 24 hr. HeLa cells were fixed using PFA and the nucleus stained with DAPI. Images taken on a confocal microscope at 40X magnification and images were analyzed using ImageJ.

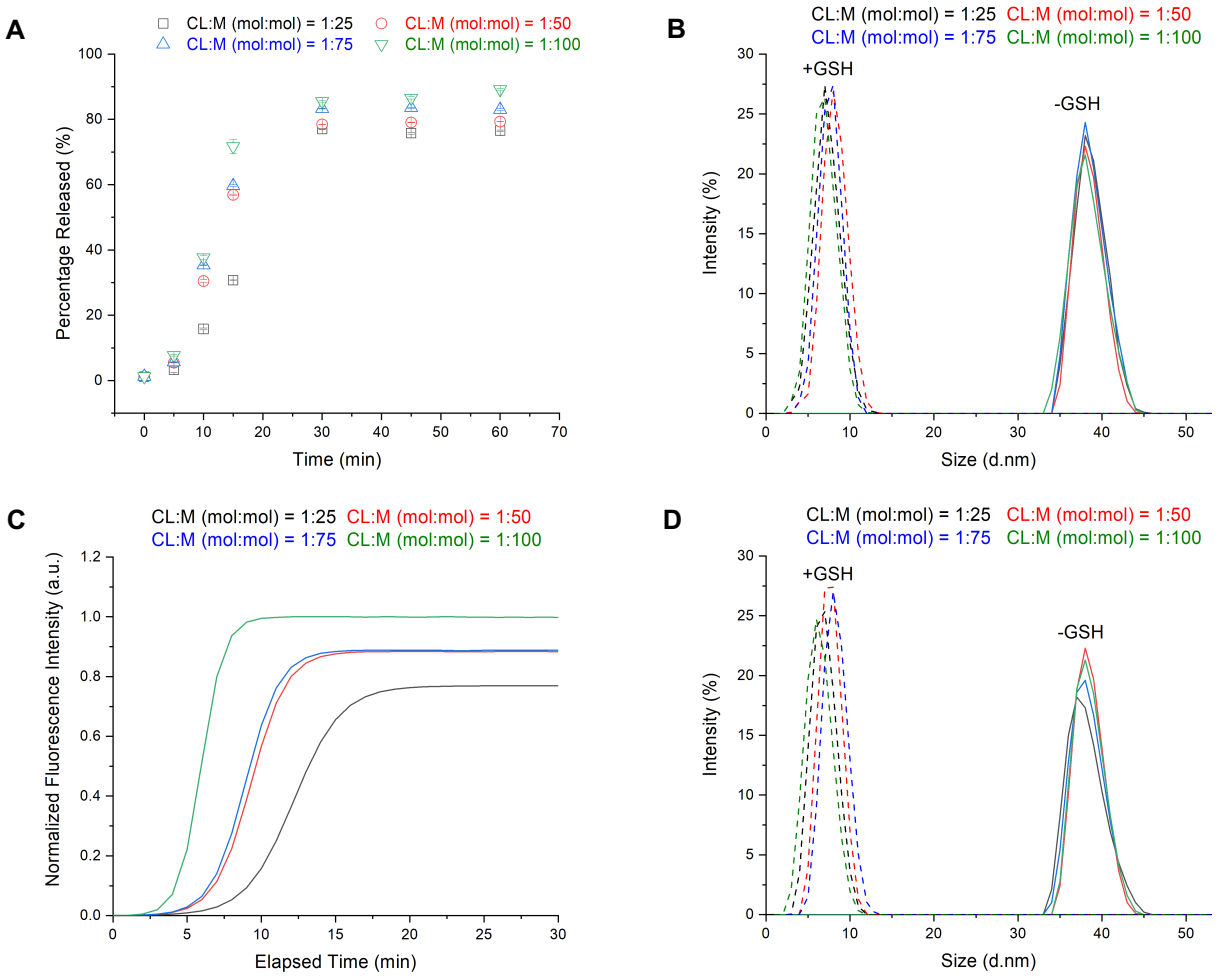

Figure 2.19. (**A**) Change in fluorescence intensity over time as nanogels loaded with rhodamine dye degraded in 11 mM GSH and (**B**) respective hydrodynamic diameters. (**C**) Change in normalized fluorescence intensity over elapsed time and (**D**) respective hydrodynamic diameters.

2.4 CONCLUSION

This chapter described the synthesis of fully degradable disulfide cross-linked nanogel drug carriers formed by oxidative radical polymerization of 2,2'-(ethylenedioxy)diethanethiol (EDDET) as a monomer with different cross-linkers, including pentaerythritol tetramercaptoacetate (PETMA). Because the poly(EDDET) backbone repeat structure and cross-linking junctions are composed entirely of disulfide bonds, these nanogels specifically degraded to small molecule dithiols intracellularly in response to the reducing agent glutathione present inside of cells. Cross-linked nanogels were synthesized using controlled microfluidic mixing in the presence of a nonionic Pluronic surfactant PLU-127 to increase the nanogel stability. Adjusting the monomer to cross-linker ratio from 1:5 to 1:100 (mol/mol) tuned the cross-linking density, resulting in swelling ratios from 1.65 to >3. Increasing the amount of stabilizing Pluronic F-127 surfactant resulted in a decrease of nanogel diameter, as expected due to increased surface area of the resulting nanogels. The monomer to cross-linker ratio in the feed had no effect on the formed nanogel diameter, providing a way to control cross-linking density with constant nanogel size but tunable drug release kinetics. Nanogels exhibited an entrapment efficiency of up to 75% for loading of Rhodamine B dye. *In vitro* studies showed low cytotoxicity, quick uptake, and fast degradation kinetics. Due to the ease of synthesis, rapid gelation times, and tunable functionality, these non-toxic and fully degradable nanogels offer excellent potential for use in a variety of drug delivery applications. Future experiments include incorporating amino thiols for mRNA delivery, where though therapeutics based on mRNA have broad potential in applications such as protein replacement therapy, cancer immunotherapy, and genomic engineering, their effective intracellular delivery remains a challenge.

2.5 BIBLIOGRAPHY

1 Anselmo, A. C. & Mitragotri, S. An Overview of Clinical and Commercial Impact of Drug Delivery Systems. *J. Control. Release* **190**, 15-28, (2014).

2 Davis, M. E., Chen, Z. G. & Shin, D. M. Nanoparticle therapeutics: an emerging treatment modality for cancer. *Nat. Rev. Drug Discov.* **7**, 771-782, (2008).

3 Jain, R. K. & Stylianopoulos, T. Delivering nanomedicine to solid tumors. *Nat. Rev. Clin. Oncol.* **7**, 653-664, (2010).

4 Peer, D., Karp, J. M., Hong, S., Farokhzad, O. C., Margalit, R. & Langer, R. Nanocarriers as an emerging platform for cancer therapy. *Nat. Nanotechnol.* **2**, 751-760, (2007).

5 Cheng, W., Gu, L., Ren, W. & Liu, Y. Stimuli-responsive polymers for anti-cancer drug delivery. *Mater. Sci. Eng. C Mater. Biol. Appl.* **45**, 600-608, (2014).

6 Kanasty, R., Dorkin, J. R., Vegas, A. & Anderson, D. Delivery materials for siRNA therapeutics. *Nat. Mater.* **12**, 967-977, (2013).

7 Lu, Y., Sun, W. & Gu, Z. Stimuli-responsive nanomaterials for therapeutic protein delivery. *J. Control. Release* **194**, 1-19, (2014).

8 Sun, W., Ji, W., Hu, Q. & Gu, Z. Leveraging physiology for precision drug delivery. *Physiol. Rev.* **97**, 189-225, (2017).

9 Albertsson, A. C. & Varma, I. K. Aliphatic polyesters: Synthesis, properties and applications. *Adv. Polym. Sci.* **157**, 1-40, (2002).

10 Tian, H., Tang, Z., Zhuang, X., Chen, X. & Jing, X. Biodegradable synthetic polymers: Preparation, functionalization and biomedical application. *Prog. Polym. Sci.* **37**, 237-280, (2012).

11 Bang, E.-K., Lista, M., Sforazzini, G., Sakai, N. & Matile, S. Poly(disulfide)s. *Chem. Sci.* **3**, 1752-1763, (2012).

12 Cheng, R., Feng, F., Meng, F., Deng, C., Feijen, J. & Zhong, Z. Glutathione-responsive nano-vehicles as a promising platform for targeted intracellular drug and gene delivery. *J. Control. Release* **152**, 2-12, (2011).

13 Schafer, F. Q. & Buettner, G. R. Redox environment of the cell as viewed through the redox state of the glutathione disulfide/glutathione couple. *Free Radic. Biol. Med.* **30**, 1191-1212, (2001).

14 Estrela, J. M., Ortega, A. & Obrador, E. Glutathione in cancer biology and therapy. *Crit. Rev. Clin. Lab Sci.* **43**, 143-181, (2006).

15 Djuric, Z., Malviya, V. K., Deppe, G., Malone, J. M., McGunagle, D. L., Heilbrun, L. K., Reading, B. A. & Lawrence, W. D. Detoxifying enzymes in human ovarian tissues: comparison of normal and tumor tissues and effects of chemotherapy. *J. Cancer Res. Clin. Oncol.* **116**, 379-383, (1990).

16 Balendiran, G. K., Dabur, R. & Fraser, D. The role of glutathione in cancer. *Cell Biochem. Funct.* **22**, 343-352, (2004).

17 Franco, R., Schoneveld, O. J., Pappa, A. & Panayiotidis, M. I. The central role of glutathione in the pathophysiology of human diseases. *Arch. Physiol. Biochem.* **113**, 234-258, (2007).

18 Valko, M., Leibfritz, D., Moncol, J., Cronin, M. T., Mazur, M. & Telser, J. Free radicals and antioxidants in normal physiological functions and human disease. *Int. J. Biochem. Cell Biol.* **39**, 44-84, (2007).

19 Wang, Y. C., Li, Y., Sun, T. M., Xiong, M. H., Wu, J., Yang, Y. Y. & Wang, J. Core-shell-corona micelle stabilized by reversible cross-linkage for intracellular drug delivery. *Macromol. Rapid Commun.* **31**, 1201-1206, (2010).

20 Lv, L.-P., Xu, J.-P., Liu, X.-S., Liu, G.-Y., Yang, X. & Ji, J. Disulfide-Crosslinked Biomimetic Micelles: Formation, Thiol Reactivity and Cytotoxicity Behavior. *Macromol. Chem. Phys.* **211**, 2292-2300, (2010).

21 Koo, A. N., Lee, H. J., Kim, S. E., Chang, J. H., Park, C., Kim, C., Park, J. H. & Lee, S. C. Disulfide-cross-linked PEG-poly(amino acid)s copolymer micelles for glutathione-mediated intracellular drug delivery. *Chem. Commun. (Camb)*, 6570-6572, (2008).

22 Zhang, A., Zhang, Z., Shi, F., Ding, J., Xiao, C., Zhuang, X., He, C., Chen, L. & Chen, X. Disulfide crosslinked PEGylated starch micelles as efficient intracellular drug delivery platforms. *Soft. Matter.* **9**, 2224-2233, (2013).

23 Oh, J. K., Siegwart, D. J., Lee, H. I., Sherwood, G., Peteanu, L., Hollinger, J. O., Kataoka, K. & Matyjaszewski, K. Biodegradable nanogels prepared by atom transfer radical polymerization as potential drug delivery carriers: Synthesis, biodegradation, in vitro release, and bioconjugation. *J. Am. Chem. Soc.* **129**, 5939-5945, (2007).

24 Oh, J. K., Siegwart, D. J. & Matyjaszewski, K. Synthesis and biodegradation of nanogels as delivery carriers for carbohydrate drugs. *Biomacromolecules* **8**, 3326-3331, (2007).

25 Oh, J., Drumright, R., Siegwart, D. & Matyjaszewski, K. The development of microgels/nanogels for drug delivery applications. *Prog. Polym. Sci.* **33**, 448-477, (2008).

26 Siegwart, D. J., Srinivasan, A., Bencherif, S. A., Karunanidhi, A., Oh, J. K., Vaidya, S., Jin, R., Hollinger, J. O. & Matyjaszewski, K. Cellular uptake of functional nanogels

prepared by inverse miniemulsion ATRP with encapsulated proteins, carbohydrates, and gold nanoparticles. *Biomacromolecules* **10**, 2300-2309, (2009).

27 Siegwart, D. J., Oh, J. K. & Matyjaszewski, K. ATRP in the design of functional materials for biomedical applications. *Prog. Polym. Sci.* **37**, 18-37, (2012).

28 Hu, X., Zhang, Y., Xie, Z., Jing, X., Bellotti, A. & Gu, Z. Stimuli-Responsive Polymersomes for Biomedical Applications. *Biomacromolecules* **18**, 649-673, (2017).

29 Kataoka, K., Harada, A. & Nagasaki, Y. Block copolymer micelles for drug delivery: design, characterization and biological significance. *Adv. Drug. Deliv. Rev.* **47**, 113-131, (2001).

30 Cheng, W., Kumar, J. N., Zhang, Y. & Liu, Y. pH- and redox-responsive poly(ethylene glycol) and cholesterol-conjugated poly(amido amine)s based micelles for controlled drug delivery. *Macromol. Biosci.* **14**, 347-358, (2014).

31 Sun, Y., Yan, X., Yuan, T., Liang, J., Fan, Y., Gu, Z. & Zhang, X. Disassemblable micelles based on reduction-degradable amphiphilic graft copolymers for intracellular delivery of doxorubicin. *Biomaterials* **31**, 7124-7131, (2010).

32 Luo, P., Luo, Y., Huang, J., Lu, W., Luo, D., Yu, J. & Liu, S. Incorporation of camptothecin into reduction-degradable supramolecular micelles for enhancing its stability. *Colloids Surf. B Biointerfaces* **109**, 167-175, (2013).

33 Liu, J., Pang, Y., Huang, W., Zhu, Z., Zhu, X., Zhou, Y. & Yan, D. Redox-Responsive Polyphosphate Nanosized Assemblies: A Smart Drug Delivery Platform for Cancer Therapy. *Biomacromolecules* **12**, 2407-2415, (2011).

34 Navath, R. S., Wang, B., Kannan, S., Romero, R. & Kannan, R. M. Stimuli-responsive star poly(ethylene glycol) drug conjugates for improved intracellular delivery of the drug in neuroinflammation. *J. Control. Release* **142**, 447-456, (2010).

35 Tsarevsky, N. V. & Matyjaszewski, K. Reversible Redox Cleavage/Coupling of Polystyrene with Disulfide or Thiol Groups Prepared by Atom Transfer Radical Polymerization. *Macromolecules* **35**, 9009-9014, (2002).

36 Paulusse, J. M., Amir, R. J., Evans, R. A. & Hawker, C. J. Free radical polymers with tunable and selective bio- and chemical degradability. *J. Am. Chem. Soc.* **131**, 9805-9812, (2009).

37 Chang, C.-C. & Emrick, T. Functional Polyolefins Containing Disulfide and Phosphoester Groups: Synthesis and Orthogonal Degradation. *Macromolecules* **47**, 1344-1350, (2014).

38 Rosenthal-Kim Emily, Q. & Puskas Judit, E. in *Pure Appl. Chem.* Vol. 84 2121 (2012).

39 Ballinger, P. & Long, F. A. Acid ionization constants of alcohols. II. Acidities of some substituted methanols and related compounds. *J. Am. Chem. Soc.* **82**, 795-798, (1960).

40 Bang, E. K., Gasparini, G., Molinard, G., Roux, A., Sakai, N. & Matile, S. Substrate-initiated synthesis of cell-penetrating poly(disulfide)s. *J. Am. Chem. Soc.* **135**, 2088-2091, (2013).

41 Gasparini, G., Bang, E.-K., Molinard, G., Tulumello, D. V., Ward, S., Kelley, S. O., Roux, A., Sakai, N. & Matile, S. Cellular Uptake of Substrate-Initiated Cell-Penetrating Poly(disulfide)s. *J. Am. Chem. Soc.* **136**, 6069-6074, (2014).

42 Chuard, N., Gasparini, G., Roux, A., Sakai, N. & Matile, S. Cell-penetrating poly(disulfide)s: the dependence of activity, depolymerization kinetics and intracellular localization on their length. *Org. Biomol. Chem.* **13**, 64-67, (2015).

43 Gasparini, G., Sargsyan, G., Bang, E. K., Sakai, N. & Matile, S. Ring Tension Applied to Thiol-Mediated Cellular Uptake. *Angew. Chem. Int. Edit.* **54**, 7328-7331, (2015).

44 Son, S., Namgung, R., Kim, J., Singha, K. & Kim, W. J. Bioreducible polymers for gene silencing and delivery. *Acc. Chem. Res.* **45**, 1100-1112, (2012).

45 Fu, J., Yu, C., Li, L. & Yao, S. Q. Intracellular Delivery of Functional Proteins and Native Drugs by Cell-Penetrating Poly(disulfide)s. *J. Am. Chem. Soc.* **137**, 12153-12160, (2015).

46 Holmgren, A. & Bjornstedt, M. Thioredoxin and thioredoxin reductase. *Methods Enzymol.* **252**, 199-208, (1995).

47 Sui, X., Feng, X., Hempenius, M. A. & Vancso, G. J. Redox active gels: synthesis, structures and applications. *J. Mater. Chem. B* **1**, 1658-1672, (2013).

48 Zhang, H., Zhai, Y., Wang, J. & Zhai, G. New progress and prospects: The application of nanogel in drug delivery. *Mater. Sci. Eng. C Mater. Biol. Appl.* **60**, 560-568, (2016).

49 Yang, S., Tang, Z., Zhang, D., Deng, M. & Chen, X. pH and redox dual-sensitive polysaccharide nanoparticles for the efficient delivery of doxorubicin. *Biomaterials Sci.* **5**, 2169-2178, (2017).

50 Curcio, M., Diaz-Gomez, L., Cirillo, G., Concheiro, A., Iemma, F. & Alvarez-Lorenzo, C. pH/redox dual-sensitive dextran nanogels for enhanced intracellular drug delivery. *Eur. J. Pharm. Biopharm.* **117**, 324-332, (2017).

51 Zhang, X. & Waymouth, R. M. 1,2-Dithiolane-Derived Dynamic, Covalent Materials: Cooperative Self-Assembly and Reversible Cross-Linking. *J. Am. Chem. Soc.* **139**, 3822-3833, (2017).

52 Cheng, X., Jin, Y., Qi, R., Fan, W., Li, H., Sun, X. & Lai, S. Dual pH and oxidation-responsive nanogels crosslinked by diselenide bonds for controlled drug delivery. *Polymer* **101**, 370-378, (2016).

53 Li, Y. L., Zhu, L., Liu, Z., Cheng, R., Meng, F., Cui, J. H., Ji, S. J. & Zhong, Z. Reversibly stabilized multifunctional dextran nanoparticles efficiently deliver doxorubicin into the nuclei of cancer cells. *Angew. Chem. Int. Edit.* **48**, 9914-9918, (2009).

CHAPTER THREE

PROGRESS TOWARDS THE SYNTHESIS OF AMINO POLYESTERS VIA RING-OPENING POLYMERIZATION (ROP) OF FUNCTIONAL LACTONES

REVIEW OF THE LITERATURE

3.1 PREFACE

The focus on my thesis work was on the synthesis and application of poly(disulfide)s. In addition to disulfide bonds, esters are another attractive functional group for creation of degradable polymers for drug delivery. In this chapter, I will review the history and state-of-the-art in the synthesis of functional polyesters that can be used in drug and gene delivery.

3.2 INTRODUCTION

Aliphatic polyesters have been widely used in biomedical applications due to their superior biocompatibility and biodegradability.[1] Introduction of functional groups to the polyester backbone allows tailoring of the physical and chemical properties and permits conjugation of different chemical moieties. Synthesizing polyesters via ring opening polymerization (ROP) is the preferred approach, where generating homo- and block-copolymers directly with controlled molecular weight and narrow polydispersity index (PDI) is possible. Though polyesters with various functional groups have been prepared and reviewed extensively,[2-7] there are limited reports on synthesizing amine-functionalized polyesters via ROP due to synthetic challenges and potential incompatibility of basic amines and esters. Yet, the amine group is an important functionality for bioconjugation with bio-related molecules such as drugs, peptides, and proteins. Positive charges are also essential to complex negatively charged nucleic acids (pDNA, siRNA, miRNA, mRNA, etc.) for gene therapy applications. Cationic polymers have been widely used in gene delivery to form polyplexes and assemble nanoparticles with nucleic acids.[8,9] Given that polyesters, notably polylactide (PLA), polyglycolic acid (PLGA), polycaprolactone (PCL), and their copolymers are

the definitive polymers used in a variety of clinically approved applications,[10-15] it is critical to review this field and aid the design of novel and facile approaches to synthesize amino polyesters.

Functional polyesters prepared by ROP are typically synthesized via (*a*) polymerization of functional lactone monomers, (*b*) post-polymerization modification reactions, or a combination of (*a*) and (*b*) (**Scheme 3.1**). Lactones are important not only as polymerization monomers, but also for their role in organic syntheses.[16] The strong advantage of using functional lactones (*route a*) is the ability to directly obtain functional polyesters in a single step with 100% grafting efficiency and without further purification needed. Grafting functional groups onto a pre-formed polymer chain is an appealing approach, where a wide range of functional groups can be attached using a single precursor polymer; however, isolation and purification of polymer at each additional step can be challenging. Also, it is hard to achieve 100% grafting efficiency, and the chance of catalyst or impurity contamination and polymer backbone degradation are increased as well. Combining polymerization of functionalized lactones and post-polymerization modification is another route that integrates the advantages of both *route a* or *b* though challenges faced with *route b* are not significantly reduced. To date, most amino polyesters have been synthesized using *route c*, where the amino moieties are introduced to the polyester backbone via post-polymerization modification. This was due to the fact that amines are weak nucleophiles and are relatively incompatible with ester bonds and/or catalysts. Thus, in this chapter, examples of protected amine and post-polymerization strategies will be primarily discussed. At the end, work described in Chapter 4 will be previewed where tertiary amine-functionalized lactone monomers and polymers were synthesized, as these are the most relevant functional groups for drug and gene delivery applications.

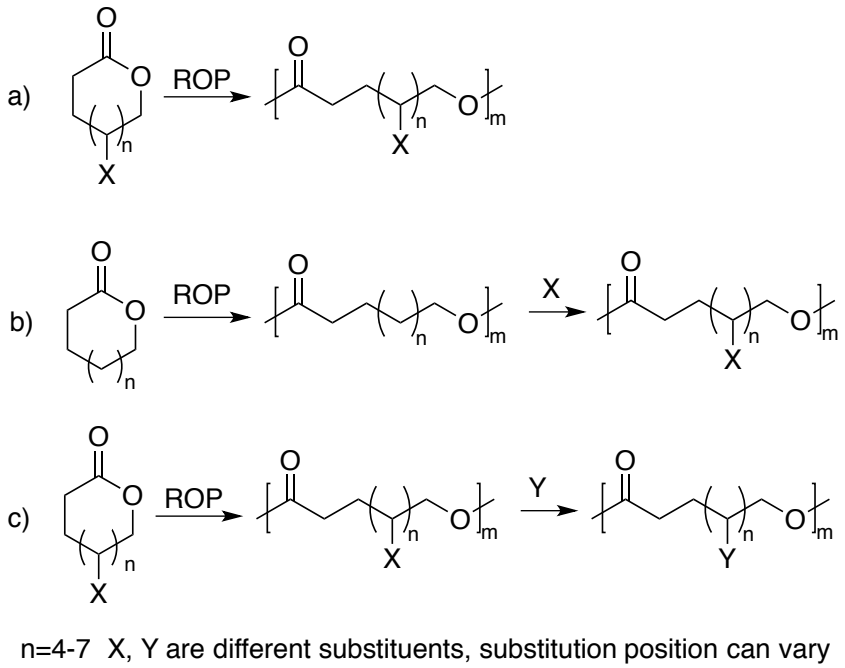

Scheme 3.1. General strategies for engineering functional polyesters via ROP a) ROP of lactone monomers substituted with various functional groups; b) Direct grafting functional groups onto polyester backbones; c) Combining polymerization of functional lactone monomers and post-polymerization modification.

3.3 POLYMERIZATION OF LACTONE MONOMERS WITH UNPROTECTED AMINE FUNCTIONALITIES

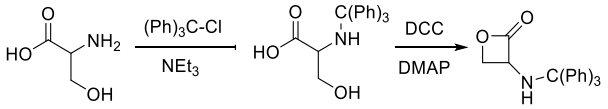

Scheme 3.2. Synthesis of β–malolactones from L-serine.

Prior to the work described in Chapter 4,[17] to the best of our knowledge, the only synthesis of unprotected amine-functionalized lactone monomers was by Fiétier et al. in 1990.[18] The lactone monomer was synthesized via cyclization to form ester bonds, which is one of the most common methods to make functionalized lactones.[4] The *N*-tritylated L-serine β-propiolactone monomer was synthesized by tritylation of the amine with triphenylchloromethane followed by cyclization with dicyclohexylcarbodiimide (DCC) and 4-(dimethylamino)pyridine (DMAP) (**Scheme 3.2**). Homopolymerization of the monomer was studied using a tetrabutylammonium acetate initiator at different temperatures, which resulted in the isolation of poly(*N*-tritylated L-serine) with narrow polydispersity index. Deprotection of the trityl group was attempted with trifluoroacetic acid, but degradation of the polymer backbone was observed.

3.4 SYNTHESIS OF AMINO FUNCTIONALIZED POLYESTERS VIA POST-POLYMERIZATION MODIFICATION OF FUNCTIONALIZED MONOMERS

As one approach, lactone monomers with protected amine or amide functionalities can be synthesized first, and the protecting group can be removed after polymerization to introduce primary amine functionality. In 2010, Coudane et al., developed a novel carbamic acid benzyl ester functionalized valerolactone monomer, 5-Z-amino-δ-valerolactone (5-NHZ-VL) (**Scheme 3.3**).[19] The monomer was cyclized via acid catalyzed transesterfication. This monomer was polymerized to give poly(5-NHZ-VL) with a molecular weight of 7000 g/mol, which was further deprotected under acidic condition to generate poly(5-NH_3^+-VL) without degradation of the polymer backbone. Furthermore, this monomer was copolymerized with caprolactone and subsequently deprotected to generate a series of copolymers with amino content from 10 to 100% in the final polymer.[20] Results indicated that these copolymers were biocompatible, exhibited amphiphilic properties, and were able to solubilize highly hydrophobic compounds.

In 2011, Lang et al. synthesized a similar monomer, γ-(carbamic acid benzyl ester)-3-caprolactone (CABCL) via another common ring-expansion strategy,[4] which covers three steps. Cyclohexanol, as a starting material, was functionalized first, and then was oxidized to the ketone. The lactone was obtained by reacting mCPBA with the functionalized ketone via Bayer-Villiger Oxidation in the last step, a series copolymers were prepared by ROP (**Scheme 3.4**). Hydrogenation converted the copolymer side chains to free amino groups, which were used for (bio)conjugation with fluorescein isothiocyanate (FITC) dye molecules.[21,22] The FITC conjugated block copolymers formed micelles and *in vitro* studies revealed that these micelles were

biocompatible and could be internalized into fibroblast cells, hence collectively proving their potential biomedical and pharmaceutical applications.

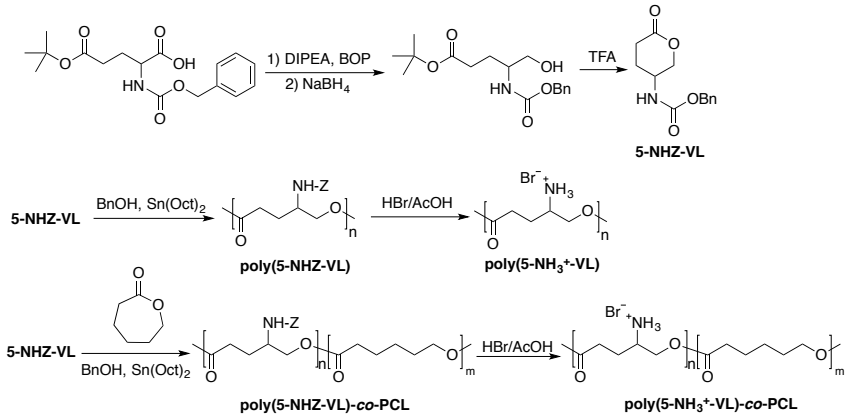

Scheme 3.3. Synthesis of 5-Z-amino-δ-valerolactone (5-NHZ-VL), poly(5-NH_3^+-VL), and poly((5-NH_3^+-VL)-*co*-CL).

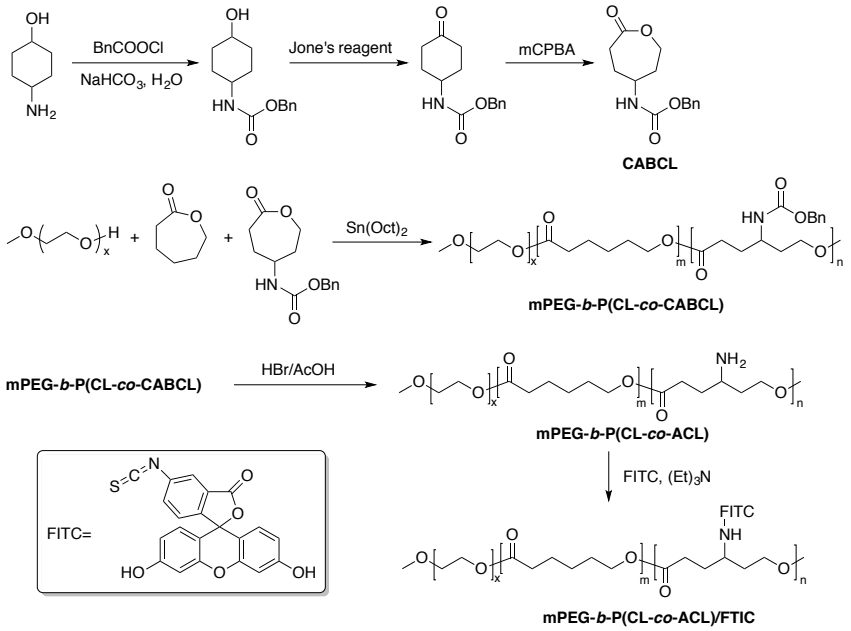

Scheme 3.4. Synthetic routes for the monomer γ-(carbamic acid benzyl ester)-ε-caprolactone (CABCL), block copolymers mPEG-*b*-P(CL-*co*-CABCL), mPEG-*b*-P(CL-*co*-ACL) and FITC-labeled mPEG-*b*-P(CL-*co*-ACL).

As a second, distinct approach, functional monomers with non-amino functionalities can be polymerized, and amine groups can be appended afterwards. In 2009, Coudane et al. synthesized a novel monomer α-iodo-ε-caprolactone (αIεCL). The monomer was synthesized via an anionic activation plus electrophilic substitution strategy,[4] which is a general strategy for the synthesis of the majority of the monomers discussed in this section. The monomer was obtained by abstracting an α H of the lactone first with a strong base (LDA) under lower temperature (-78 °C) and attaching an electrophile I^+ to the same α position afterwards. The monomer was copolymerized with caprolactone to produce poly(α-iodo-ε-caprolactone-*co*-ε-caprolactone) (**Scheme 3.5**).[23] This polymer was further modified into poly(α-amino-ε-caprolactone-*co*-ε-caprolactone) by two different strategies. The first route was the reaction of poly(αIεCL-*co*-εCL) with ammonia and the second route was the reduction of poly(αN3εCL-*co*-εCL) by hydrogenolysis. This method established a new way to synthesize cationic and water-soluble amino PCL-based degradable polyesters.

In 2008, Xiong et al. synthesized a novel monomer via a similar strategy. A different electrophile, benzyl chloroformate, was attached to the α position. A novel class of biodegradable poly(ethylene oxide-*b*-caprolactone) copolymers were synthesized from the monomer. The PCL blocks were substituted with polyamine groups, such as spermine (SP), tetraethylenepentamine (TP), or *N*,*N*-dimethyldipropylenetriamine (DP) (**Scheme 3.6**).[24] The family of polymers self-assembled into polyion complex micelles, which were evaluated for the encapsulation and delivery of siRNA. All three polymers bound siRNA, formed micelles, and shielded siRNA from nuclease degradation. MDR-1-targeted siRNA formulated in PEO-*b*-P(CL-*g*-SP) and PEO-*b*-P(CL-*g*-TP) micelles exhibited efficient cellular update and effective gene silencing of P-gp expression.[24]

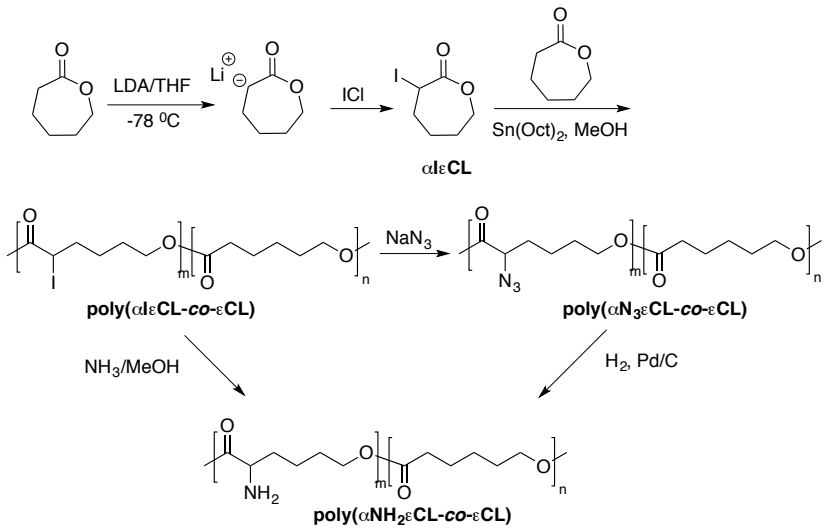

Scheme 3.5. Synthetic pathway for the preparation of αIεCL, poly(αIεCL-*co*-εCL), poly(αN$_3$εCL-*co*-εCL), and poly(αNH$_2$εCL-*co*-εCL).

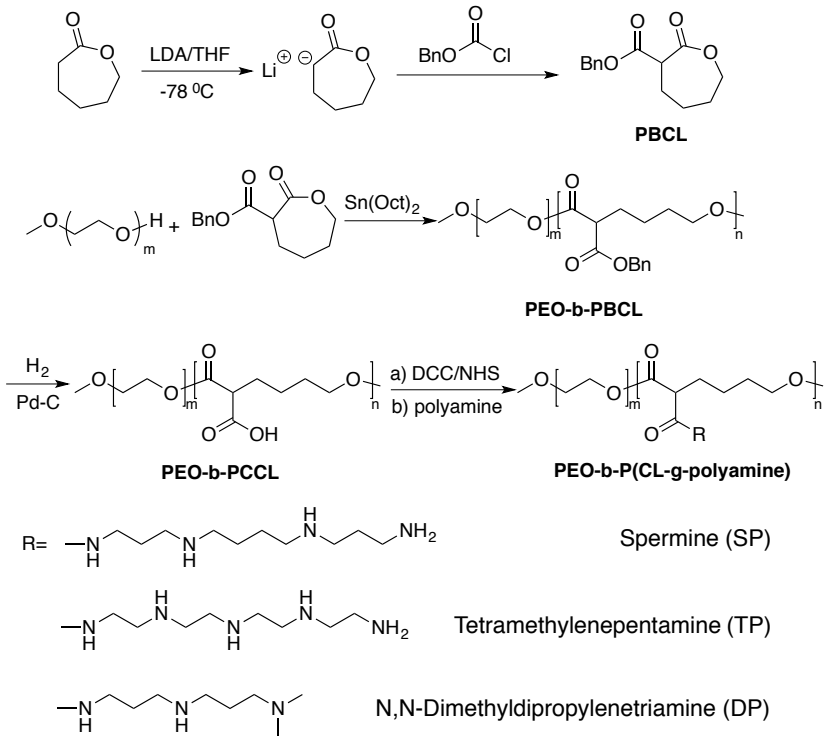

Scheme 3.6. Synthetic procedure for the preparation of PEO-b-PCL with grafted SP, TP, and DP.

In 2005, Jerome et al. synthesized azide substituted caprolactone. The monomer was copolymerized with caprolactone using the initiator 2,2-dibutyl-2-stanna-1,3-dioxepane (DSDOP), which works under a similar mechanism as with $Sn(Oct)_2$. The generated copolymer was further derivatized into tertiary amines, ammonium salts, and other functionalities via 1,3-Husgen cycloaddition under mild conditions, and no backbone degradation was observed (**Scheme 3.7**).[25] Although amino polyesters were not prepared, a number of other reports have explored the use of bromo-, chloro, and azido-functionalized lactones towards the synthesis of functional polyesters.[26-29]

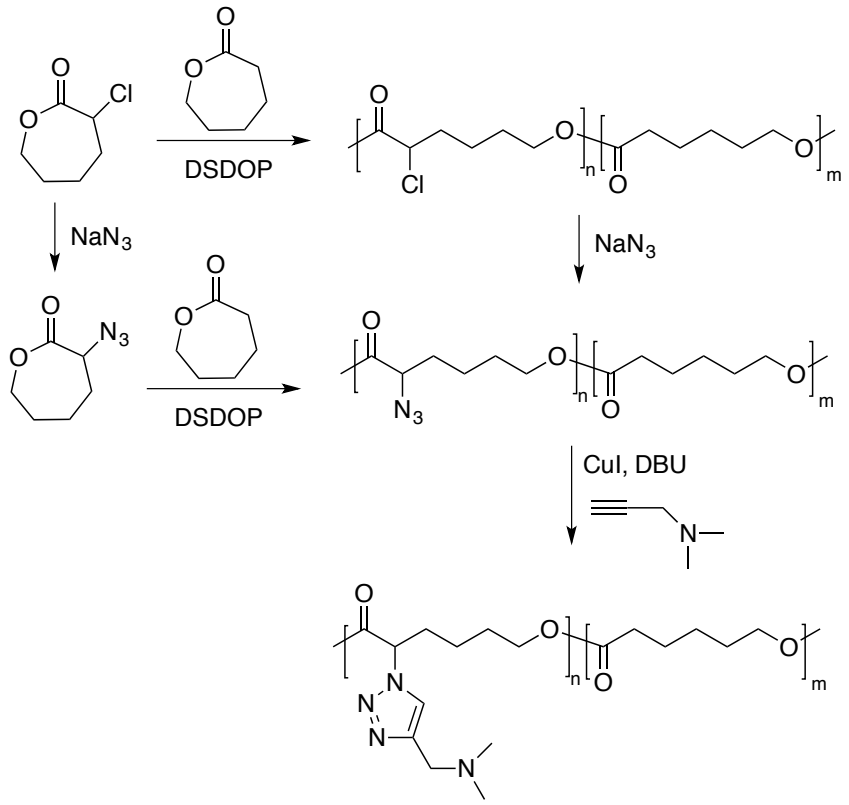

Scheme 3.7 Derivatization of PCL by combining ROP and "click" chemistry.

In 2008, Harth et al. synthesized copolymers from valerolactone, α-allyl-δ-valerolactone, and/or α-propargyl-δ-valerolactone and 2-oxepane-1,5-dione. Allyl functionality in the block copolymer was further oxidized to epoxide groups. The diamine 2,2'-(ethylenedioxy)bis(ethylamine) was used as a cross-linkers to react with epoxide units on the polymer chains and led to controlled preparation of amine cross-linked polyester nanoparticles. The size of the nanoparticles could be controlled by the number of epoxide units present on the polymers and the amount of diamine used during cross-linking (**Scheme 3.8**).[30]

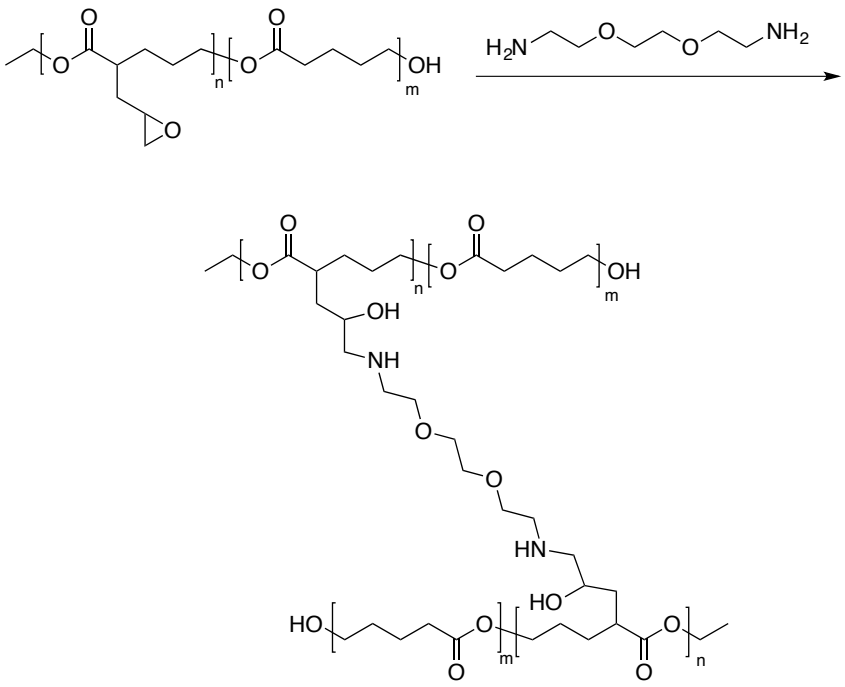

Scheme 3.8 Crosslinking of epoxide-functionalized polyvalerolactone copolymers with 2,2'-(ethylenedioxy)bis(ethylamine)

In 2011, Coudane et al. prepared novel amino polyeseters via thiol-ene addition (**Scheme 3.9**).[31] First, allyl functionalizd CL was synthesized and copolymerizaed with CL to generate copolymers. Then, a thiol-ene reaction of the alkene-functional PCL with 2-(Boc-amino)ethanethiol was used to generate polyesters bearing protected amino groups without chain degradation. Finally, water-soluble polyesters bearing free amino groups were recovered by cleavage of the Boc protecting group. Similarly, a number of other reports have explored the use of ene-functionalized lactones towards the synthesis of functional polyesters, even though amino-polyesters have not been prepared.[32-36] It is worth noting that this short review focuses exclusively on ROP of lactones and the resulting functional polyesters. Reports of functional polymers via step-growth polymerization,[37-42] amino functional polycarbonates,[43-46] and functional lactide derivatives[47,48] have greatly contributed to the field of drug and gene delivery.

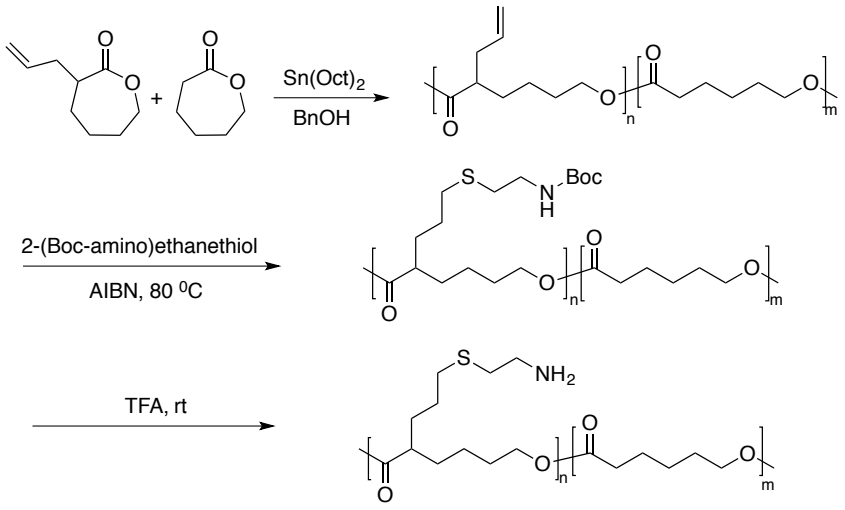

Scheme 3.9. General pathway for the synthesis of aminated poly(ε-caprolactone).

3.5 DESIGN OF NOVEL AMINO FUNCTIONALIZED LACTONE MONOMERS AND DIRECT SYNTHESIS OF AMINO POLYESTERS

To date, only a few methods to synthesize amino functionalized polyesters have been reported. Moreover, most synthetic routes involve multiple steps to access functional monomers, protection/deprotection after polymerization, with problems like partial conversion, and polymer chain degradation involved. Thus, there is an ongoing need to develop more efficient and robust chemical routes to directly synthesize amino polyesters. Among polymerization methods, direct ROP of functional monomers without protecting groups provides the best and most atom economical route towards functional polyesters. ROP offers the best control over polymerization length, polydispersity, and the ability to make block copolymers. The direct polymerization of functional monomers has the added advantage of 100% grafting efficiency with no purification needed after polymerization.

With those factors in mind, we were motivated to synthesize a new type of amine-functionalized lactone monomer via a facile synthetic approach (see Chapter 4). Because tertiary amines are more compatible with esters than primary and secondary amines with no protection needed, and tertiary amine with precise pKa and hydrophobic alkyl chains have been implicated as essential design components for gene delivery. We focused on those functional groups in our monomer design. We set out to achieve a number of challenging criteria: (1) Scalable (gram+) monomer synthesis (which to us prohibited the use of ring closure reactions); (2) Direct synthesis of amino polyesters (no protecting groups); (3) Tunable hydrophobicity and amine pKa; (4) 100% functional group incorporation efficiency; (5) No polyester degradation; and (6) Ability to form serum-stable nanoparticles for *in vivo* siRNA delivery. To pursue these goals, a library of 13 functional monomers via the one step reaction of aminothiols (or alkyl thiols) with 5,6-dihydro-

2H-pyran-2-one (DPO) that was scalable, robust, and easy to work up was synthesized. The chemistry for this work was inspired by research using DPO and related compounds.[7,49-51] Monomers can be synthesized within one hour upon mixing via the simple, catalyst free addition reaction. Homo- and random-(co)polymerizations were carried out in bulk and reached high monomer conversion (90% on average), which allowed for siRNA delivery screening directly without purification. Polymerization was completed within five minutes via anionic polymerization using methyl lithium as initiator. In total, we synthesized 139 copolymers with different monomer ratios and combinations (**Scheme 3.10**), which accomplished the goal of scalable and direct synthesis of amino polyesters.[17]

The synthesized library of polymers was formulated with siRNA, DSPC, cholesterol, PEG lipid into nanoparticles, exhibiting tunable sizes from 40 nm to 300 nm. These nanoparticles were evaluated for cytotoxicity and siRNA delivery efficacy *in vitro* to luciferase-expressing HeLa cancer cells. A clear structure-activity relationship (SAR) can be drawn from the resulting heat map (**Figure 3.1**). Results indicate that an ideal pKa (6.0-6.2) and a fine balance of charge and hydrophobicity must be reached to impart high delivery efficiency. These conclusions are in agreement with other literature reports concerning lipid- and polymer-mediated siRNA delivery.[52-54] Dose-response experiments indicated that >90% silencing can be reached at a dosage of only 2.4 nM for two of the copolymers which is more effective than RNAiMax under the same dose and conditions (only 18% silencing). *In vivo* studies of the lead polymer, N1C4 (2:2), nanoparticles in tumor-bearing mice demonstrated effective tumor uptake and high knockdown capability.

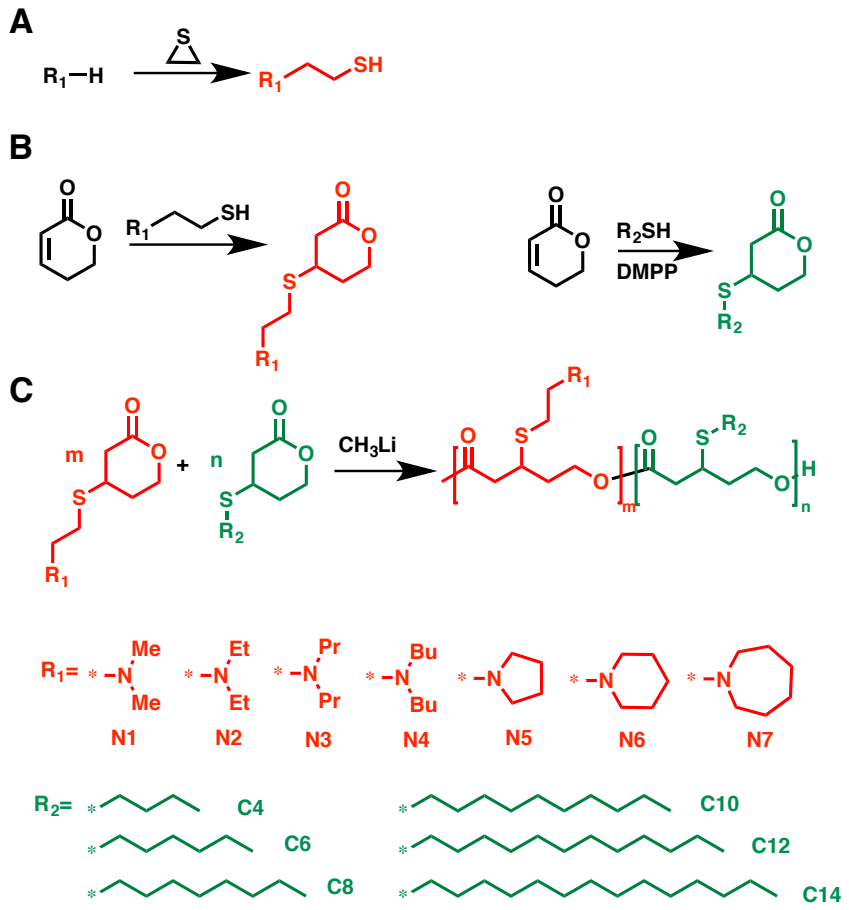

Scheme 3.10. (A) Synthesis of aminothiols (N1-N7). (B) One step monomer synthesis from commercially available DPO with aminothiols (N1-N7) and alkylthiols (C4-C14) (C) Combinatorial synthesis of a library of 139 lipocationic polyesters.

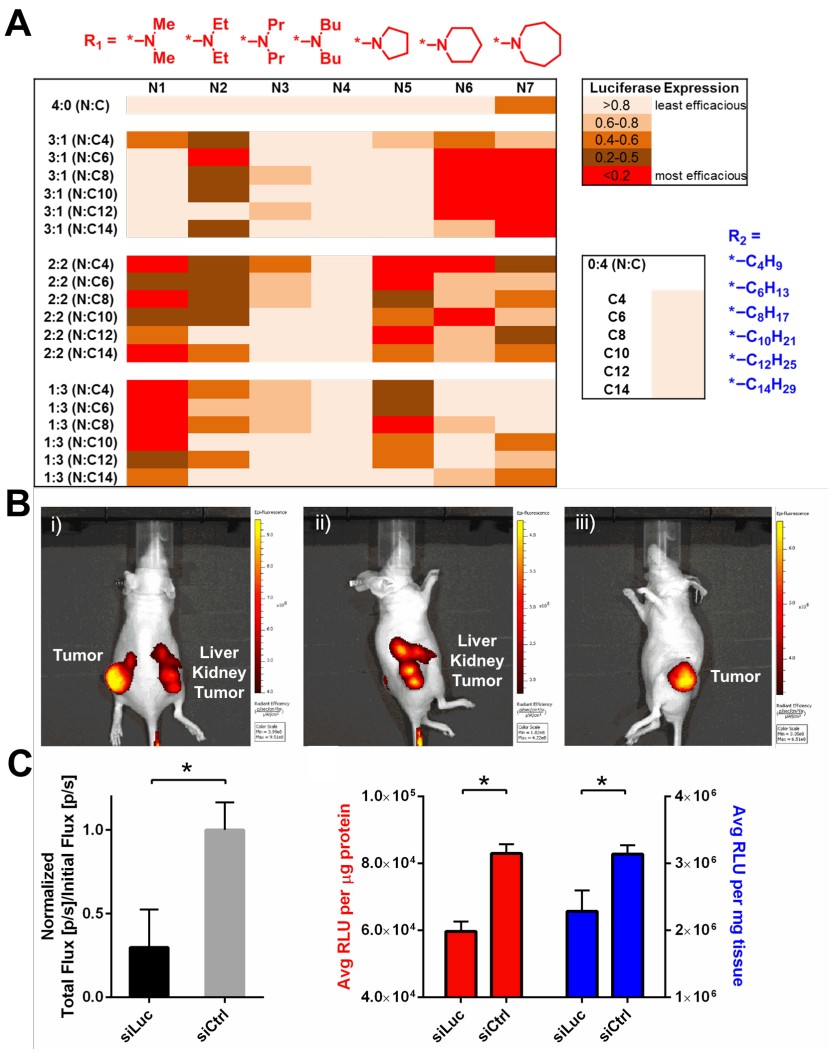

Figure 3.1 (A) Heat map showing *in vitro* siRNA delivery and structure− activity relationships (SAR) for the formulated polyester library in HelaLuc cells. (B) N1C4 (2:2) NPs provided effective accumulation in tumor xenografts after IV injection. A representative mouse is shown from three angles. (C) Luciferase silencing was measured in tumors 24 hours after injection by bioluminescence imaging or in tissue lysates normalized against total protein level or total tissue amount. Reprinted with permission from *J. Am. Chem. Soc.* **2015**, *137*, 9206. Copyright 2015 American Chemical Society.[17]

3.6 CONCLUSION

In conclusion, the synthesis of amino polyesters via ROP has been reviewed. Most of these polymers were synthesized via post polymerization modification due to the challenge of synthesizing amine functionalized lactone monomers. The discovery on synthesizing tertiary amine functionalized lactone monomers and polymers via a facile synthetic method and their applications in siRNA delivery was highlighted and is further described in Chapter 4. 139 polymers were synthesized in high yield, fast time (minutes), and gram scale. Precise monomer incorporation ratios were achieved to enable tunable hydrophobicity and pKa. NPs formulated with these polymers were able to enable gene silencing *in vitro* and *in vivo* at low doses. The versatility of this synthetic method may allow preparation of functional polyesters for a variety of applications and inspire development of even better reactions for the synthesis of amino polyesters.

3.7 BIBLIOGRAPHY

1 Albertsson, A.-C. & Varma, I. K. Recent Developments in Ring Opening Polymerization of Lactones for Biomedical Applications. *Biomacromolecules* **4**, 1466-1486, (2003).

2 Philippe, L., Raphaël, R., Stéphanie, S., Jutta, R., Kathy Van, B., Christine, J. & Robert, J. New Prospects for the Grafting of Functional Groups onto Aliphatic Polyesters. Ring-Opening Polymerization of α- or γ-Substituted ε-Caprolactone Followed by Chemical Derivatization of the Substituents. *Macromol. Sym.* **240**, 157-165, (2006).

3 Jerome, C. & Lecomte, P. Recent advances in the synthesis of aliphatic polyesters by ring-opening polymerization. *Adv. Drug Delivery Rev.* **60**, 1056-1076, (2008).

4 Pounder, R. & Dove, A. Towards poly(ester) nanoparticles: recent advances in the synthesis of functional poly(ester)s by ring-opening polymerization. *Polym. Chem.* **1**, 260-271, (2010).

5 Seyednejad, H., Ghassemi, A. H., van Nostrum, C. F., Vermonden, T. & Hennink, W. E. Functional aliphatic polyesters for biomedical and pharmaceutical applications. *J. Control. Release* **152**, 168-176, (2011).

6 Tian, H., Tang, Z., Zhuang, X., Chen, X. & Jing, X. Biodegradable synthetic polymers: Preparation, functionalization and biomedical application. *Prog. Polym. Sci.* **37**, 237-280, (2012).

7 Hao, J., Rainbolt, E. A., Washington, K., Biewer, M. C. & Stefan, M. C. Synthesis of Functionalized Poly(caprolactone)s and Their Application as Micellar Drug Delivery Systems. *Curr. Org. Chem.* **17**, 930-942, (2013).

8 Pack, D. W., Hoffman, A. S., Pun, S. & Stayton, P. S. Design and development of polymers for gene delivery. *Nat. Rev. Drug Discov.* **4**, 581-593, (2005).

9 Kanasty, R., Dorkin, J. R., Vegas, A. & Anderson, D. Delivery materials for siRNA therapeutics. *Nat. Mater.* **12**, 967-977, (2013).

10 Uhrich, K. E., Cannizzaro, S. M., Langer, R. S. & Shakesheff, K. M. Polymeric systems for controlled drug release. *Chem. Rev.* **99**, 3181-3198, (1999).

11 Lü, J.-M., Wang, X., Marin-Muller, C., Wang, H., Lin, P. H., Yao, Q. & Chen, C. Current advances in research and clinical applications of PLGA-based nanotechnology. *Expert Rev. Mol. Diagn.* **9**, 325-341, (2009).

12 Ulery, B. D., Nair, L. S. & Laurencin, C. T. Biomedical Applications of Biodegradable Polymers. *J. Polym. Sci., Part B: Polym. Phys.* **49**, 832-864, (2011).

13 Anselmo, A. C. & Mitragotri, S. An Overview of Clinical and Commercial Impact of Drug Delivery Systems. *J. Control. Release* **190**, 15-28, (2014).

14 Cheng, C. J., Tietjen, G. T., Saucier-Sawyer, J. K. & Saltzman, W. M. A holistic approach to targeting disease with polymeric nanoparticles. *Nat. Rev. Drug Discov.* **14**, 239-247, (2015).

15 Kamaly, N., Yameen, B., Wu, J. & Farokhzad, O. C. Degradable Controlled-Release Polymers and Polymeric Nanoparticles: Mechanisms of Controlling Drug Release. *Chem. Rev.* **116**, 2602-2663, (2016).

16 El Ali, B. & Alper, H. The application of transition metal catalysis for selective cyclocarbonylation reactions. Synthesis of lactones and lactams. *Synlett*, 161-171, (2000).

17 Hao, J., Kos, P., Zhou, K., Miller, J. B., Xue, L., Yan, Y., Xiong, H., Elkassih, S. & Siegwart, D. J. Rapid synthesis of a lipocationic polyester library via ring-opening polymerization of functional valerolactones for efficacious siRNA delivery. *J. Am. Chem. Soc.* **137**, 9206-9209, (2015).

18 Fietier, I., Le Borgne, A. & Spassky, N. Synthesis of functional polyesters derived from serine. *Polym. Bull. (Berlin)* **24**, 349-353, (1990).

19 Blanquer, S., Tailhades, J., Darcos, V., Amblard, M., Martinez, J., Nottelet, B. & Coudane, J. Easy synthesis and ring-opening polymerization of 5-Z-amino-δ-valerolactone: New degradable amino-functionalized (Co)polyesters. *J. Polym. Sci., Part A: Polym. Chem.* **48**, 5891-5898, (2010).

20 Nottelet, B., Patterer, M., François, B., Schott, M.-A., Domurado, M., Garric, X., Domurado, D. & Coudane, J. Nanoaggregates of Biodegradable Amphiphilic Random Polycations for Delivering Water-Insoluble Drugs. *Biomacromolecules* **13**, 1544-1553, (2012).

21 Yan, J., Zhang, Y., Xiao, Y., Zhang, Y. & Lang, M. Novel poly(ε-caprolactone)s bearing amino groups: Synthesis, characterization and biotinylation. *React. Funct. Polym.* **70**, 400-407, (2010).

22 Yan, J., Ye, Z., Luo, H., Chen, M., Zhou, Y., Tan, W., Xiao, Y., Zhang, Y. & Lang, M. Synthesis, characterization, fluorescence labeling and cellular internalization of novel amine-functionalized poly(ethylene glycol)-block-poly(?-caprolactone) amphiphilic block copolymers. *Polym. Chem.* **2**, 1331-1340, (2011).

23 El Habnouni, S., Blanquer, S., Darcos, V. & Coudane, J. Aminated PCL-based copolymers by chemical modification of poly(α-iodo-ε-caprolactone-co-ε-caprolactone). *J. Polym. Sci., Part A: Polym. Chem.* **47**, 6104-6115, (2009).

24 Xiong, X.-B., Uludağ, H. & Lavasanifar, A. Biodegradable amphiphilic poly(ethylene oxide)-block-polyesters with grafted polyamines as supramolecular nanocarriers for efficient siRNA delivery. *Biomaterials* **30**, 242-253, (2009).

25 Riva, R., Schmeits, S., Stoffelbach, F., Jerome, C., Jerome, R. & Lecomte, P. Combination of ring-opening polymerization and "click" chemistry towards functionalization of aliphatic polyesters. *Chem. Commun.*, 5334-5336, (2005).

26 Detrembleur, C., Mazza, M., Lou, X., Halleux, O., Lecomte, P., Mecerreyes, D., Hedrick, J. L. & Jérôme, R. New Functional Aliphatic Polyesters by Chemical Modification of Copolymers of ε-Caprolactone with γ-(2-Bromo-2-methylpropionate)-ε-caprolactone, γ-Bromo-ε-caprolactone, and a Mixture of β- and γ-Ene-ε-caprolactone. *Macromolecules* **33**, 7751-7760, (2000).

27 Detrembleur, C., Mazza, M., Halleux, O., Lecomte, P., Mecerreyes, D., Hedrick, J. L. & Jérôme, R. Ring-Opening Polymerization of γ-Bromo-ε-caprolactone: A Novel Route to Functionalized Aliphatic Polyesters. *Macromolecules* **33**, 14-18, (2000).

28 Lenoir, S., Riva, R., Lou, X., Detrembleur, C., Jérôme, R. & Lecomte, P. Ring-Opening Polymerization of α-Chloro-ε-caprolactone and Chemical Modification of Poly(α-chloro-ε-caprolactone) by Atom Transfer Radical Processes. *Macromolecules* **37**, 4055-4061, (2004).

29 Riva, R., Chafaqi, L., Jerome, R. & Lecomte, P. Synthesis of new substituted lactones by "click" chemistry. *Arkivoc*, 292-306, (2007).

30 van der Ende, A., Kravitz, E. & Harth, E. Approach to formation of multifunctional polyester particles in controlled nanoscopic dimensions. *J. Am. Chem. Soc.* **130**, 8706-8713, (2008).

31 Darcos, V., Antoniacomi, S., Paniagua, C. & Coudane, J. Cationic polyesters bearing pendent amino groups prepared by thiol-ene chemistry. *Polym. Chem.* **3**, 362-368, (2012).

32 Mecerreyes, D., Miller, R. D., Hedrick, J. L., Detrembleur, C. & Jerome, R. Ring-opening polymerization of 6-hydroxynon-8-enoic acid lactone: novel biodegradable copolymers containing allyl pendent groups. *J. Polym. Sci., Part A: Polym. Chem.* **38**, 870-875, (2000).

33 Mecerreyes, D., Humes, J., Miller, R. D., Hedrick, J. L., Detrembleur, C., Lecomte, P., Jerome, R. & San Roman, J. First example of an unsymmetrical difunctional monomer polymerizable by two living/controlled methods. *Macromol. Rapid Commun.* **21**, 779-784, (2000).

34 Lou, X., Detrembleur, C., Lecomte, P. & Jerome, R. Living Ring-Opening (Co)polymerization of 6,7-Dihydro-2(5H)-oxepinone into Unsaturated Aliphatic Polyesters. *Macromolecules* **34**, 5806-5811, (2001).

35 Lou, X., Detrembleur, C., Lecomte, P. & Jerome, R. Controlled synthesis and chemical modification of unsaturated aliphatic (Co)polyesters based on 6,7-dihydro-2(3H)-oxepinone. *J. Polym. Sci., Part A: Polym. Chem.* **40**, 2286-2297, (2002).

36 Li, H., Jeroeme, R. & Lecomte, P. Synthesis of tadpole-shaped copolyesters based on living macrocyclic poly(ϵ-caprolactone). *Polymer* **47**, 8406-8413, (2006).

37 Lynn, D. M. & Langer, R. Degradable Poly(β-amino esters): Synthesis, Characterization, and Self-Assembly with Plasmid DNA. *J. Am. Chem. Soc.* **122**, 10761-10768, (2000).

38 Green, J., Langer, R. & Anderson, D. A combinatorial polymer library approach yields insight into nonviral gene delivery. *Accounts Chem. Res.* **41**, 749-759, (2008).

39 Tian, H. Y., Tang, Z. H., Zhuang, X. L., Chen, X. S. & Jing, X. B. Biodegradable synthetic polymers: Preparation, functionalization and biomedical application. *Prog. Polym. Sci.* **37**, 237-280, (2012).

40 Gokhale, S., Xu, Y. & Joy, A. A Library of Multifunctional Polyesters with "Peptide-Like" Pendant Functional Groups. *Biomacromolecules* **14**, 2489-2493, (2013).

41 Yan, Y. & Siegwart, D. J. Scalable synthesis and derivation of functional polyesters bearing ene and epoxide side chains. *Polym. Chem.* **5**, 1362-1371, (2014).

42 Yan, Y. F., Xue, L., Miller, J. B., Zhou, K. J., Kos, P., Elkassih, S., Liu, L., Nagai, A., Xiong, H. & Siegwart, D. J. One-pot synthesis of functional poly(amino ester sulfide)s and utility in delivering pDNA and siRNA. *Polymer* **72**, 271-280, (2015).

43 Nederberg, F., Zhang, Y., Tan, J. P. K., Xu, K. J., Wang, H. Y., Yang, C., Gao, S. J., Guo, X. D., Fukushima, K., Li, L. J., Hedrick, J. L. & Yang, Y. Y. Biodegradable nanostructures with selective lysis of microbial membranes. *Nat. Chem.* **3**, 409-414, (2011).

44 Geihe, E. I., Cooley, C. B., Simon, J. R., Kiesewetter, M. K., Edward, J. A., Hickerson, R. P., Kaspar, R. L., Hedrick, J. L., Waymouth, R. M. & Wender, P. A. Designed guanidinium-rich amphipathic oligocarbonate molecular transporters complex, deliver and release siRNA in cells. *Proc. Natl. Acad. Sci. USA* **109**, 13171-13176, (2012).

45 Zhang, X. J., Cai, M. M., Zhong, Z. L. & Zhuo, R. X. A Water-Soluble Polycarbonate With Dimethylamino Pendant Groups Prepared by Enzyme-Catalyzed Ring-Opening Polymerization. *Macromol. Rapid Commun.* **33**, 693-697, (2012).

46 Blake, T. R. & Waymouth, R. M. Organocatalytic Ring-Opening Polymerization of Morpholinones: New Strategies to Functionalized Polyesters. *J. Am. Chem. Soc.* **136**, 9252-9255, (2014).

47 Zhang, Z. H., Yin, L. C., Xu, Y. X., Tong, R., Lu, Y. B., Ren, J. & Cheng, J. J. Facile Functionalization of Polyesters through Thiol-yne Chemistry for the Design of Degradable,

Cell-Penetrating and Gene Delivery Dual-Functional Agents. *Biomacromolecules* **13**, 3456-3462, (2012).

48 Jones, C. H., Chen, C. K., Jiang, M., Fang, L., Cheng, C. & Pfeifer, B. A. Synthesis of Cationic Polylactides with Tunable Charge Densities as Nanocarriers for Effective Gene Delivery. *Mol. Pharmaceut.* **10**, 1138-1145, (2013).

49 Kim, H., Olsson, J. V., Hedrick, J. L. & Waymouth, R. M. Facile Synthesis of Functionalized Lactones and Organocatalytic Ring-Opening Polymerization. *ACS. Macro. Lett.* **1**, 845-847, (2012).

50 Winkler, M., Raupp, Y. S., Kohl, L. A. M., Wagner, H. E. & Meier, M. A. R. Modified Poly(epsilon-caprolactone)s: An Efficient and Renewable Access via Thia-Michael Addition and Baeyer-Villiger Oxidation. *Macromolecules* **47**, 2842-2846, (2014).

51 Li, X. W., Li, H., Zhao, Y. Y., Tang, X. Y., Ma, S. F., Gong, B. & Li, M. F. Facile synthesis of well-defined hydrophilic polyesters as degradable poly(ethylene glycol)-like biomaterials. *Polym. Chem.* **6**, 6452-6456, (2015).

52 Jayaraman, M., Ansell, S. M., Mui, B. L., Tam, Y. K., Chen, J. X., Du, X. Y., Butler, D., Eltepu, L., Matsuda, S., Narayanannair, J. K., Rajeev, K. G., Hafez, I. M., Akinc, A., Maier, M. A., Tracy, M. A., Cullis, P. R., Madden, T. D., Manoharan, M. & Hope, M. J. Maximizing the Potency of siRNA Lipid Nanoparticles for Hepatic Gene Silencing In Vivo. *Angew. Chem. Int. Edit.* **51**, 8529-8533, (2012).

53 Wittrup, A., Ai, A., Liu, X., Hamar, P., Trifonova, R., Charisse, K., Manoharan, M., Kirchhausen, T. & Lieberman, J. Visualizing lipid-formulated siRNA release from endosomes and target gene knockdown. *Nat. Biotechnol.* **33**, 870-976, (2015).

54 Zhou, K., Nguyen, L. H., Miller, J. B., Yan, Y., Kos, P., Xiong, H., Li, L., Hao, J., Minnig, J. T., Zhu, H. & Siegwart, D. J. Modular degradable dendrimers enable small RNAs to extend survival in an aggressive liver cancer model. *Proc. Natl. Acad. Sci. USA* **113**, 520-525, (2016).

CHAPTER FOUR

RAPID SYNTHESIS OF A LIPOCATIONIC POLYESTER LIBRARY VIA RING-OPENING POLYMERIZATION OF FUNCTIONAL VALEROLACTONES FOR EFFICACIOUS siRNA DELIVERY

4.1 PREFACE

The central independent project for my thesis was on the synthesis of poly(disulfide) nanogels (see Chapters 1 and 2). In addition to that area of research, I was also able to work closely with Dr. Jing Hao, a postdoc in the Siegwart lab who worked on synthesis and application of functional lipocationic polyesters. In this chapter, I will summarize the experiments and research that I worked on with Dr. Hao to show how polyesters can be synthesized in a controlled fashion and how they can be used to deliver siRNA molecules *in vitro* and *in vivo*.

4.2 INTRODUCTION

Gene silencing via the RNA Interference (RNAi) mechanism is a promising strategy to treat major diseases including cancer, genetic disorders, and viral infections. However, the success of short interfering RNA (siRNA)-based therapies has been limited by the difficulty of delivering these highly anionic biomacromolecular drugs into cells.[1-3] Polymers are an important class of materials for drug and nucleic acid delivery due to the versatility in constructing different nanostructures including micelles, polyplexes, dendrimers, and polymer-siRNA conjugates. Yet they currently lag behind in efficacy compared to lipid-based carriers.[3]

Cationic polymers, such as polyethyleneimine and polylysine,[1] are widely used as nucleic acid carriers; however, application of these materials to *in vivo* disease models is often limited by their cytotoxicity. Since incorporating biodegradable bonds will facilitate elimination of materials used in biomedical applications, the development of degradable polymer-based siRNA delivery systems represents an important goal. Aliphatic polyesters are used in FDA-approved products, but lack the required functional groups to complex and deliver nucleic acids.[4] Numerous studies of lipids and non-degradable polymers have implicated tertiary amines and alkyl chains as key

functional groups for effective siRNA delivery.[5-8] Yet, their potential incompatibility with esters has made direct synthesis of degradable polymers with amino groups challenging. Step-growth polymerization can be used to overcome this issue, [9-13] but these methods do not offer control over molecular weight and molecular weight distribution.

Direct synthesis of polymers using ring opening polymerization (ROP) offers greater control over polymer composition and the ability to make block copolymers.[9,14-17] A number of excellent examples of functional polyesters have been reported via direct polymerization of functional lactones and/or post-polymerization modification routes.[18-27] To date however, low yields due to multi-step synthetic pathways has limited the scale and chemical scope of polymer production.[14] Moreover, there has been no report on polymerization of amine bearing lactones. The development of combinatorial polymer libraries is an effective way to discover efficacious nucleic acid carriers.[6,10,11] We were therefore motivated to employ a strategy to prepare functional lactone monomers in one step from commercially available starting materials that could be polymerized with high monomer conversion to yield a scalable polymer library. These attributes are essential to be able to synthesize and screen a variety of copolymer compositions and discover optimal delivery materials.

In this Chapter, we describe a library of 139 degradable lipocationic polyesters that were directly synthesized from tertiary amine bearing valerolactone and alkylated valerolactone monomers, thereby overcoming current synthetic limitations in functionality and scalability. Initiation with methyl lithium promoted rapid polymerization with high monomer conversion and decent control over molecular weight. Cationic and hydrophobic moieties were incorporated at precise ratios, which allowed us to fine tune the material composition and correlate structure with siRNA delivery activity. Formulated polymeric nanoparticles (NPs) exhibited high delivery

efficiency, enabling >95% knockdown *in vitro* for the top performing materials using only a 5 nM siRNA dose. Automated, high throughput screening of this library revealed a strong correlation between delivery efficacy and chemical structure. NPs could localize to tumors *in vivo* after intravenous delivery and were able to silence gene expression in tumor-bearing mice. We believe that this chemistry introduces a versatile way to directly synthesize lipocationic polymers for gene delivery and is a promising step towards closing the activity gap between lipids and polymers.

4.3 METHODOLOGY

4.3.1 MATERIALS

Ethylene sulfide, cholesterol, all thiols, all amines, and all otherwise unpecified chemicals were purchased from Sigma-Aldrich. 5,6-dihydro-2H-pyran-2-one (DPO) and luciferin (monosodium salt) were purchased from Fisher Scientific. DSPC was purchased from Avanti Lipids. siRNA against luciferase (sense strand: 5'-GAUUAUGUCCGGUUAUGUA[dT][dT]-3'; anti-sense strand: 3'-UACAUAACCGGACAUAAUC[dT][dT]-5'), Dulbecco's Modified Eagle Media (DMEM), and fetal bovine serum (FBS) were purchased from Sigma-Aldrich. Cy5.5-siLuc had the same sequence but was labeled with the Cy5.5 dye at one end. PEG-lipid was chemically synthesized. OptiMEM was purchased from Life Technologies. RNAiMax was purchased from Invitrogen and used following the supplier's recommended protocols. Cell Mask Orange was purchased from Molecular Probes. ONE-Glo + Tox was purchased from Promega. All organic

solvents were purchased from Fisher Scientific and purified with a solvent purification system (Innovative Technology).

4.3.2 METHODS

4.3.2.1 Experimental Details

In vitro siRNA Transfection Assays

HeLa cells stably expressing luciferase (HeLa-Luc) were derived from HeLa cells (ATCC) by stable transfection of the Firefly Luciferase gene using Lentiviral infection followed by clonal selection. HeLa-Luc cells were seeded (10,000 cells/well) into each well of an opaque white 96-well plate (Corning) and allowed to attach overnight in phenol red-free DMEM supplemented with 5% FBS. Polymer stock solutions were diluted to 1 mM in ethanol. 58.45 μL DSPC/Cholesterol/PEG lipid mixture in EtOH (DPSC = 211.14 μM, Chol = 802.33 μM, PEG Lipid = 42.228 μM) was mixed with 61.55 μL polymer (1 mM stock solution in EtOH). This was mixed thoroughly by pipette mixing. 33 μL of this ethanol lipid mixture was added to 55 μL siRNA stock solution in citrate buffer (40 ng/μL siRNA) (citrate buffer pH = 4.2) and rapidly mixed. It was allowed to complex for 20 minutes at room temperature. 132 μL sterile PBS was added to complete the preparation of formulated NPs. 20, 10, 5, 2.5, and 1.5 μL were added to growing cells (n = 4) depending on desired dose.

For the high-throughput screen (**Figures 4.2-4.3**), cells were transfected with 100 ng (38.4 nM) of firefly-specific siLuc. Crude polymers were utilized in this phase to screen for hits. Subsequently, we re-synthesized lead polymers and purified them by dialysis into THF. All

polymers used in the dose response (**Figure 4.4**) and animal experiments (**Figure 4.5**) were purified polymers free of all residual solvents and any unreacted monomers. For the dose response curves, 6.25 to 100 ng were added (2.4 to 38.4 nM). Cells were incubated for 36 h at 37 °C, 5% CO_2 and then firefly luciferase activity and viability was analyzed using "One Glo + Tox" assay kits (Promega). RNAiMax control experiments used OptiMEM during the initial mixing stage according to the manufacturer's recommended protocol. All polymeric NP experiments were performed in full 5% serum-containing DMEM. Results were normalized to untreated cells (n=4). To evaluate statistical significance, two-tailed T tests with the 95% confidence level were conducted. As an example, N1C8 (2:2) was compared to RNAiMax: ****, $p<0.0001$.

Confocal Microscopy

Cellular uptake studies were performed using the top performing materials from the polymer screen. HeLa-Luc cells were seeded at a density of 30,000 cells per well in 8-chambered coverglass slides (Nunc) and allowed to attach for 24 hours. NP formulations were prepared by manual mixing using a similar protocol to the *in vitro* transfection assays above (Section 1.3) using Cy5.5-labeled siRNA. The formulation was performed in 10 mM citrate buffer pH 4.3 at a final mole ratio of 100:1 polymer:siRNA, and the lipid mixture of the formulation consisted of molar ratios 50:38:10:2 lipocationic polymer: cholesterol: DSPC: PEG-lipid. The nanoparticles were added to the cells at a final siRNA dose of 100 ng/well. After 3h incubation, the medium was aspirated, washed with PBS, and cell membrane staining was performed (Cell Mask Orange, Molecular Probes) using the manufacturer's protocol. Confocal microscopy imaging was performed using a Nikon Eclipse TE2000-E and images were analyzed using ImageJ (NIH).

In vivo Biodistribution and Luciferase Silencing in Mice

Animals

Female athymic Nude-Foxn1^{nu} mice were purchased from Harlan Laboratories (Indianapolis, IN). All experiments were approved by the Institutional Animal Care and Use Committees of The University of Texas Southwestern Medical Center and were consistent with local, state and federal regulations as applicable.

In vivo Biodistribution

MDA-MB-231-Luc tumor cells ($5*10^6$) in 100 μL PBS were injected subcutaneously into each flank of the mice. After three weeks when the tumors reached the adequate size, N1C4 (2:2) NPs (N1C4 (2:2):cholesterol:DSPC:PEG-lipid = 50:35:10:5; polymer:siRNA = 20:1 (weight); aqueous:EtOH = 3:1 (volume)) containing 50 μg siLuc (50 % Cy5.5-labeled) in 200 μL were injected intravenously (2.5 mg/kg dose IV). After 2.5 h, mice were anesthetized with 2.5 % isofluorane in oxygen and the whole body and ex vivo organs fluorescence imaging was performed on an IVIS Lumina System (Caliper Life Sciences).

In vivo Bioluminescence Imaging

MDA-MB-231-Luc tumor-bearing mice (see above) were anesthetized with 2.5 % isofluorane in oxygen. D-Luciferin, monosodium salt (Fisher Scientific) was dissolved in PBS (40 mg/mL) and administered intraperitoneally at a dose of 200 mg/kg body weight. Bioluminescence imaging was performed 10 min after luciferin administration on the IVIS Lumina System (Caliper Life Sciences). Mice were then injected intratumorally with the N1C4 (2:2) NPs (N1C4

(2:2):cholesterol:DSPC:PEG-lipid = 50:35:10:5; polymer:siRNA = 20:1 (weight); aqueous:EtOH = 3:1 (volume)) NPs with the siRNA concentration of 50 μg/100 μL (siLuc or control siGFP) in a total volume of 150 μL per mouse distributed between the two tumors on both flanks. Twenty-four hours after NP administration, luminescence imaging was performed again as described above. The BLI signal intensities from the tumors were quantified by the fixed regions of interest (ROI) as the total flux of photons per second and normalized against the initial values obtained prior to the first injection.

Quantitative Luciferase and Total Protein Measurements

MDA-MB-231-Luc tumor-bearing mice were administered N1C4 (2:2) NPs intratumorally at the concentrations described above for the bioluminescence imaging. On the following day, the NPs were injected again. Two days after second injection, mice were sacrificed and tumor tissues collected, weighed and homogenized in RLB buffer (Promega) using T 25 digital ULTRA-TURRAX (Ika). Tumor homogenates were centrifuged and the supernatant applied in protein concentration and luciferase activity measurements. Luciferase assay reagent (Promega) was added to the supernatant (20 μL) and the luminescence was detected using Infinite 200 PRO micro plate reader (Tecan). Background signals were subtracted. The protein concentrations were determined using the BCA Protein Assay Kit (Pierce) according to the manufacturer's protocol. The luminescence data were calculated as relative light units per milligram of tissue or microgram of proteins. To evaluate statistical significance, student's T tests with the 95% confidence level were conducted. * $p<0.1$. (**Figure 4.5B**): n=4; p=0.0121. (**Figure 4.5**) left: n=4; p=0.0300 (**Figure 4.5C**) right: n=4; p=0.0386.

siRNA Retention in Tumor

The MDA-MB-231-Luc tumor-bearing mice were injected intratumorally with the N1C4 (2:2) NPs (N1C4 (2:2):cholesterol:DSPC:PEG-lipid = 50:35:10:5; polymer:siRNA = 20:1 (weight); aqueous:EtOH = 3:1 (volume)) NPs with the siRNA concentration of 50 μg/100 μL (siLuc; 20 % Cy5.5-siLuc) in a total volume of 150 μL per mouse distributed between the tumors on both flanks. Two days later, whole body fluorescence imaging was performed on an IVIS Lumina System (Caliper Life Sciences).

4.3.2.2 Chemical Synthesis

Aminothiol (AT) Synthesis

2-(dimethylamino)ethane-1-thiol (**AT1**)

A 250 mL round bottom flask was dried overnight, degassed, and refilled with nitrogen prior to being placed in a liquid nitrogen bath. Then, dimethylamine was released into the flask where it solidified into a white solid. The liquid nitrogen bath was removed, and the solid dimethylamine was weighed to be 10.5 g (0.23 mol). 50 mL dry dichloromethane (DCM) was added and the flask was placed in an ice bath. 18 g ethylene sulfide (0.30 mol) was dissolved in 25 mL dry DCM and added into the flask drop wise. The reaction solution was stirred for 2 hours from 0 °C to room temperature under nitrogen. The solution was concentrated via rotary evaporation at 40 °C. Sodium ascorbate was added and filtered to yield 15.6 g (0.15 mol) product (yield: 65%) as a colorless liquid. The structure was verified by NMR (**Figure A1**) and LC-MS. 2-(diethylamino)ethane-1-thiol (**AT2**), 2-(dipropylamino)ethane-1-thiol (**AT3**), 2-

(dibutylamino)ethane-1-thiol (**AT4**), 2-(pyrrolidin-1-yl)ethane-1-thiol (**AT5**), 2-(piperidine-1-yl)ethane-1-thiol (**AT6**), and 2-(azepan-1-yl)ethane-1-thiol (**AT7**)

The secondary amine (0.1 mol) was dissolved in 100 mL DCM in a pre-dried flask, followed by addition of 12 g ethylene sulfide (0.2 mol) in 50 mL DCM solution. The reaction solution was stirred at room temperature for 2 hours under nitrogen, and then concentrated via rotary evaporation and distilled under vacuum to yield a colorless liquid. The yields (based on secondary amine) for compounds (AT2-AT7) were 42%, 40%, 22%, 47%, 54%, 35%, respectively. The structures were verified by NMR and LC-MS.

2-(dimethylamino)ethane-1-thiol (AT1)

^{1}H NMR (500 MHz, $CDCl_3$): δ 2.61 (t, 2H), 2.48 (t, 2H), 2.24 (s, 6H)

2-(diethylamino)ethane-1-thiol (AT2)

^{1}H NMR (500 MHz, $CDCl_3$): δ 2.61 (m, 2H), 2.59 (m, 2H), 2.52 (q, 4H), 1.02 (t, 6H) m/z=133.1

2-(dipropylamino)ethane-1-thiol (AT3)

^{1}H NMR (500 MHz, $CDCl_3$): δ 2.62 (m, 2H), 2.56 (m, 2H), 2.36 (m, 4H), 1.45 (m, 4H), 0.88 (t, 6H). m/z=161.2

2-(dibutylamino)ethane-1-thiol (AT4)

^{1}H NMR (500 MHz, $CDCl_3$): δ 2.60 (m, 2H), 2.58 (m, 2H), 2.41 (t, 4H), 1.41 (m, 4H), 1.31 (m, 4H), 0.91 (t, 6H). m/z= 189.2

2-(pyrrolidin-1-yl)ethane-1-thiol (AT5)

^{1}H NMR (500 MHz, $CDCl_3$): δ 2.65 (br, 4H), 2.51 (br, 4H), 1.78 (m, 4H). m/z=131.2

2-(piperidin-1-yl)ethane-1-thiol (AT6)

^{1}H NMR (500 MHz, $CDCl_3$): δ 2.62 (m, 2H), 2.50 (m, 2H), 2.38 (br, 4H), 1.57 (m, 4H), 1.42 (m, 2H). m/z=145.2

2-(azepan-1-yl)ethane-1-thiol (AT7)

^{1}H NMR (500 MHz, $CDCl_3$): δ 2.69 (t, 2H), 2.63 (t, 4H), 2.59 (t, 2H), 1.63 (br, 4H), 1.58 (br. 4H). m/z=159.1

4.3.2.3 Monomer Synthesis

General Procedure for Synthesis of Aminothiol Monomer N1-N7

5,6-dihydro-2H-pyran-2-one (DPO) reacted with an aminothiol (AT1-AT7) at a mole ratio of 1 to 1, and the reaction was stirred at 50 °C for two hours. Complete reactant conversion to product was reached with ~100% yield. The structures were verified by NMR and LC-MS.

4-((2-(dimethylamino)ethyl)thio)tetrahydro-2H-pyran-2-one (N1)

^{1}H NMR (500 MHz, $CDCl_3$): δ 4.45 (ddd, 1H), 4.22 (ddd, 1H), 3.20 (m, 1H), 2.88 (ddd, 1H), 2.62 (t, 2H), 2.47 (m, 3H), 2.19 (s, 6H), 2.16 (m, 1H), 1.81 (ddd, 1H). $[MH]^+$ m/z=204.1

^{13}C NMR (500 MHz, $CDCl_3$) δ 169.25, 67.25, 58.95, 45.27, 37.14, 35.92, 29.49, 28.58 $[MH]^+$ m/z=204.1

4-((2-(diethylamino)ethyl)thio)tetrahydro-2H-pyran-2-one (N2)

^{1}H NMR (500 MHz, $CDCl_3$): δ 4.48 (ddd, 1H), 4.25 (ddd, 1H), 3.24 (m, 1H), 2.92 (ddd, 1H), 2.63 (br. 4H), 2.51 (m, 5H), 2.18 (ddd, 1H), 1.85 (ddd, 1H), 0.99 (t, 6H). $[MH]^+$ m/z=232.2

^{13}C NMR (500 MHz, $CDCl_3$) δ 169.28, 67.27, 52.77, 46.92, 37.21, 36.02, 29.58, 28.50, 11.71 $[MH]^+$ m/z=232.2

4-((2-(dipropylamino)ethyl)thio)tetrahydro-2H-pyran-2-one (N3)

^{1}H NMR (500 MHz, $CDCl_3$): δ 4.49 (ddd, 1H), 4.26 (ddd, 1H), 3.25 (m, 1H), 2.92 (ddd, 1H), 2.63 (br, 4H), 2.49 (dd, 1H), 2.36 (m, 4H), 2.17 (ddd, 1H), 1.83 (ddd, 1H), 1.43 (m, 4H), 0.85 (t, 6H). $[MH]^+$ m/z=260.2

^{13}C NMR (500 MHz, $CDCl_3$) δ 169.27, 67.25, 56.15, 54.10, 37.29, 35.99, 29.61, 28.64, 20.30, 11.87. $[MH]^+$ m/z=260.2

4-((2-(dibutylamino)ethyl)thio)tetrahydro-2H-pyran-2-one (N4)

^{1}H NMR (500 MHz, $CDCl_3$): δ 4.50 (ddd, 1H), 4.26 (ddd, 1H), 3.25 (m, 1H), 2.93 (dd, 1H), 2.63 (br, 4H), 2.50 (dd, 1H), 2.40 (t, 4H), 2.19 (m, 1H), 1.82 (m, 1H), 1.38 (m, 4H), 1.28 (m, 4H), 0.89 (t, 6H). $[MH]^+$ m/z=288.2

^{13}C NMR (500 MHz, $CDCl_3$): δ 169.26, 67.24, 54.04, 53.96, 37.25, 36.01, 29.62, 29.27, 28.63, 20.62, 14.07. $[MH]^+$ m/z=288.2

4-((2-(pyrrolidin-1-yl)ethyl)thio)tetrahydro-2H-pyran-2-one (N5)

^{1}H NMR (500 MHz, $CDCl_3$): δ 4.46 (ddd, 1H), 4.23 (ddd, 1H), 3.21 (m, 1H), 2.90 (ddd, 1H), 2.66 (m, 4H), 2.48 (m, 5H), 2.18 (ddd, 1H), 1.84 (ddd, 1H), 1.74 (m, 4H). $[MH]^+$ m/z=230.1

^{13}C NMR (500 MHz, $CDCl_3$): δ 169.21, 67.23, 56.10, 54.05, 37.17, 36.03, 29.63, 29.55, 23.40. $[MH]^+$ m/z=230.1

4-((2-(piperidin-1-yl)ethyl)thio)tetrahydro-2H-pyran-2-one (N6)

^{1}H NMR (500 MHz, $CDCl_3$): δ 4.48 (ddd, 1H), 4.24 (ddd, 1H), 3.24 (m, 1H), 2.91 (ddd, 1H), 2.64 (m, 2H), 2.51 (m, 3H), 2.36 (br, 4H), 2.19 (ddd, 1H), 1.84 (ddd, 1H), 1.54 (m, 4H), 1.40 (m, 2H). $[MH]^+$ m/z=244.1

^{13}C NMR (500 MHz, $CDCl_3$): δ 169.24, 67.25, 59.13, 54.50, 37.21, 36.04, 29.60, 27.90, 25.85, 24.22. $[MH]^+$ m/z=244.1

4-((2-(azepan-1-yl)ethyl)thio)tetrahydro-2H-pyran-2-one (N7)

^{1}H NMR (500 MHz, $CDCl_3$): δ 4.46 (ddd, 1H), 4.24 (ddd, 1H), 3.23 (m, 1H), 2.91 (dd, 1H), 2.63 (m, 8H), 2.50 (dd, 1H), 2.20 (ddd, 1H), 1.84 (ddd, 1H), 1.54 (m, 8H). $[MH]^+$ m/z=258.1

^{13}C NMR of 4-((2-(azepan-1-yl)ethyl)thio)tetrahydro-2H-pyran-2-one. ^{13}C NMR (500 MHz, $CDCl_3$): δ 169.28, 67.26, 57.77, 55.29, 37.26, 35.97, 29.62, 28.69, 28.03, 26.97. $[MH]^+$ m/z=258.1

General Procedure for Synthesis of Alkylthiol Monomers C4/C6/C10/C12/C14

DPO was reacted with an alkylthiol at a mole ratio of 1 to 1.2. Dimethylphenylphosphine (DMPP) (0.5 % by mol) was added to the reaction mixture, and the reaction was stirred at room temperature until all the DPO was converted (100%). The reaction mixture was then separated by flash chromatography (with hexane: ethyl acetate=10:0~9:1) to obtain pure monomers. The structures were verified by NMR and LC-MS.

4-(butylthio)tetrahydro-2H-pyran-2-one (C4)

^{1}H NMR (500 MHz, $CDCl_3$): δ 4.52 (ddd, 1H), 4.29 (ddd, 1H), 3.19 (m, 1H), 2.93 (ddd, 1H), 2.57 (m, 3H), 2.20 (ddd, 1H) 1.85 (ddd, 1H), 1.57 (m, 2H), 1.42 (m, 2H), 0.92 (t, 3H). $[MH]^+$ m/z=189.1

^{13}C NMR (500 MHz, $CDCl_3$) δ 169.42, 67.34, 37.19, 35.73, 31.57, 30.27, 29.49, 22.00, 13.65; $[MH]^+$ m/z=189.1

4-(hexylthio)tetrahydro-2H-pyran-2-one (C6)

^{1}H NMR (500 MHz, $CDCl_3$): δ 4.48 (ddd, 1H), 4.25 (ddd, 1H), 3.17 (m, 1H), 2.90 (ddd, 1H), 2.54 (m, 3H), 2.17 (ddd, 1H), 1.84 (ddd, 1H), 1.54 (m, 2H), 1.36 (m, 2H), 1.25 (m, 4H), 0.85 (t, 3H). $[MH]^+$ m/z=217.2

^{13}C NMR (500 MHz, $CDCl_3$) δ 169.36, 67.30, 37.18, 35.74, 31.33, 30.59, 29.48, 28.54, 22.49, 14.01. $[MH]^+$ m/z=217.2

4-(octylthio)tetrahydro-2H-pyran-2-one (C8)

^{1}H NMR (500 MHz, $CDCl_3$): δ 4.51 (ddd, 1H), 4.28 (ddd, 1H), 3.19 (m, 1H), 2.92 (ddd, 1H), 2.55 (m, 3H), 2.19 (ddd, 1H), 1.87 (ddd, 1H), 1.57 (m, 2H), 1.26 (m, 10H), 0.85 (t, 3H). $[MH]^+$ m/z=245.2

^{13}C NMR δ 169.40, 67.33, 37.20, 35.75, 31.78, 30.61, 29.53, 29.51, 29.15, 29.14, 28.91, 22.64, 14.11; $[MH]^+$ m/z=245.2

4-(decylthio)tetrahydro-2H-pyran-2-one (C10)

^{1}H NMR (500 MHz, $CDCl_3$): δ 4.52 (ddd, 1H), 4.29 (ddd, 1H), 3.19 (m, 1H), 2.93 (ddd, 1H), 2.56 (m, 3H), 2.18 (ddd, 1H), 1.87 (ddd, 1H), 1.57 (m, 2H), 1.24 (m, 14H), 0.86 (t, 3H). $[MH]^+$ m/z=273.3

^{13}C NMR δ169.38, 67.32, 37.20, 35.76, 31.90, 30.61, 29.53, 29.51, 29.48, 29.29, 29.18, 28.90, 22.67, 14.13; $[MH]^+$ m/z=273.3

4-(dodecylthio)tetrahydro-2H-pyran-2-one (C12)

^{1}H NMR (500 MHz, $CDCl_3$): δ 4.50 (ddd, 1H), 4.27 (ddd, 1H), 3.20 (m, 1H), 2.92 (ddd, 1H), 2.54 (m, 3H), 2.18 (ddd, 1H), 1.87 (ddd, 1H), 1.57 (m, 2H), 1.24 (m, 18H), 0.86 (t, 3H). $[MH]^+$ m/z=301.4

^{13}C NMR δ 169.38, 67.32, 37.20, 35.75, 31.91, 30.61, 29.64, 29.62, 29.58, 29.54, 29.51, 29.49, 29.35, 29.19, 28.91, 22.69, 14.14; $[MH]^+$ m/z=301.4

4-(tetradecylthio)tetrahydro-2H-pyran-2-one (C14)

^{1}H NMR (500 MHz, $CDCl_3$): δ 4.51(ddd, 1H), 4.29 (ddd, 1H), 3.20 (m, 1H), 2.95 (ddd, 1H), 2.56 (m, 3H), 2.21 (ddd, 1H), 1.88 (ddd, 1H), 1.60 (m, 4H), 1.37 (m, 2H), 1.25 (m, 18H), 0.88 (t, 3H). $[MH]^+$ m/z=329.3

^{13}C NMR of 4-(tetradecylthio)tetrahydro-2H-pyran-2-one. ^{13}C NMR 169.35, 67.31, 37.20, 35.76, 31.92, 30.62, 29.68, 29.66, 29.65, 29.64, 29.58, 29.54, 29.52, 29.49, 29.36, 29.18, 28.91, 22.69, 14.13. $[MH]^+$ m/z=329.3

4.3.2.4 Polymer Synthesis

N1C4 (2:2), N1C8 (2:2), and N1C8 (1:3) are described as typical polymerizations.

N1C4 (2:2): *Synthesis of poly{4-((2-(dimethylamino)ethyl)thio)tetrahydro-2H-pyran-2-one}-r-poly{4-(butylthio)tetrahydro-2H-pyran-2-one}*. Glass vials with stir bars were dried in an oven for

two days and then cooled under vacuum. All of the vials were transferred into the glove box. Monomers N1 (0.104 g, 5.10×10^{-4} mol) and C4 (0.096 g, 5.10×10^{-4} mol) were added to each vial at a fixed mole ratio listed in Table S1. 32 μL Methyl lithium (1.6 M in ether) was then added into the reaction vial to initiate the reaction. The polymer was collected after 5 minutes. Purified polymer was obtained by dialysis against THF for 4 hours. The polymer was then concentrated and dried via vacuum pump for 24 hours. The polymer was characterized by NMR and GPC (**Table 2.1**). ^{1}H NMR (500 MHz, CDCl3): δ 4.27 (br, 4H), 3.12 (br, 2H), 2.61 (m, 6H), 2.52 (m, 4H), 2.24 (s, 6H), 1.98 (br, 2H), 1.84 (br, 2H), 1.55 (m, 2H), 1.28 (m, 2H), 0.88 (t, 3H).

N1C8 (2:2): *Synthesis of poly{4-((2-(dimethylamino)ethyl)thio)tetrahydro-2H-pyran-2-one}-r-poly{4-(octylthio)tetrahydro-2H-pyran-2-one}*. Glass vials with stir bars were dried in an oven for two days and then cooled under vacuum. All of the vials were transferred into the glove box. Monomers N1 (0.104 g, 5.10×10^{-4} mol) and C8 (0.125 g, 5.10×10^{-4} mol) were added to each vial at a fixed mole ratio listed in **Table 4.1**. 32 μL Methyl lithium (1.6 M in ether) was then added into the reaction vial to initiate the reaction. The polymer was collected after 5 minutes. Purified polymer was obtained by dialysis against THF for 4 hours. The polymer was then concentrated and dried via vacuum pump for 24 hours. The polymer was characterized by NMR and GPC (**Table 4.1**). ^{1}H NMR (500 MHz, CDCl3): δ 4.27 (br, 4H), 3.12 (br, 2H), 2.61 (m, 6H), 2.52 (m, 4H), 2.24 (s, 6H), 1.98 (br, 2H), 1.84 (br, 2H), 1.55 (m, 2H), 1.28 (m, 10H), 0.88 (t, 3H).

N1C8 (1:3): *Synthesis of poly{4-((2-(dimethylamino)ethyl)thio)tetrahydro-2H-pyran-2-one}-r-poly{4-(octylthio)tetrahydro-2H-pyran-2-one}*. Glass vials with stir bars were dried in an oven for two days and then cooled under vacuum. All of the vials were transferred into the glove box.

Monomers N1 (0.052 g, 2.55×10^{-4} mol) and C8 (0.187 g, 7.65×10^{-4} mol) were added to each vial at a fixed mole ratio listed in **Table 4.1**. 32 µl Methyl lithium (1.6 M in ether) was then added into the reaction vial to initiate the reaction. The polymer was collected after 5 minutes. Purified polymer was obtained by dialysis against THF for 4 hours. The polymer was then concentrated and dried via vacuum pump for 24 hours. The polymer was characterized by NMR (**Appendix Figure A30**) and GPC (**Table 4.1**). ^{1}H NMR (500 MHz, CDCl3): δ 4.27 (br, 4H), 3.12 (br, 2H), 2.61 (m, 6H), 2.52 (m, 4H), 2.24 (s, 6H), 1.98 (br, 2H), 1.84 (br, 2H), 1.55 (m, 2H), 1.28 (m, 10H), 0.88 (t, 3H).

All the other polymers were synthesized using an identical procedure with different monomers.

The exact moles of monomers used for different copolymers were:

M1:M2 (2:2): 5.10×10^{-4} mol : 5.10×10^{-4} mol

M1:M2 (1:3): 2.55×10^{-4} mol : 7.65×10^{-4} mol

M1:M2 (3:1): 7.65×10^{-4} mol : 2.55×10^{-4} mol

4.3.2.5 Scalability Verification

A gram scale reaction was carried out for copolymer N1C6 (1:3) to examine scalability

N1C6 (1:3): Synthesis of *poly{4-((2-(dimethylamino)ethyl)thio)tetrahydro-2H-pyran-2-one}-r-poly{4-(hexylthio)tetrahydro-2H-pyran-2-one}*. Monomer **N1** (0.25 g, 1.2×10^{-3} mol) and Monomer **C6** (0.8 g, 3.6×10^{-3} mol) were added to a flame-dried glass vial. 153 µL Methyl lithium

(1.6 M in ether) was then added into the reaction vial to initiate the polymerization. The polymer was collected after 5 minutes and dialyzed against THF for 4 hours. The polymer was then concentrated and dried via vacuum pump for 24 hours. Yield = 87.7%. The polymer was characterized via NMR and GPC (**Figure 4.1**). ^{1}H NMR (500 MHz, CDCl3): δ 4.27 (br, 4H), 3.12 (br, 2H), 2.61 (m, 6H), 2.52 (m, 4H), 2.24 (s, 6H), 1.98 (br, 2H), 1.84 (br, 2H), 1.55 (m, 2H), 1.28 (m, 6H), 0.88 (t, 3H).

4.3.2.6 Mechanistic Study

According to previous studies, we propose that the initiation step involves nucleophilic attack of the carbonyl carbon in the monomer by methyl anion in CH_3Li resulting in the scission of acyl oxygen bond to generate alcoholate ion, which initiates ring-opening polymerization.[28 29,30] To verify the initiation step in the proposed mechanism, we carried out the following model reaction. After quenching the reaction with water, we identified a diol compound as a major product (**Appendix Figure A31**), clearly indicating that the polymerization is initiated by the nucleophilic attack of carbonyl carbon by methyl anion. The model reaction proceeds via nucleophilic acyl substitution in the lactone ring first with one equivalent of CH_3Li, and then nucleophilic addition to the carbonyl bond with one more equivalent of CH_3Li. 0.64 mL of CH_3Li (1.6 M in ether) was added in a flame-dried Schlenk flask. The flask was cooled to 0 °C. 0.1 g **C6** was diluted in 2 mL of dried toluene, and was added drop wise into the CH_3Li solution. The reaction was left at 0 °C for 10 more minutes and was then quenched with H_2O. The product was separated via column chromatography to yield compound **1** (0.075 g, 75%). The product was confirmed by ^{1}H NMR and MS. ^{1}H NMR (500 MHz, $CDCl_3$) δ 3.80 (m, 2H), 3.01 (p, 1H), 2.57 (m, 2H), 2.40 (br, 2H),

1.85 (m, 2H), 1.75 (d, 2H), 1.58 (p, 2H), 1.38 (p, 2H), 1.28 (br, 4H), 1.25 (s, 6H), 0.88 (t, 3H). [M-18] m/z = 230.1.

4.3.2.7 Measurement of pKa

pKa Measurement Through pH Titration

The selected copolymer (15 mg) was first dissolved in 100 μL THF and transferred into 20 mL deionized and purified water with 90 μL 1.0 M HCl (*aq.*). The pH titration was carried out by adding 5 μL of 1M NaOH solution (*aq.*) under stirring. The pH increase in the range of 2 to 12 was monitored as a function of total added volume of NaOH (V_{NaOH}). The pH values were measured using a Mettler Toledo pH meter with a microelectrode.

4.3.3 INSTRUMENTATION

4.3.3.1 Robotic Automation

Nanoparticle (NP) formulations and *in vitro* screening were performed on a Tecan Freedom EVO 200 fluid handling robot equipped with an 8-channel liquid handling arm (LiHa), multi-channel arm with 96-channel head (MCA), robotic manipulator arm (RoMa), and an integrated InfiniTe F/M200 Pro microplate reader (Tecan). Two integrated custom heating and stirring chemical reaction stations (V&P Scientific 710E-3HM Series Tumble Stirrers) provided reaction and mixing support. All operations were programmed in EVOware Standard software (Tecan).

4.3.3.2 Nuclear Magnetic Resonance (NMR) Spectroscopy

^{1}H and ^{13}C NMR were performed on a Varian 500 MHz spectrometer.

4.3.3.3 Molecular Weight Analysis

For polymers soluble in DMF, the molecular weight was measured by Gel Permeation Chromatography (GPC) (Viscotek) equipped with RI detection and ViscoGEL I-series columns (Viscoteck I-MBLMW-3078) using DMF as the eluent at 0.75 mL/min and 45 °C. For polymers not soluble in DMF, the molecular weight were measured by GPC with THF as the eluent at 1 mL/min and 35 ºC (Malvern / Viscotek) equipped with an RI detector (Malvern / Viscotek). The instruments were calibrated with a series of 10 narrow polydispersity polystyrene standards (500 to 200,000 g/mol).

4.3.3.4 Flash Chromatography

Flash chromatography was performed on a Teledyne Isco CombiFlash Rf-200i chromatography system equipped with UV-vis and evaporative light scattering detectors (ELSD).

4.3.3.5 Transmission Electron Microscopy (TEM)

TEM was performed on a FEI Tecnai G2 Spirit Biotwin at an accelerated voltage of 120 kW. For sample preparation, a drop of formulated NP was placed on a carbon film covered TEM grid, excess liquid was then wicked by filter paper. The copper grid was then dried under vacuum for one hour.

4.3.3.6 NP Size Analysis

Particle sizes were measured by Dynamic Light Scattering (DLS) using a Malvern Zetasizer Nano ZS (He-Ne laser, $\lambda = 632$ nm).

4.3.3.7 Nanoparticle Formulation for *In Vivo* Studies

Formulated polymeric nanoparticles for *in vivo* studies were prepared using a microfluidic mixing instrument with herringbone rapid mixing features (Precision Nanosystems NanoAssemblr). Ethanol solutions of polymers, DSPC, cholesterol, and PEG lipid were rapidly combined with acidic solutions of siRNA. The typical ratio of aqueous:EtOH was 3:1 (volume) and the typical flow rate was 12 mL/minute.

4.4 RESULTS

To develop an efficacious degradable polymer delivery system, we used a unique synthetic strategy to rapidly build a library of lipocationic polyesters via anionic ROP. As previously noted, tertiary amines and alkyl chains are critical functional groups for effective siRNA delivery.[3,6-8,31-33] However, the synthesis of amine-containing lactones (and polyesters) is not straightforward because nucleophilic amines can hydrolyze esters over time. To pursue this goal, we initially explored aza-Michael addition of secondary amines to 5,6-dihydro-2H-pyran-2-one (DPO), but the resulting functionalized valerolactones could not be polymerized. Monomers were successfully synthesized, but underwent retro-Michael addition in the presence of Lewis acid catalysts and did not open under basic conditions. Concurrent to these efforts, successful thiol-Michael addition to DPO was reported.[23] Inspired by that paper, we adapted our protocol to utilize functional thiols. We synthesized seven tertiary amine containing aminothiols via reaction with ethylene sulfide (**Scheme 4.1**). The resulting amino thiols were reacted with DPO at a 1:1 ratio to give tertiary amine functionalized valerolactone monomers (**Scheme 4.2**). Six alkylated valerolactone monomers were also synthesized via a similar strategy but required addition of dimethylphenylphosphine (DMPP) to catalyze the reaction. In this way, monomers were synthesized through a single step, which enabled functional monomer/polymer synthesis in gram scale (**Figure 4.1**). Although we purified most of the monomers reported herein, complete reaction conversion enabled the polymerization to be conducted in one pot from monomer synthesis to polymer synthesis.

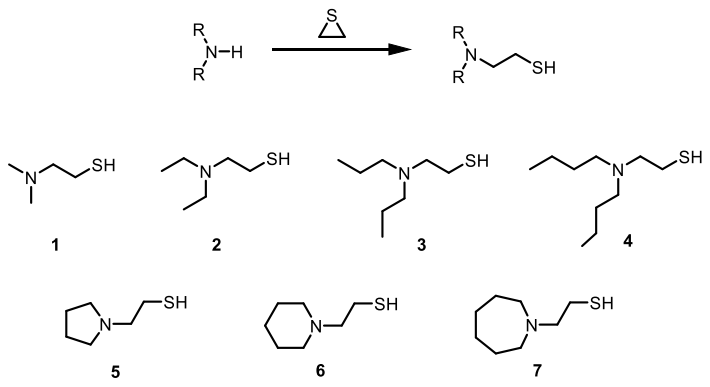

Scheme 4.1. Synthesis of aminothiols via reaction of secondary amines with ethylene sulfide (**AT1-AT7**).

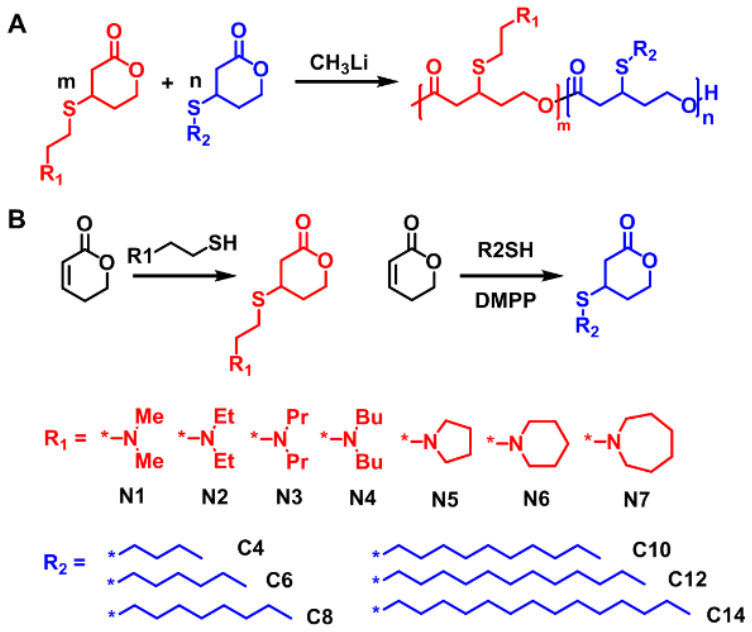

Scheme 4.2. (A) A combinatorial library of 139 lipocationic polyesters was synthesized. (B) Unprotected monomers were synthesized in one step from commercially available DPO with aminothiols (N1-N7) and alkylthiols (C4-C14).

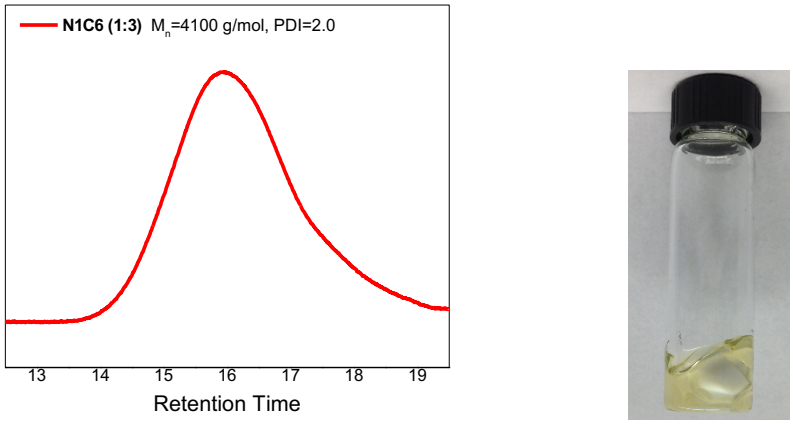

Figure 4.1. GPC trace (left) and photograph of polymerization mixture of viscous polymer **N1C6 (1:3)** synthesized on 1+ gram scale (right).

To explore structure-activity relationships (SAR), we synthesized random copolymers from all monomers through anionic ROP using methyl lithium[29] as the initiator (**Scheme 4.2**). This allowed us to prepare polymers without initiator chain end functionality, so that delivery ability could be better correlated with the polymer composition. Homo- and random (co)polymerizations were carried out in bulk in a glove box and reached high monomer conversion (90% on average) (**Table 4.1**), which allowed for siRNA delivery screening directly without purification (**Figure 4.2** and **Figure 4.3**). The library consists of different combinations of the two monomer types at three different mole ratios in the feed (3:1, 2:2, and 1:3) (**Figure 4.4**). The final monomer incorporation was very close to the feed ratio (**Table 4.2**). There was good agreement of molecular weight to theoretical molecular weight based on Gel Permeation Chromatography (GPC) and ^{1}H NMR (**Table 4.1-4.2**). The mechanism of this reaction involves the nucleophilic attack of carbonyl carbon on the monomer by methyl anion in the initiator, which results in scission of acyl-oxygen bond, and the polymerization propagates via an alcoholate ion (**Scheme 4.3**). It is worth noting

that polymerization with some conventional ROP catalysts including tin (II) octanoate, alkoxides and organocatalysts[23,34,35] were not successful. However, Grignard reagents were able to initiate the functional valerolactones reported in this communication (**Table 4.3**). In this way, polymers with functional groups at the chain ends could be prepared. The use of addition reactions and easily obtainable starting materials allowed us to rapidly build a library of 139 functional polyesters in about one week. Polymer degradation analysis was also carried out (**Table 4.4** and **Figure 4.5**).

Table 4.1. GPC analysis of lipocationic polymers synthesized at different monomer ratios.
[a] M_n[a], and PDI[a] were analyzed by DMF GPC; M_n and PDI of all other polymers were analyzed by THF GPC; [b] Monomer conversion were determined by ^{1}H NMR.

Polymer	Mon 1	Mon 2	M1:M2 (mol)	M_n (theo)	M_n (GPC)	PDI (GPC)	Conversion[b]
N1	N1		4:0	3616	3018[a]	2.01[a]	89.0
N1C4 (2:2)	N1	C4	2:2	3360	2340	1.65	85.9
N1C4 (3:1)	N1	C4	3:1	3515	3332[a]	2.06[a]	88.2
N1C4 (1:3)	N1	C4	1:3	3342	4010	1.85	87.1
N1C6 (2:2)	N1	C6	2:2	3588	2687	1.62	85.6
N1C6 (3:1)	N1	C6	3:1	3546	3618[a]	1.86[a]	85.9
N1C6 (1:3)	N1	C6	1:3	3609	3770	1.71	84.8
N1C8 (2:2)	N1	C8	2:2	3950	3315	1.80	88.3
N1C8 (3:1)	N1	C8	3:1	3722	3510[a]	2.00[a]	87.2

N1C8 (1:3)	N1	C8	1:3	4057	5660	1.90	86.7
N1C10 (2:2)	N1	C10	2:2	4144	3760	1.70	87.2
N1C10 (3:1)	N1	C10	3:1	3817	3556[a]	1.96[a]	86.6
N1C10 (1:3)	N1	C10	1:3	4425	6670	1.74	86.8
N1C12 (2:2)	N1	C12	2:2	4653	5010	1.70	92.5
N1C12 (3:1)	N1	C12	3:1	4189	2922[a]	1.88[a]	92.1
N1C12 (1:3)	N1	C12	1:3	5045	8990	1.77	91.4
N1C14 (2:2)	N1	C14	2:2	4922	6164	1.59	92.6
N1C14 (3:1)	N1	C14	3:1	4245	3777[a]	1.32[a]	90.6
N1C14 (1:3)	N1	C14	1:3	5319	8430	1.61	89.6
N2	N2		4:0	4038	2392[a]	1.74[a]	87.3
N2C4 (2:2)	N2	C4	2:2	3746	3340	1.76	89.3
N2C4 (3:1)	N2	C4	3:1	3905	2258	1.78	88.5
N2C4 (1:3)	N2	C4	1:3	3599	5230	1.73	90.5
N2C6 (2:2)	N2	C6	2:2	4261	4525	1.67	95.2
N2C6 (3:1)	N2	C6	3:1	4320	2480	1.72	94.9
N2C6 (1:3)	N2	C6	1:3	4056	7020	1.70	92.2
N2C8 (2:2)	N2	C8	2:2	4255	4610	1.59	89.5
N2C8 (3:1)	N2	C8	3:1	4194	2571	1.70	89.4
N2C8 (1:3)	N2	C8	1:3	4514	7700	1.52	93.7
N2C10 (2:2)	N2	C10	2:2	4561	5720	1.54	90.6
N2C10 (3:1)	N2	C10	3:1	4262	2960	1.63	88.2
N2C10 (1:3)	N2	C10	1:3	4765	8250	1.55	90.9

N2C12 (2:2)	N2	C12	2:2	5000	6750	1.56	94.1
N2C12 (3:1)	N2	C12	3:1	4581	2536	1.52	92.2
N2C12 (1:3)	N2	C12	1:3	5156	10280	1.52	91.1
N2C14 (2:2)	N2	C14	2:2	4992	7300	1.61	89.2
N2C14 (3:1)	N2	C14	3:1	4667	4070	1.66	91.4
N2C14 (1:3)	N2	C14	1:3	5342	11220	1.71	87.9
N3	N3		4:0	4559	4270	1.49	87.9
N3C4 (2:2)	N3	C4	2:2	3957	6680	1.55	88.4
N3C4 (3:1)	N3	C4	3:1	4227	5873	1.34	87.5
N3C4 (1:3)	N3	C4	1:3	3710	7600	1.57	90.1
N3C6 (2:2)	N3	C6	2:2	4149	7623	1.48	87.3
N3C6 (3:1)	N3	C6	3:1	4350	6860	1.45	87.5
N3C6 (1:3)	N3	C6	1:3	3982	8930	1.60	87.7
N3C8 (2:2)	N3	C8	2:2	4453	8160	1.48	88.4
N3C8 (3:1)	N3	C8	3:1	4490	7120	1.42	87.8
N3C8 (1:3)	N3	C8	1:3	4321	8900	1.55	87.1
N3C10 (2:2)	N3	C10	2:2	4645	8510	1.50	87.4
N3C10 (3:1)	N3	C10	3:1	4654	6480	1.50	88.6
N3C10 (1:3)	N3	C10	1:3	4673	10320	1.53	86.9
N3C12 (2:2)	N3	C12	2:2	5115	10360	1.65	91.4
N3C12 (3:1)	N3	C12	3:1	4903	8970	1.59	91.0
N3C12 (1:3)	N3	C12	1:3	5239	11660	1.53	90.3
N3C14 (2:2)	N3	C14	2:2	5244	9540	1.66	89.3

N3C14 (3:1)	N3	C14	3:1	4967	8120	1.64	89.9
N3C14 (1:3)	N3	C14	1:3	5618	9120	1.71	90.3
N4	N4		4:0	5023	3560	1.46	87.4
N4C4 (2:2)	N4	C4	2:2	4379	5980	1.62	92.1
N4C4 (3:1)	N4	C4	3:1	4729	5183	1.53	90.0
N4C4 (1:3)	N4	C4	1:3	3843	6580	1.63	90.2
N4C6 (2:2)	N4	C6	2:2	4542	6590	1.59	90.2
N4C6 (3:1)	N4	C6	3:1	4835	5720	1.62	89.7
N4C6 (1:3)	N4	C6	1:3	4272	8010	1.67	91.3
N4C8 (2:2)	N4	C8	2:2	4815	7070	1.54	90.6
N4C8 (3:1)	N4	C8	3:1	4978	5810	1.55	90.0
N4C8 (1:3)	N4	C8	1:3	4578	8800	1.55	89. 8
N4C10 (2:2)	N4	C10	2:2	5041	7870	1.56	90.1
N4C10 (3:1)	N4	C10	3:1	5077	6270	1.59	89.5
N4C10 (1:3)	N4	C10	1:3	4895	9030	1.69	88.7
N4C12 (2:2)	N4	C12	2:2	5296	9110	1.75	90.2
N4C12 (3:1)	N4	C12	3:1	5230	9630	1.54	90.0
N4C12 (1:3)	N4	C12	1:3	5323	9260	1.87	89.6
N4C14 (2:2)	N4	C14	2:2	5524	9770	1.74	89.8
N4C14 (3:1)	N4	C14	3:1	5531	8270	1.68	93.0
N4C14 (1:3)	N4	C14	1:3	5734	9880	1.82	90.2
N5	N5		4:0	3878	2180[a]	1.80[a]	84.5
N5C4 (2:2)	N5	C4	2:2	3673	3200[a]	2.13[a]	88.0

N5C4 (3:1)	N5	C4	3:1	3928	2560[a]	2.00[a]	89.7
N5C4 (1:3)	N5	C4	1:3	3511	3652	1.90	88.5
N5C6 (2:2)	N5	C6	2:2	4004	3364[a]	2.13[a]	89.9
N5C6 (3:1)	N5	C6	3:1	4023	2460[a]	2.07[a]	89.0
N5C6 (1:3)	N5	C6	1:3	3933	5880	1.71	89.6
N5C8 (2:2)	N5	C8	2:2	4220	2568	1.70	89.1
N5C8 (3:1)	N5	C8	3:1	4164	2310[a]	1.94[a]	89.3
N5C8 (1:3)	N5	C8	1:3	4336	5750	1.65	90.2
N5C10 (2:2)	N5	C10	2:2	4436	3260	1.67	88.5
N5C10 (3:1)	N5	C10	3:1	4187	3380[a]	2.11[a]	87.2
N5C10 (1:3)	N5	C10	1:3	4665	8700	1.58	89.2
N5C12 (2:2)	N5	C12	2:2	4997	4190	1.61	94.4
N5C12 (3:1)	N5	C12	3:1	4434	2390[a]	1.96[a]	89.8
N5C12 (1:3)	N5	C12	1:3	5311	11650	1.55	94.0
N5C14 (2:2)	N5	C14	2:2	5230	5268	1.65	93.8
N5C14 (3:1)	N5	C14	3:1	4707	2500[a]	2.02[a]	92.7
N5C14 (1:3)	N5	C14	1:3	5363	7010	1.67	88.4
N6	N6		4:0	4387	2810[a]	1.85[a]	90.1
N6C4 (2:2)	N6	C4	2:2	3900	4291	1.65	90.4
N6C4 (3:1)	N6	C4	3:1	4163	2740	1.71	90.7
N6C4 (1:3)	N6	C4	1:3	3652	5940	1.60	90.4
N6C6 (2:2)	N6	C6	2:2	4188	5400	1.59	91.1
N6C6 (3:1)	N6	C6	3:1	4361	3440	1.64	92.2

N6C6 (1:3)	N6	C6	1:3	4051	8180	1.51	90.9
N6C8 (2:2)	N6	C8	2:2	4464	6013	1.53	91.6
N6C8 (3:1)	N6	C8	3:1	4547	3765	1.69	93.4
N6C8 (1:3)	N6	C8	1:3	4540	8124	1.46	93.1
N6C10 (2:2)	N6	C10	2:2	4791	7326	1.49	92.9
N6C10 (3:1)	N6	C10	3:1	4687	4100	1.64	93.5
N6C10 (1:3)	N6	C10	1:3	4922	9680	1.52	92.9
N6C12 (2:2)	N6	C12	2:2	4912	8050	1.69	90.4
N6C12 (3:1)	N6	C12	3:1	4593	4320	1.67	89.2
N6C12 (1:3)	N6	C12	1:3	5216	8880	1.69	91.2
N6C14 (2:2)	N6	C14	2:2	5199	6480	1.75	91.0
N6C14 (3:1)	N6	C14	3:1	4897	4800	1.40	92.6
N6C14 (1:3)	N6	C14	1:3	5511	10897	1.70	89.8
N7	N7		4:0	4639	2840[a]	2.26[a]	90.1
N7C4 (2:2)	N7	C4	2:2	4131	2285	1.85	92.7
N7C4 (3:1)	N7	C4	3:1	4389	1614	1.91	91.4
N7C4 (1:3)	N7	C4	1:3	3728	5838	1.85	90.8
N7C6 (2:2)	N7	C6	2:2	4316	5520	1.71	91.2
N7C6 (3:1)	N7	C6	3:1	4483	2950	1.76	90.7
N7C6 (1:3)	N7	C6	1:3	4094	7853	1.75	90.4
N7C8 (2:2)	N7	C8	2:2	4532	5481	1.69	90.4
N7C8 (3:1)	N7	C8	3:1	4583	3170	1.71	90.2
N7C8 (1:3)	N7	C8	1:3	4478	8090	1.63	90.5

N7C10 (2:2)	N7	C10	2:2	4814	5950	1.79	90.9
N7C10 (3:1)	N7	C10	3:1	4887	3930	1.77	93.6
N7C10 (1:3)	N7	C10	1:3	5066	8860	1.70	94.3
N7C12 (2:2)	N7	C12	2:2	5027	6670	1.76	90.2
N7C12 (3:1)	N7	C12	3:1	4931	4072	1.77	92.0
N7C12 (1:3)	N7	C12	1:3	5399	8367	1.68	93.3
N7C14 (2:2)	N7	C14	2:2	5290	7052	1.71	90.4
N7C14 (3:1)	N7	C14	3:1	5013	3412	1.60	91.2
N7C14 (1:3)	N7	C14	1:3	5680	8628	1.67	91.5
C4		C4	0:4	3310	2360[a]	1.74[a]	87.6
C6		C6	0:4	3732	2600[a]	1.92[a]	86.4
C8		C8	0:4	4215	3350[a]	1.69[a]	86.3
C10		C10	0:4	4696	2750[a]	1.31[a]	86.3
C12		C12	0:4	5178	2860[a]	1.53[a]	86.4
C14		C14	0:4	2247	1510[a]	1.21[a]	34.6

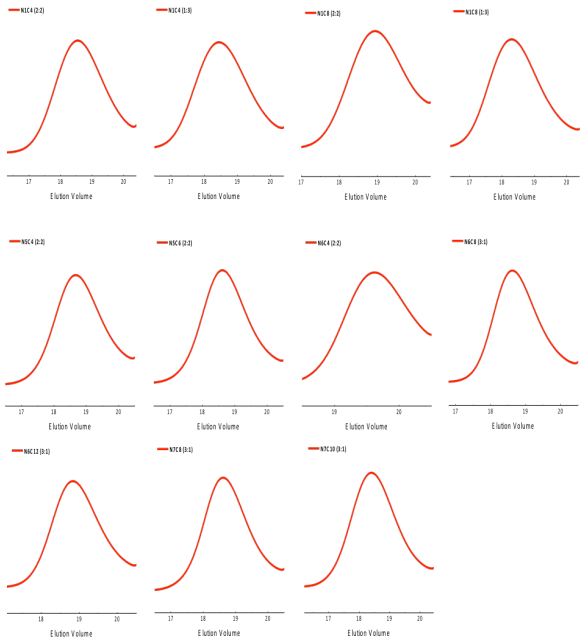

Figure 4.2. GPC traces of top performing polymers using DMF line.

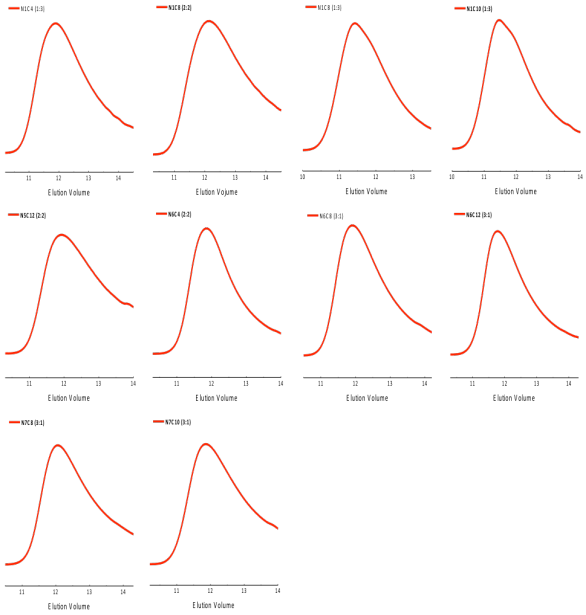

Figure 4.3. GPC traces of top performing polymers using THF line. Tailing at low MW side is due to amine interactions with the column (no base was added to the THF mobile phase).

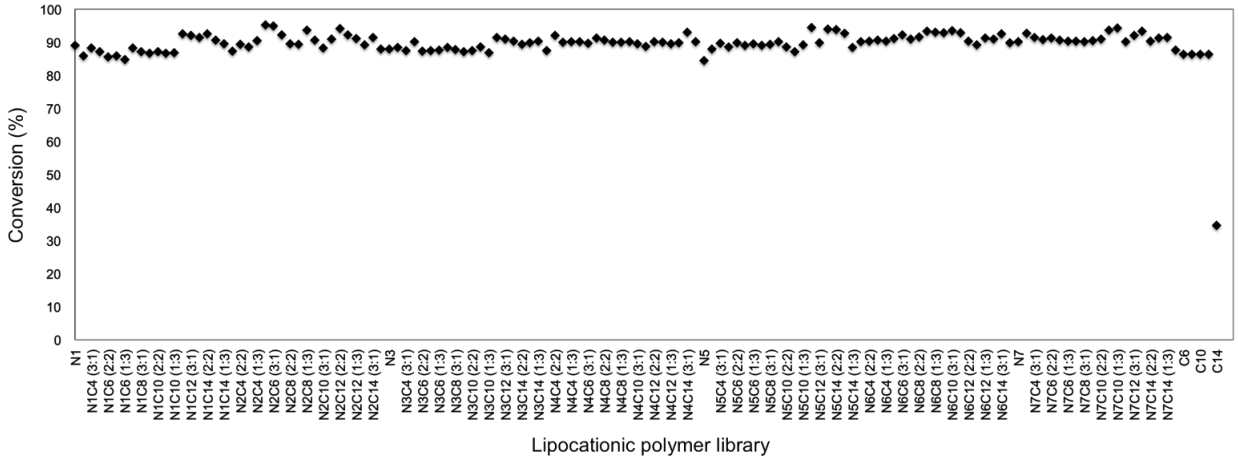

Figure 4.4. Plot of monomer conversion to polymer for all polymerizations. Calculated by ^{1}H NMR.

Table 4.2. ^{1}H NMR analysis to compare the monomer feed ratio to final copolymer composition.

Polymer	Mon 1	Mon 2	M1:M2 (mol)	N1 in feed (%)	N1 in final copolymer (%)
N1C4 (2:2)	N1	C4	2:2	50 %	49.2 %
N1C8 (2:2)	N1	C8	2:2	50 %	47.5 %
N1C8 (1:3)	N1	C8	1:3	25 %	25.1 %

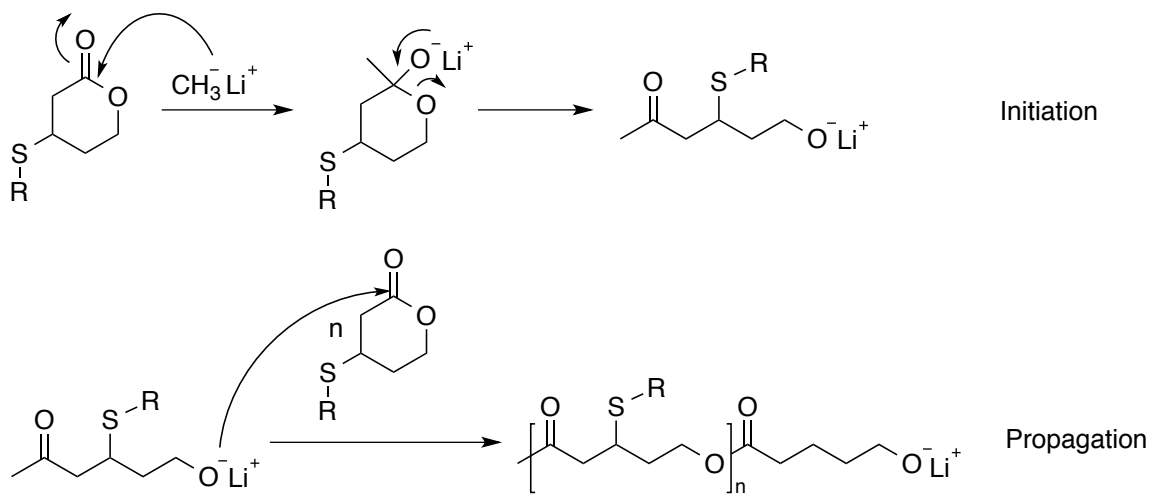

Scheme 4.3. Proposed mechanism of ring-opening polymerization by CH_3Li.

Table 4.3. Grignard reagents are also able to initiate polymerization. Various conditions were attempted, and are summarized below.

Mon	M:I ratio	Initiator	Solvent	T (ºC)	Conv. (%)	M_n (GPC)	PDI
N1	20:1	$C_{12}H_{25}MgBr$	bulk	r.t.	68.3	4,680	1.66
N2	10:1	CH_3MgBr	THF	r.t.	17.5	2,470	1.56
N2	20:1	CH_3MgBr	bulk	r.t.	78.11	5,740	1.58
N2	20:1	CH_3MgBr	toluene	r.t.	26.5	3,580	1.64
N2	20:1	CH_3MgBr	THF	-78	28.82	3,720	1.86
N2	20:1	CH_3MgBr	bulk	r.t.	59.0	7,200	1.39
N2	20:1	CH_3MgBr	toluene	r.t.	23.0	3,820	1.41
N2	20:1	CH_3MgBr	THF	r.t.	25.3	5,550	1.54

N3	20:1	CH_3MgBr	bulk	r.t.	59.0	4,730	1.46
N4	20:1	CH_3MgBr	bulk	r.t.	73.6	6,480	1.33
N4	20:1	CH_3MgBr	bulk	r.t.	82.3	4,280	1.27
N5	20:1	CH_3MgBr	bulk	r.t.	66.7	3,110	1.44
N6	20:1	CH_3MgBr	bulk	r.t.	60.9	3,180	1.43
C8	20:1	CH_3MgBr	bulk	r.t.	84.19	5,700	1.37
C8	20:1	CH_3MgBr	toluene	r.t.	16.32	2,620	1.43
N1+C8	10:10:1	CH_3MgBr	bulk	r.t.	84.02	7,100	1.51
N1+C8	15:5:1	CH_3MgBr	bulk	r.t.	74.45	4,600	1.46
N1+C8	5:15:1	CH_3MgBr	bulk	r.t.	81.1	8,590	1.40

Table 4.4. GPC analysis to confirm polyester degradation in this class of materials. Two representative copolymers were chosen and dissolved in 1M HCl (*aq.*). The molecular weight was measured before degradation and also after 24 hours.

Polymer	**Initial M_n (GPC)**	**Initial M_w (GPC)**	**Initial PDI (GPC)**	**After 24 hrs M_n (GPC)**	**After 24 hrs M_w (GPC)**	**After 24 hrs PDI (GPC)**
N3C8 (2:2)	4000	5900	1.5	1700	2800	1.6
N2C8 (1:3)	4200	8600	2.1	2500	5400	2.2

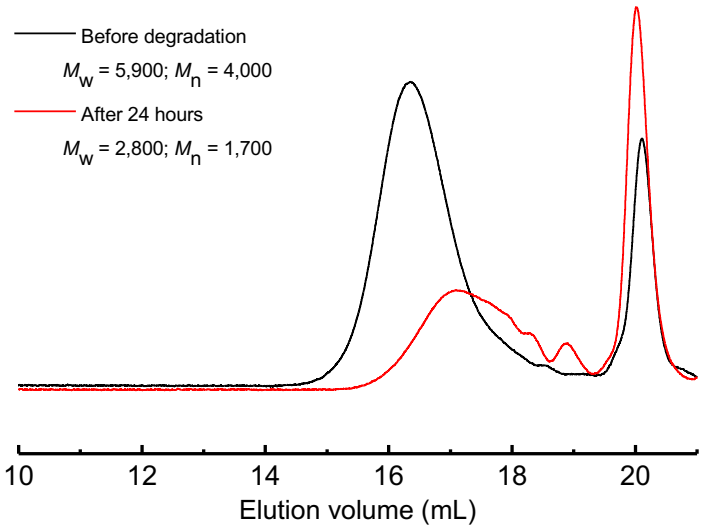

Figure 4.5. Degradation study on N3C8 (2:2) to confirm hydrolysis of ester bonds in polymer backbone. MW was measured before degradation and after 24 hours.

To date, the most efficacious materials for *in vivo* siRNA delivery have been lipid nanoparticles (LNPs) composed of a cationic or ionizable lipid, 1,2-distearoyl-sn-glycero-3-phosphocholine (DSPC), cholesterol, and lipid poly(ethylene glycol) (PEG).[7,31,32] These components reduce aggregation and provide enhanced NP stability at physiological conditions. In order to prepare *in vivo* ready NPs and to mitigate potential toxicity of cationic polymers, we employed a similar strategy in this work, replacing cationic lipids with lipocationic polymers (**Figure 4.6A**). A NP formulation consisting of polymer:DSPC:cholesterol:PEG lipid = 50:10:35:5 (mole) typically had an average diameter of ~75 nm in PBS by dynamic light scattering (DLS) (**Figure 4.6C**). The size could be tuned from 40 nm to 300 nm by adjusting the mixing conditions and the formulation components. For example, increasing the PEG lipid amount yielded smaller NPs (**Figure 4.7**). The morphology of an efficacious polymeric NP N1C8 (2:2) was studied using Transmission Electron Microscopy (TEM) (**Figure 4.6D**). An average diameter of 70 nm was

observed, which is in agreement with DLS results. The NPs exhibit spherical morphology where a less dense particle shell consists mainly of PEG lipid and a more textured and electron dense core consists of siRNA in aqueous pockets surrounded by DSPC and lipocationic polymers. This is consistent with previous computational modeling reports of nanostructured LNPs.[36] The cellular uptake of various lead polymeric NPs was monitored in HeLa-Luc cells using confocal microscopy. NPs were internalized into cells within 3 hours (**Figures 4.6B and 4.8**).

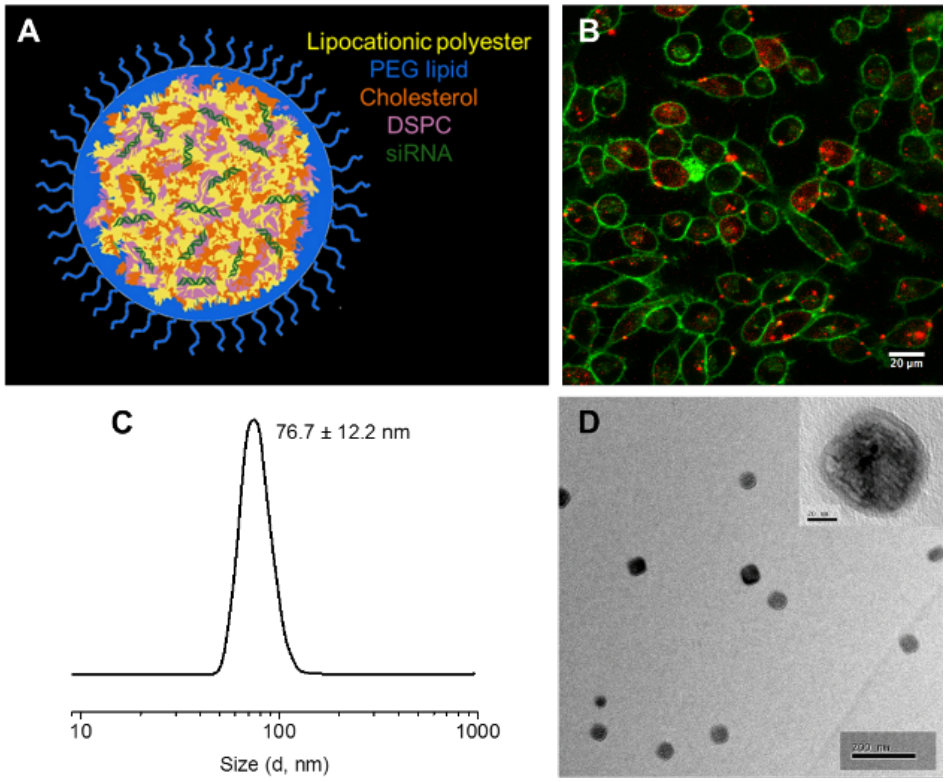

Figure 4.6. (A) Representative scheme of polymeric nanoparticle composition. (B) Cellular internalization of Cy5.5-siRNA loaded N1C8 (2:2) NPs (red) after 3hr of incubation in HeLa-Luc cells. The cell membrane was stained with CellMask (green). (C) Particle Size distribution measured by DLS and (D) TEM image obtained for formulated NP N1C8 (2:2).

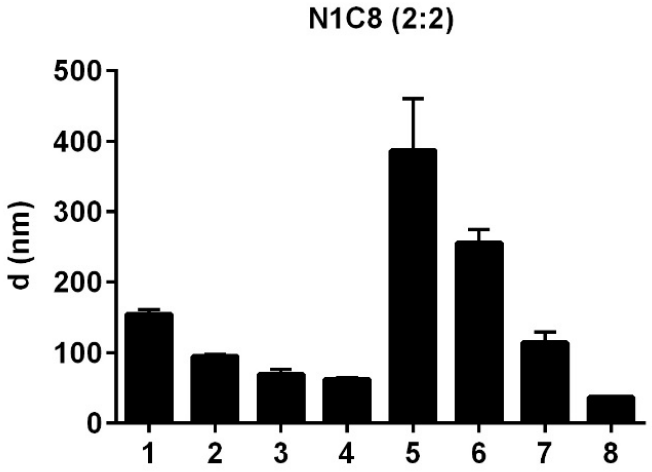

Entry	Total delivery components:siRNA (wt)	N1C8(2:2):cholesterol:DSPC:PEG-lipid (mol)	d (nm)
1	7:1	50:38.5:10:1.5	154
2	7:1	50:35:10:5	95
3	15:1	50:35:10:5	69
4	20:1	50:35:10:5	62
5	20:1	70:15:10:5	387
6	25:1	50:35:10:5	255
7	25:1	50:30:10:10	114
8	30:1	50:30:10:10	36

Figure 4.7. Nanoparticle size can be controlled by mixing rations and conditions. DLS results for N1C8 (2:2) NPs with different ratio of components (n=5) (mean ± SEM). Within groups of fixed polymer:siRNA (wt) ratios, the size decreased when increasing the PEG-lipid amount. NPs were prepared using the NanoAssemblr. Ethanol solutions of polymers, DSPC, cholesterol, and PEG lipid were rapidly combined with acidic solutions of siRNA. The ratio of aqueous:EtOH was 3:1 (volume) and the flow rate was 12 mL/minute.

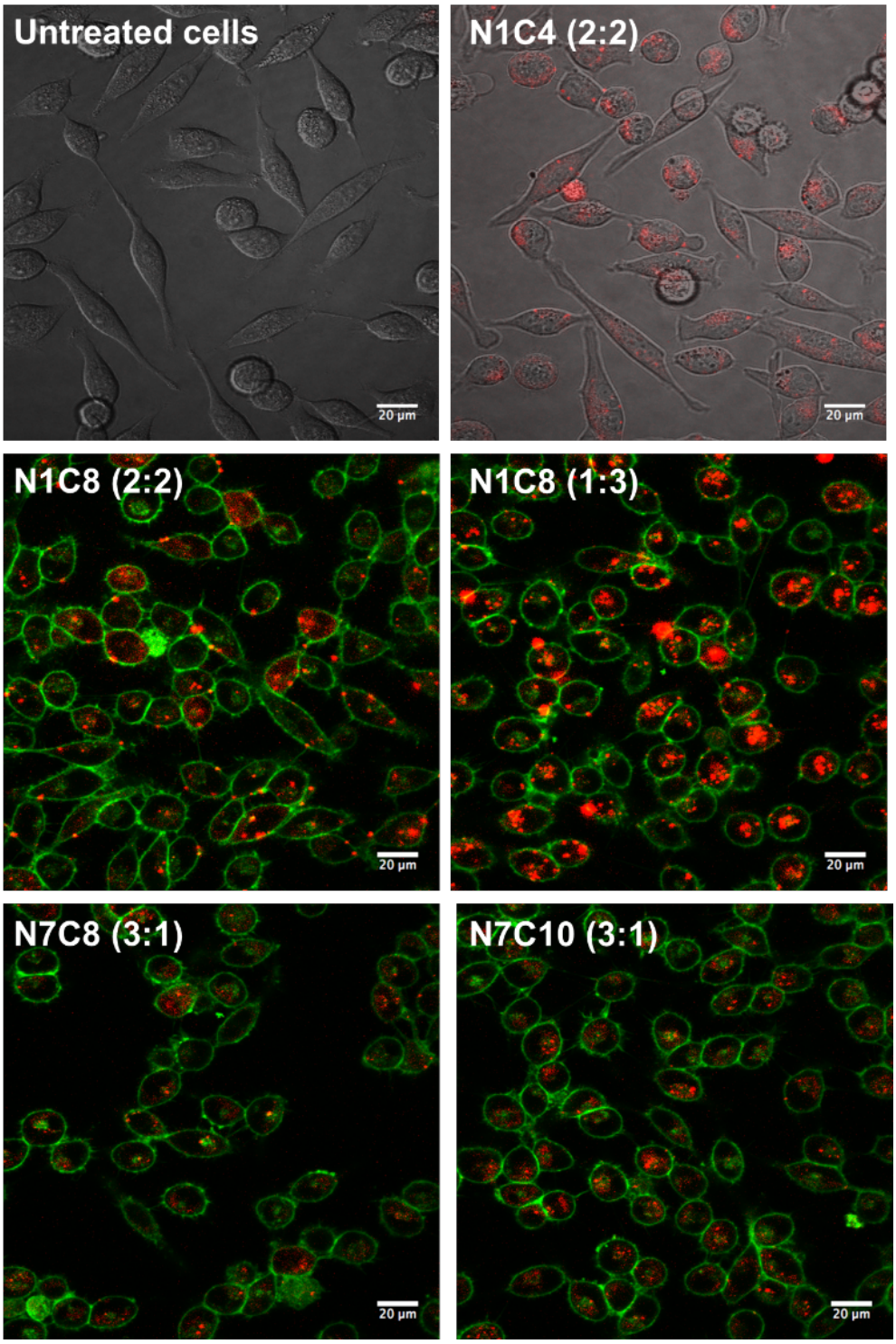

Figure 4.8. Cellular uptake of formulated Cy5.5-siLuc containing nanoparticles. The NPs are red, and the cell membrane is green (Cell Mask Orange).

The lipocationic polyester library was screened for siRNA delivery efficacy using an *in vitro* luciferase reporter assay in HeLa-Luc cells with the aid of an automated, fluid-handling robot (**Figure 4.9**). NPs were formulated by rapidly combining an ethanol solution of lipocationic polymers, DSPC, cholesterol and lipid PEG with an acidic aqueous buffer containing siRNA at a final molar ratio of 100:1 (polymer:siRNA). After dilution in PBS, the formulated nanoparticles were directly added to growing cells (**Figure 4.10**). Luciferase activity and cytotoxicity were measured after 48 hours relative to untreated cells (**Figure 4.11**). The polymeric NPs were non-toxic to cells at the screening dose (blue dots), with ~15 % of the polymer library enabling more than 80% knockdown efficiency (red bars) Six polymers enabled >90% silencing at a screening dose of 38.4 nM. Delivery using only DSPC, cholesterol, and lipid PEG did not exhibit significant silencing at this dose (**Figure 4.9**). Delivery efficiency strongly correlated with chemical structure because cationic and hydrophobic moieties were incorporated at precise ratios (**Table 4.2**). A heat map organized by feeding ratio of the aminothiol monomer vs. alkylthiol monomer elucidated trends related to hydrophobicity and pKa (**Figure 4.12**). In the top third of the heat map (3:1 amino:alkyl) ratio, the greatest activity is seen with the most hydrophobic amines, piperidine (N6) and azepane (N7). Moreover, N7 was only homopolymer that showed activity. For polymers containing the dimethylamine group (N1), additional hydrophobic content is required to promote NP stability at pH 7.4 and enable delivery (see bottom left third of heat map). When the hydrophobicity was increased (going from N1 to N3 left to right), less additional hydrophobic content from the alkyl comonomers was required to give a high delivery efficiency. Within a defined series that showed a smooth decrease of activity: N1C8 (2:2) → N2C8 (2:2) → N3C8 (2:2) → N4C8 (2:2), the pKa decreased from 6.1 to 4.0 (**Figure 4.13**). This is in agreement with reported pKa data for LNPs.[7] Dibutylamine (N4) polymers were completely inactive, likely due to

steric hindrance that reduced binding combined with a decreased pKa (**Figure 4.13**). For monomers containing cyclic amine side chains, N5 displayed a similar trend as N1, where more hydrophobic co-monomer was needed to give better delivery efficiency. N6-N7 were more hydrophobic, and therefore were most active when copolymerized with less hydrophobic monomers (3:1 ratio) (top third of the heat map). Overall, the 2:2 group showed the largest number of hits because this feed ratio provides the highest degree of balance of lipocationic properties. These data suggest an optimized combination of amino monomers and hydrophobic monomers is necessary to impart delivery activity.

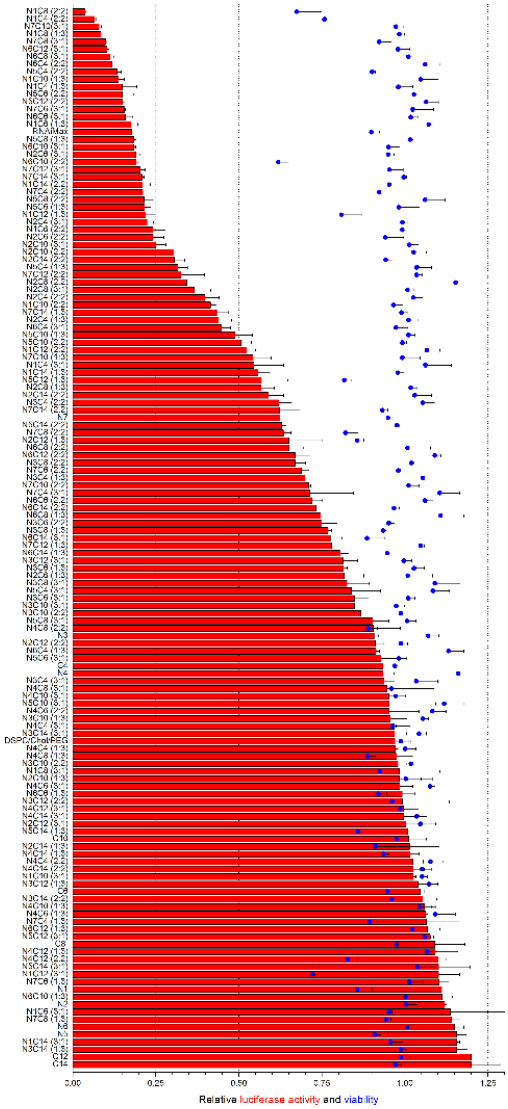

Figure 4.9. In vitro screening of formulated polyester library in Hela-Luc cells. Luciferase expression (red bars) and viability (blue dots) were measured after addition of NPs containing 100 ng (38.4 nM) siLuc and 48 hours incubation compared to untreated cells (n=4).

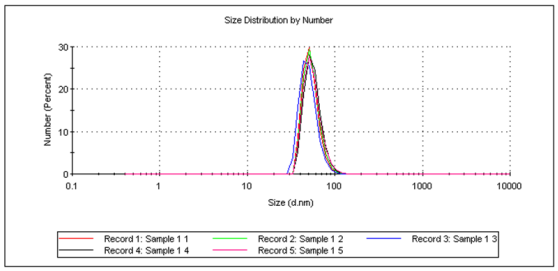

Figure 4.10. siRNA NP DLS sizing result. 5 runs of the same sample were performed and overlaid. N1C4 (2:2) NPs (N1C4 (2:2):cholesterol:DSPC:PEG-lipid = 50:35:10:5; polymer:siRNA = 20:1 (weight); aqueous:EtOH = 3:1 (volume)).

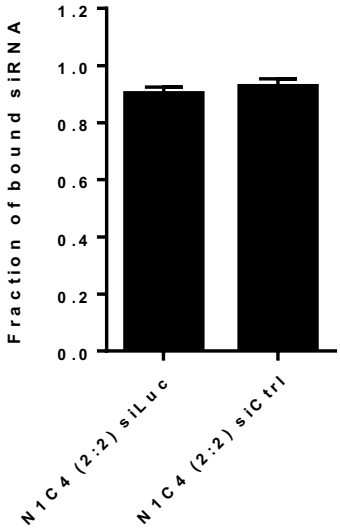

Figure 4.11. siRNA binding results for NPs used in *in vivo* experiments (siLuc and siControl). N1C4 (2:2) NPs (N1C4 (2:2):cholesterol:DSPC:PEG-lipid = 50:35:10:5; polymer:siRNA = 20:1 (weight); aqueous:EtOH = 3:1 (volume)).

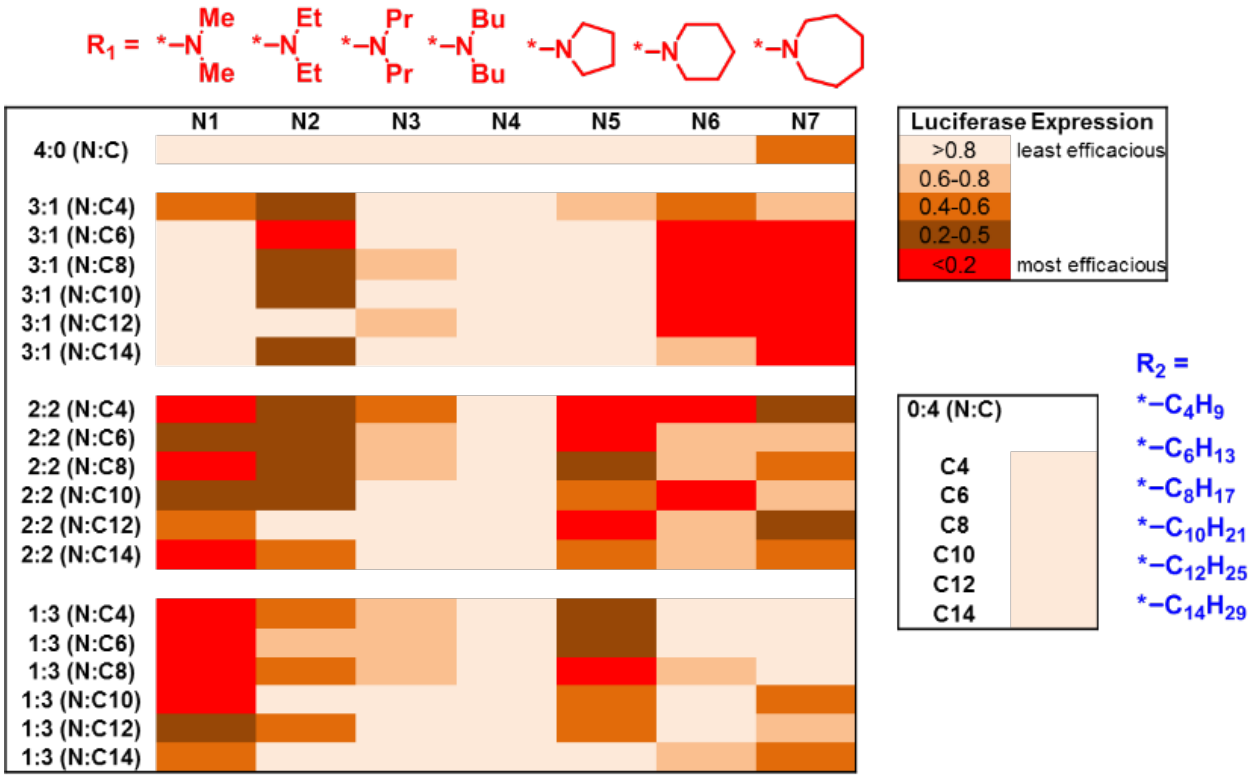

Figure 4.12. Heat map showing *in vitro* siRNA delivery and Structure Activity Relationships (SAR) for the formulated polyester library in Hela-Luc cells. The formulation consisted of polymer:DSPC:cholesterol:PEG lipid = 50:10:38:2 (mole). Hydrophobicity generally increases from top to bottom, by increasing the feed ratio of the alkyl monomer (4:0 to 1:3) and by increasing the alkyl length (C4 to C14).

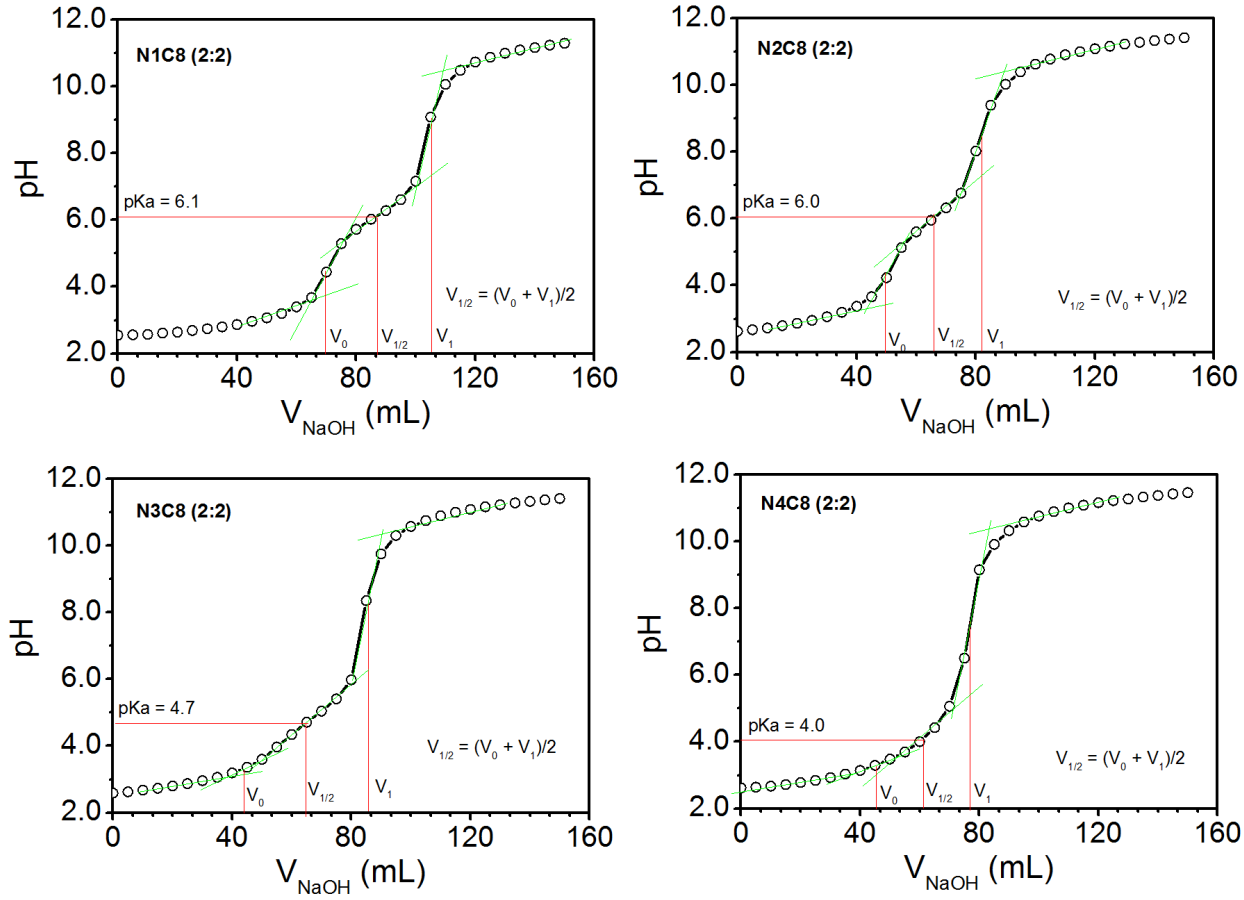

Figure 4.13. To further explore structure-activity relationships, pH titrations were performed to measure the pKa of a polymer series that displayed a clear siRNA delivery efficacy trend. Within the C8 (2:2) group, polymers N1C8 (2:2), N2C8 (2:2), N3C8 (2:2), and N4C8 (2:2) were analyzed. The pKa decreased from N1 to N4.

To investigate *in vitro* efficacy at low doses of siRNA, a dose response was conducted for the top 10 performing polymers (**Figure 4.14**). Polymers were re-synthesized and purified by dialysis to verify activity. NPs were incubated with cells at doses between 2.4 and 38.4 nM siRNA. Dose dependent silencing was observed for all the polymers tested. Five polymers facilitated greater than 80% silencing at a siRNA dosage of 9.6 nM. Also, two polymers enabled >90% silencing at a dosage of only 2.4 nM. In contrast, RNAiMax was less effective in silencing luciferase expression head-to-head at the same doses. To our knowledge, this is among the most potent polymer-based delivery systems reported to date.

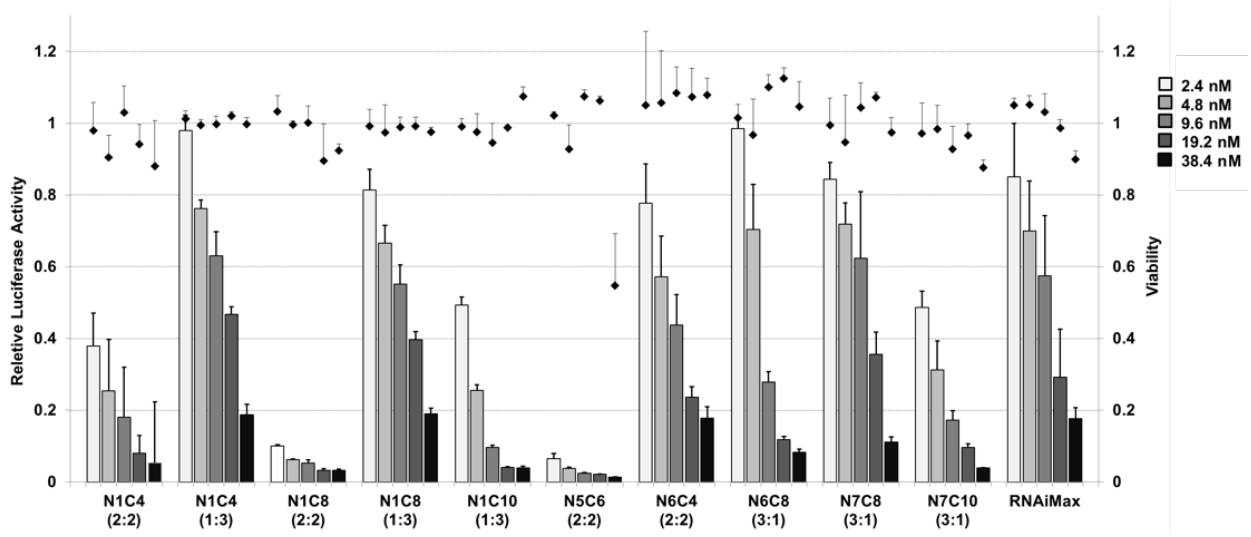

Figure 4.14. Dose-response of silencing in Hela-Luc cells for selection of the top performing polymers. The dose scale is 6.25 ng (2.4 nM), 12.5 ng (4.8 nM), 25 ng (9.6 nM), 50 ng (19.2 nM), and 100 ng (38.4 nM) going from left to right. Bars represent relative luciferase activity, while dots represent cell viability. Results were normalized to untreated cells (n=4). N1C8 (2:2) vs. RNAiMax.

Cancer therapy is one of the most promising applications for siRNA delivery. We therefore evaluated the ability of lipocationic polyester NPs to localize and deliver siRNA to tumors. We delivered a single dose of 2.5 mg/kg siRNA (1.25 mg/kg siLuc + 1.25 mg/kg Cy5.5-siLuc) via intravenous (IV) tail vein injection to nude mice bearing MDA-MB-231-Luc xenograft tumors in both flanks. After 2.5 hours, remarkably high tumor accumulation of N1C4 (2:2) NPs was measured (**Figure 4.15A**). Fluorescence signals from the liver and kidneys were also visualized. *Ex vivo* imaging of harvested organs confirmed effective tumor uptake (**Figure 4.16**). Moreover, luciferase activity in the tumors was greatly reduced after intratumoral (IT) injection of 2.5 mg/kg siLuc (**Figure 4.17**). Luciferase was quantified by bioluminescence (**Figure 4.15B**) and by tissue homogenization on total protein and tissue levels (**Figure 4.15C**).

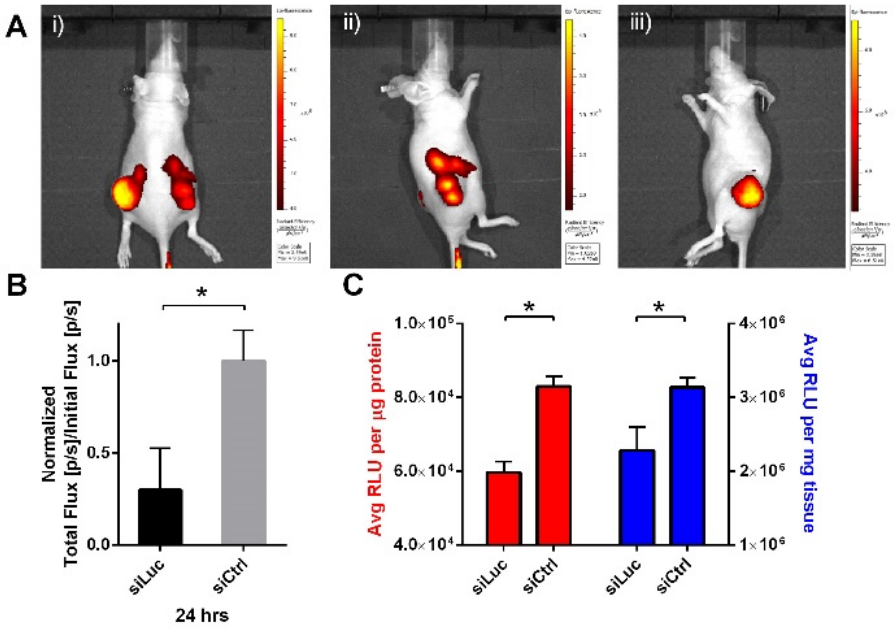

Figure 4.15. (A) N1C4 (2:2) NPs provided effective accumulation in tumor xenografts after IV injection. A representative mouse is shown from three angles. Luciferase silencing was measured in tumors 24 hours after injection by (B) bioluminescence imaging or (C) in tissue lysates normalized against total protein level or total tissue amount (n=4; *P < 0.05).

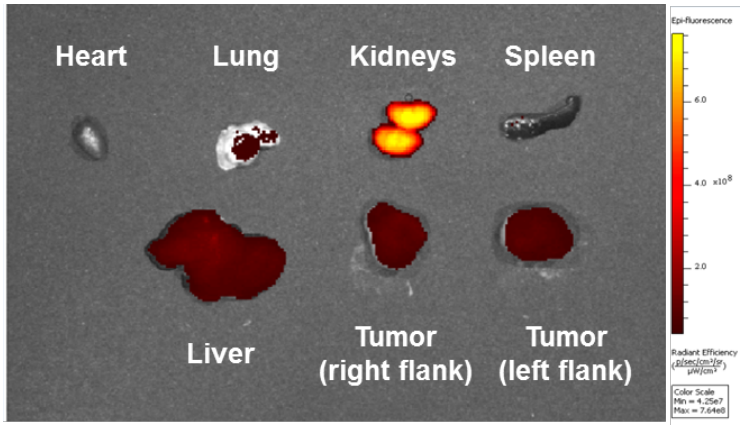

Figure 4.16. Organ distribution of siRNA-containing polymeric NPs 2.5 hours after IV injection. The MDA-MB-231 tumor-bearing mice were injected intravenously at a siRNA dose of 2.5 mg/kg. N1C4 (2:2) NPs (N1C4 (2:2):cholesterol:DSPC:PEG-lipid = 50:35:10:5; polymer:siRNA = 20:1 (weight); aqueous:EtOH = 3:1 (volume)).

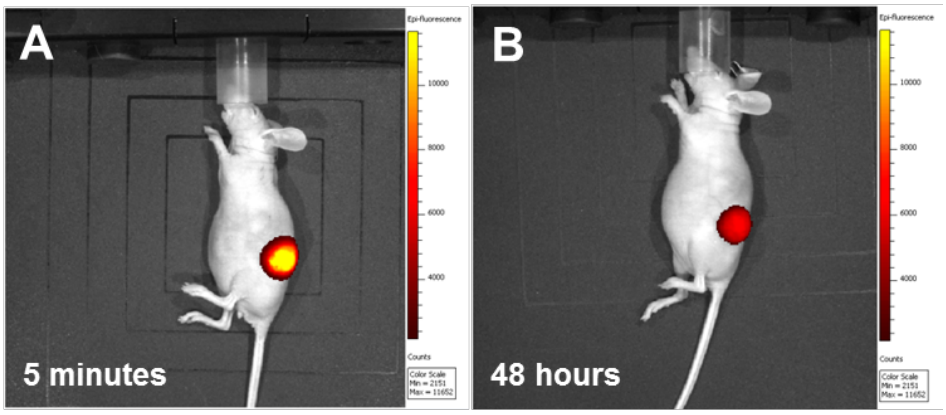

Figure 4.17. Tumor retention of siRNA-containing polymeric NPs 5 minutes (**A**) and 48 hours (**B**) after IT injection. The MDA-MB-231 tumor-bearing mice were injected intratumorally at a siRNA dose of 2.5 mg/kg. = 50:35:10:5; polymer:siRNA = 20:1 (weight); aqueous:EtOH = 3:1 (volume)).

4.5 CONCLUSION

In the spectrum of delivery systems, polymers have many advantages including tunable structural composition, degradability, and biocompatibility. Yet, they are currently less effective than lipid-based delivery vehicles. To overcome this challenge, we have incorporated key ionizable amines and hydrophobic alkyl chains into polyesters. We synthesized a library of lipocationic polyesters directly from functional monomers in high yield, fast time (~2 minutes), and in gram scale. This was accomplished with precise monomer incorporation ratios to enable tunable hydrophobicity and pKa. Formulated NPs enabled siRNA mediated silencing *in vitro* and *in vivo* at low dose. Notably, NPs could localize to tumors *in vivo* after IV delivery and were able to silence gene expression in tumor-bearing mice. This new class of lipocationic polyesters is a promising step towards closing the activity gap between lipids and polymers. Finally, we envision that the versatility of the chemical methods may allow preparation of functional polyesters for a variety of applications (in addition to gene delivery) because nearly any thiol can be used to synthesize functional monomers.

4.6 BIBLIOGRAPHY

1 Pack, D. W., Hoffman, A. S., Pun, S. & Stayton, P. S. Design and development of polymers for gene delivery. *Nat. Rev. Drug Discov.* **4**, 581-593, (2005).

2 Whitehead, K., Langer, R. & Anderson, D. Knocking down barriers: advances in siRNA delivery. *Nat. Rev. Drug Discov.* **8**, 129-138, (2009).

3 Kanasty, R., Dorkin, J. R., Vegas, A. & Anderson, D. Delivery materials for siRNA therapeutics. *Nat. Mater.* **12**, 967-977, (2013).

4 Albertsson, A. C. & Varma, I. K. Aliphatic polyesters: Synthesis, properties and applications. *Adv. Polym. Sci.* **157**, 1-40, (2002).

5 Akinc, A., Zumbuehl, A., Goldberg, M., Leshchiner, E. S., Busini, V., Hossain, N., Bacallado, S. A., Nguyen, D. N., Fuller, J. & Alvarez, R. A combinatorial library of lipid-like materials for delivery of RNAi therapeutics. *Nat. Biotechnol.* **26**, 561, (2008).

6 Siegwart, D. J., Whitehead, K. A., Nuhn, L., Sahay, G., Cheng, H., Jiang, S., Ma, M. L., Lytton-Jean, A., Vegas, A., Fenton, P., Levins, C. G., Love, K. T., Lee, H., Cortez, C., Collins, S. P., Li, Y. F., Jang, J., Querbes, W., Zurenko, C., Novobrantseva, T., Langer, R. & Anderson, D. G. Combinatorial synthesis of chemically diverse core-shell nanoparticles for intracellular delivery. *Proc. Natl. Acad. Sci. USA* **108**, 12996-13001, (2011).

7 Jayaraman, M., Ansell, S. M., Mui, B. L., Tam, Y. K., Chen, J. X., Du, X. Y., Butler, D., Eltepu, L., Matsuda, S., Narayanannair, J. K., Rajeev, K. G., Hafez, I. M., Akinc, A., Maier, M. A., Tracy, M. A., Cullis, P. R., Madden, T. D., Manoharan, M. & Hope, M. J. Maximizing the Potency of siRNA Lipid Nanoparticles for Hepatic Gene Silencing In Vivo. *Angew. Chem. Int. Edit.* **51**, 8529-8533, (2012).

8 Scholz, C. & Wagner, E. Therapeutic plasmid DNA versus siRNA delivery: Common and different tasks for synthetic carriers. *J. Control. Release* **161**, 554-565, (2012).

9 Tian, H., Tang, Z., Zhuang, X., Chen, X. & Jing, X. Biodegradable synthetic polymers: Preparation, functionalization and biomedical application. *Prog. Polym. Sci.* **37**, 237-280, (2012).

10 Lynn, D. M. & Langer, R. Degradable Poly(β-amino esters): Synthesis, Characterization, and Self-Assembly with Plasmid DNA. *J. Am. Chem. Soc.* **122**, 10761-10768, (2000).

11 Green, J., Langer, R. & Anderson, D. A combinatorial polymer library approach yields insight into nonviral gene delivery. *Accounts Chem. Res.* **41**, 749-759, (2008).

12 Gokhale, S., Xu, Y. & Joy, A. A Library of Multifunctional Polyesters with "Peptide-Like" Pendant Functional Groups. *Biomacromolecules* **14**, 2489-2493, (2013).

13 Yan, Y. & Siegwart, D. J. Scalable synthesis and derivation of functional polyesters bearing ene and epoxide side chains. *Polym. Chem.* **5**, 1362-1371, (2014).

14 Jerome, C. & Lecomte, P. Recent advances in the synthesis of aliphatic polyesters by ring-opening polymerization. *Adv. Drug Delivery Rev.* **60**, 1056-1076, (2008).

15 Pounder, R. & Dove, A. Towards poly(ester) nanoparticles: recent advances in the synthesis of functional poly(ester)s by ring-opening polymerization. *Polym. Chem.* **1**, 260-271, (2010).

16 Seyednejad, H., Ghassemi, A. H., van Nostrum, C. F., Vermonden, T. & Hennink, W. E. Functional aliphatic polyesters for biomedical and pharmaceutical applications. *J. Control. Release* **152**, 168-176, (2011).

17 Hao, J., Rainbolt, E. A., Washington, K., Biewer, M. C. & Stefan, M. C. Synthesis of Functionalized Poly(caprolactone)s and Their Application as Micellar Drug Delivery Systems. *Curr. Org. Chem.* **17**, 930-942, (2013).

18 van der Ende, A., Kravitz, E. & Harth, E. Approach to formation of multifunctional polyester particles in controlled nanoscopic dimensions. *J. Am. Chem. Soc.* **130**, 8706-8713, (2008).

19 Nederberg, F., Zhang, Y., Tan, J. P. K., Xu, K. J., Wang, H. Y., Yang, C., Gao, S. J., Guo, X. D., Fukushima, K., Li, L. J., Hedrick, J. L. & Yang, Y. Y. Biodegradable nanostructures with selective lysis of microbial membranes. *Nat. Chem.* **3**, 409-414, (2011).

20 Zhang, X. J., Cai, M. M., Zhong, Z. L. & Zhuo, R. X. A Water-Soluble Polycarbonate With Dimethylamino Pendant Groups Prepared by Enzyme-Catalyzed Ring-Opening Polymerization. *Macromol. Rapid Commun.* **33**, 693-697, (2012).

21 Darcos, V., Antoniacomi, S., Paniagua, C. & Coudane, J. Cationic polyesters bearing pendent amino groups prepared by thiol-ene chemistry. *Polym. Chem.* **3**, 362-368, (2012).

22 Zhang, Z. H., Yin, L. C., Xu, Y. X., Tong, R., Lu, Y. B., Ren, J. & Cheng, J. J. Facile Functionalization of Polyesters through Thiol-yne Chemistry for the Design of Degradable, Cell-Penetrating and Gene Delivery Dual-Functional Agents. *Biomacromolecules* **13**, 3456-3462, (2012).

23 Kim, H., Olsson, J. V., Hedrick, J. L. & Waymouth, R. M. Facile Synthesis of Functionalized Lactones and Organocatalytic Ring-Opening Polymerization. *ACS. Macro. Lett.* **1**, 845-847, (2012).

24 Geihe, E. I., Cooley, C. B., Simon, J. R., Kiesewetter, M. K., Edward, J. A., Hickerson, R. P., Kaspar, R. L., Hedrick, J. L., Waymouth, R. M. & Wender, P. A. Designed

guanidinium-rich amphipathic oligocarbonate molecular transporters complex, deliver and release siRNA in cells. *Proc. Natl. Acad. Sci. USA* **109**, 13171-13176, (2012).

25 Jones, C. H., Chen, C. K., Jiang, M., Fang, L., Cheng, C. & Pfeifer, B. A. Synthesis of Cationic Polylactides with Tunable Charge Densities as Nanocarriers for Effective Gene Delivery. *Mol. Pharmaceut.* **10**, 1138-1145, (2013).

26 Winkler, M., Raupp, Y. S., Kohl, L. A. M., Wagner, H. E. & Meier, M. A. R. Modified Poly(epsilon-caprolactone)s: An Efficient and Renewable Access via Thia-Michael Addition and Baeyer-Villiger Oxidation. *Macromolecules* **47**, 2842-2846, (2014).

27 Blake, T. R. & Waymouth, R. M. Organocatalytic Ring-Opening Polymerization of Morpholinones: New Strategies to Functionalized Polyesters. *J. Am. Chem. Soc.* **136**, 9252-9255, (2014).

28 Albertsson, A. C. & Varma, I. K. Recent developments in ring opening polymerization of lactones for biomedical applications. *Biomacromolecules* **4**, 1466-1486, (2003).

29 Sutar, A. K., Maharana, T., Dutta, S., Chen, C. T. & Lin, C. C. Ring-opening polymerization by lithium catalysts: an overview. *Chem. Soc. Rev.* **39**, 1724-1746, (2010).

30 Maurice, M. & Meiyan, W. U. in *Ring-Opening Polymerization* Vol. 286 *ACS Symposium Series* Ch. 13, 175-182 (American Chemical Society, 1985).

31 Akinc, A., Zumbuehl, A., Goldberg, M., Leshchiner, E. S., Busini, V., Hossain, N., Bacallado, S. A., Nguyen, D. N., Fuller, J., Alvarez, R., Borodovsky, A., Borland, T., Constien, R., de Fougerolles, A., Dorkin, J. R., Narayanannair Jayaprakash, K., Jayaraman, M., John, M., Koteliansky, V., Manoharan, M., Nechev, L., Qin, J., Racie, T., Raitcheva, D., Rajeev, K. G., Sah, D. W., Soutschek, J., Toudjarska, I., Vornlocher, H. P.,

Zimmermann, T. S., Langer, R. & Anderson, D. G. A combinatorial library of lipid-like materials for delivery of RNAi therapeutics. *Nat. Biotechnol.* **26**, 561-569, (2008).

32 Love, K., Mahon, K., Levins, C., Whitehead, K., Querbes, W., Dorkin, J., Qin, J., Cantley, W., Qin, L., Racie, T., Frank-Kamenetsky, M., Yip, K., Alvarez, R., Sah, D., de Fougerolles, A., Fitzgerald, K., Koteliansky, V., Akinc, A., Langer, R. & Anderson, D. Lipid-like materials for low-dose, in vivo gene silencing. *Proc. Natl. Acad. Sci. USA* **107**, 1864-1869, (2010).

33 Nelson, C. E., Kintzing, J. R., Hanna, A., Shannon, J. M., Gupta, M. K. & Duvall, C. L. Balancing Cationic and Hydrophobic Content of PEGylated siRNA Polyplexes Enhances Endosome Escape, Stability, Blood Circulation Time, and Bioactivity in Vivo. *ACS Nano* **7**, 8870-8880, (2013).

34 Tempelaar, S., Mespouille, L., Dubois, P. & Dove, A. P. Organocatalytic Synthesis and Postpolymerization Functionalization of Allyl-Functional Poly(carbonate)s. *Macromolecules* **44**, 2084-2091, (2011).

35 Silvers, A. L., Chang, C. C. & Emrick, T. Functional aliphatic polyesters and nanoparticles prepared by organocatalysis and orthogonal grafting chemistry. *J. Polym. Sci. A* **50**, 3517-3529, (2012).

36 Leung, A. K. K., Hafez, I. M., Baoukina, S., Belliveau, N. M., Zhigaltsev, I. V., Afshinmanesh, E., Tieleman, D. P., Hansen, C. L., Hope, M. J. & Cullis, P. R. Lipid Nanoparticles Containing siRNA Synthesized by Microfluidic Mixing Exhibit an Electron-Dense Nanostructured Core. *J. Phys. Chem. C* **116**, 18440-18450, (2012).